University of Alberta

MATHEMATICAL ANALYSIS IN NONLINEAR AEROELASTICITY

by

Liping Liu ©

A thesis submitted to the Faculty of Graduate Studies and Research
in partial fulfillment of the requirements for the degree of
Doctor of Philosophy

in

Applied Mathematics

Department of Mathematical and Statistical Sciences
Edmonton, Alberta
Spring 2002

National Library
of Canada

Acquisitions and
Bibliographic Services

395 Wellington Street
Ottawa ON K1A 0N4
Canada

Bibliothèque nationale
du Canada

Acquisitions et
services bibliographiques

395, rue Wellington
Ottawa ON K1A 0N4
Canada

Your file Votre référence

Our file Notre référence

The author has granted a non-exclusive licence allowing the National Library of Canada to reproduce, loan, distribute or sell copies of this thesis in microform, paper or electronic formats.

L'auteur a accordé une licence non exclusive permettant à la Bibliothèque nationale du Canada de reproduire, prêter, distribuer ou vendre des copies de cette thèse sous la forme de microfiche/film, de reproduction sur papier ou sur format électronique.

The author retains ownership of the copyright in this thesis. Neither the thesis nor substantial extracts from it may be printed or otherwise reproduced without the author's permission.

L'auteur conserve la propriété du droit d'auteur qui protège cette thèse. Ni la thèse ni des extraits substantiels de celle-ci ne doivent être imprimés ou autrement reproduits sans son autorisation.

0-612-68598-5

Canada

University of Alberta

Library Release Form

Name of Author: Liping Liu

Title of Thesis: Mathematical Analysis in Nonlinear Aeroelasticity

Degree: Doctor of Philosophy

Year This Degree Granted: 2002

Permission is hereby granted to the University of Alberta Library to reproduce single copies of this thesis and to lend or sell such copies for private, scholarly, or scientific research purposes only.

The author reserves all other publication and other rights in association with the copyright in the thesis, and except as herein before provided, neither the thesis nor any substantial portion thereof may be printed or otherwise reproduced in any material form whatever without the author's prior written permission.

608F
Michener Park
Edmonton, Alberta
Canada, T6H 5A1

Date: December 19, 2001

UNIVERSITY OF ALBERTA

Faculty of Graduate Studies and Research

The undersigned certify that they have read, and recommend to the Faculty of Graduate Studies and Research for acceptance, a thesis entitled **Mathematical Analysis in Nonlinear Aeroelasticity** submitted by **Liping Liu** in partial fulfillment of the requirements for the degree of **Doctor of Philosophy** in Applied Mathematics.

Dr. Joseph So (Chair)

Dr. Yau Shu Wong (Supervisor)

Dr. B. H. K. Lee (Co-Supervisor)

Dr. Peter Minev

Dr. Henry Van Roessel

Dr. Chongqing Ru (Mechanical Engineering)

December 6, 2001 for Dr. Xinzhi Liu (University of Waterloo)

ABSTRACT

Aeroelasticity is concerned with the physical phenomena which involve significant mutual interaction among inertial, elastic, and aerodynamic forces. The study of aeroelasticity began in earnest in the early stages of the World War II when airplane speeds increased and aircraft designers encountered a wide variety of problems classified later as aeroelastic problems. The classic works on aeroelasticity are based on linear dynamics, linear aerodynamics, and linear structures. However, nonlinear structures arise from various sources, and an understanding of the nonlinear behavior of the system is crucial to the efficient and safe design of aircraft wings and control surfaces. In this thesis, we consider a two-dimensional airfoil oscillating in pitch and plunge with subsonic aerodynamics and with cubic, freeplay, and hysteresis structural nonlinearities. Some analytical techniques—center manifold theory, the principle of normal form, the perturbation method, and the point transformation method—were used to investigate the effects of the structural nonlinearities on flutter. For a self-excited aeroelastic system with cubic hard springs, the amplitudes and frequencies of limit cycle oscillations in the post-Hopf bifurcation can be predicted analytically. An excellent agreement was found between the results of numerical simulations and analytical predictions. For an aeroelastic system with freeplay and hysteresis models, convergent motions, period-one and period-two stable limit cycle oscillations, and chaotic motions are detected and the amplitudes and frequencies of limit cycle oscillations are predicted for the velocity below the linear flutter speed. Although time-integration numerical methods have often been used to study the response of an aeroelastic system with structural nonlinearities, the importance and necessity of analytical techniques are addressed through a detailed study of the numerical errors resulting from the Runge-Kutta method. The analytical techniques developed in this thesis are suitable for many other non-aeroelastic systems: the center manifold theory and the principle of normal form can be generalized for nonlinear systems of ordinary differential equations with polynomial nonlinearities; the point transformation method can be extended for general piecewise linear systems.

ACKNOWLEDGEMENT

I sincerely thank my supervisor Professor Yau Shu Wong and my co-supervisor Dr. Ben H. K. Lee for their kind patience and invaluable guidance. Also, I deeply indebted to several professors for helpful comments and criticisms, including, in particular, Professor Joseph W.H. So, Professor Peter D. Minev, Professor Chongqing Ru, Professor Henry Van Roessel and Professor Xinzhi Liu. In the long process of this study, I received kind help from many friends, among which Wieslaw Kracewicz, Micheal Y. Li, Eric Woolgar and Ming Mei are the most helpful ones. Thanks are due also to my husband, who always strongly supports me by doing much house work, looking after our baby son and reading the first draft of this thesis. Last but not least, I wish to thank Mr. Dave Clyburn, director of University Writing Resources, for his patience in correcting all grammatical errors.

To my husband,
Quanli Wang,
and my son,
Kelvin Ray Wang

Table of Contents

1 Introduction 1

1.1 Background 1

1.2 Nonlinear Aeroelasticity 3

1.3 A Review of Flutter Analysis on Aeroelastic Systems with Structural Nonlinearities 5

1.3.1 Cubic Springs 6

1.3.2 Freeplay Springs 9

1.3.3 Hysteresis Nonlinearities 14

1.4 Main Contributions 15

2 Equations for Airfoils with Structural Nonlinearities and Subsonic Aerodynamics 18

2.1 Introduction 18

2.2 A Two-degree-of-freedom Airfoil Motion 19

2.3 Model Reformulation 21

2.4 Structural Nonlinearities 24

2.4.1 Cubic Springs 24

2.4.2 Freeplay Springs 25

2.4.3 Hysteresis Nonlinearities 25

3 Cubic Springs 27

3.1 Introduction 27

3.2 The Reduced System on A Center Manifold 28

3.3 The Principle of Normal Form 32
3.4 Amplitudes of Limit Cycle Oscillations 34
3.5 Case Studies and Discussion 35
3.6 Concluding Remarks 42

4 Freeplay Models **44**
4.1 Introduction 44
4.2 Rational Polynomial Approximations for Freeplay Springs 46
4.3 The Point Transformation Method 48
  4.3.1 Formulation 1 54
  4.3.2 Formulation 2 58
4.4 Results and Discussions 61
4.5 Concluding Remarks 71

5 Hysteresis Nonlinearities **73**
5.1 Introduction 73
5.2 The Point Transformation Method 74
  5.2.1 Formulation 1 79
  5.2.2 Formulation 2 81
5.3 Case Studies and Discussions 84
5.4 Concluding Remarks 89

6 Error Analysis of RK's Discretizations of Aeroelastic Systems **91**
6.1 Introduction 91
6.2 A Simple Sinusoidal Motion and Aeroelastic Systems with Cubic Springs 93
6.3 A Rapidly Time-Variant System 99
6.4 An Aeroelastic System with A Piecewise Linear Model 104
6.5 Concluding Remarks 117

7 Conclusion **120**

Bibliography **124**

A Nomenclature **134**

B Center Manifold Theory **137**

B.1 Definitions and Theorems 137

B.2 Properties of Center Manifolds 139

List of Figures

1.1 A triangle of forces for problems in aeroelasticity. 1

2.1 Two-degree-of-freedom airfoil motion 20
2.2 General sketch of a cubic spring: (a). cubic hard spring; (b). cubic soft spring. 24
2.3 General sketch of a freeplay spring: (a). without any preload; (b). with a preload. 25
2.4 General sketch of a hysteresis spring. 26

3.1 Dynamic response for Case 1. (a). frequency; (b). amplitude of pitch motion; (c). amplitude of plunge motion. 39
3.2 Dynamic response for Case 2. (a). frequency; (b). amplitude of pitch motion. 40
3.3 Dynamic response for Case 3. (a). frequency; (b). amplitude of pitch motion; (c). amplitude of plunge motion. 41
3.4 Dynamic response for Case 4. (a). frequency; (b). amplitude of pitch motion. 42

4.1 The original freeplay model and its approximations, (a). with $R_1(x_1)$; (b). with $R_2(x_1)$. Solid line: $M(x_1)$; open circle: approximated values of $R_1(x_1)$ or $R_2(x_1)$. 47
4.2 The system response when the freeplay model is replaced by $R_1(x_1)$: divergent motion (a), and by $R_2(x_1)$: periodic motion (b). 48
4.3 General sketch of a freeplay model. 50

4.4 General trajectory of system (2.2) with a freeplay stiffness in pitch. 51
4.5 Trajectories for system Eq.(2.2) with a freeplay stiffness in pitch: period-one with harmonics where (a) the smaller loop covers R_1 and R_2; (b) the smaller loop covers R_2 and R_3. 52
4.6 Trajectories for system Eq.(2.2) with a freeplay stiffness in pitch: period-two LCO (a) without harmonics and (b) with harmonics where two smaller loops cover R_1 and R_2. 53
4.7 Bifurcation diagram for $\alpha(0) = 3^\circ$ and $\alpha'(0) = \xi(0) = \xi'(0) = 0$. 62
4.8 Period diagram for $\alpha(0) = 3^\circ$ and $\alpha'(0) = \xi(0) = \xi'(0) = 0$. . 63
4.9 Frequency diagram for $\alpha(0) = 3^\circ$ and $\alpha'(0) = \xi(0) = \xi'(0) = 0$. 64
4.10 The time history (a) and power spectral density (b) of pitch motion for Case 1 in Table 4.1. Solid line: Runge-Kutta time-integration result; filled circle: point transformation result. . . 66
4.11 The time history (a) and power spectral density (b) of pitch motion for Case 2 in Table 4.1. Solid line: Runge-Kutta time-integration result; filled circle: point transformation result. . . 67
4.12 The time history (a) and power spectral density (b) of pitch motion for Case 3 in Table 4.1. Solid line: Runge-Kutta time-integration result; filled circle: point transformation result. . . 68
4.13 Chaotic motion of Case 4 in Table 4.1: (a) the switching points by using point transformation method; (b) the phase path by using Runge-Kutta time-integration; (c) the PSD plot. 70
4.14 The time history (a) and phase path (b) for Case 5 in Table 4.2. Solid line: Runge-Kutta time-integration result; filled circle: point transformation result. 71

5.1 General sketch of a freeplay spring. 76
5.2 General trajectory (a) and a period-one LCO (b) of the aeroelastic system Eq.(2) with hysteresis structure. Filled circles: switching points. 76

5.3 General trajectories for period-one with harmonics: (a) the smaller loop covers IR_1 and IR_2; (b) the smaller loop covers DR_1 and DR_2. Filled circles: switching points. 78
5.4 Trajectories for a period-two with harmonics (a) and a period-four with harmonics (b) LCOs. Filled circles: switching points. 79
5.5 The flutter boundary diagram of an aeroelastic system with a hysteresis model. Filled dot: damped motion, star: LCO, open circle: divergent motion. 84
5.6 Case 1 in Table 5.1: (a) time history; (b) trajectory of α-α'. Solid line: numerical result, filled circles: point transformation method. 86
5.7 Case 2 in Table 5.1: (a) time history. (b) PSD plot. Solid line: numerical result, filled circles: point transformation method. . 87
5.8 Time histories for Cases 3 and 4 in Table 5.1: (a) Case 3; (b) Case 4. Solid line: numerical result, filled circles: point transformation method. 88
5.9 Case 5 in Table 5.1: (a) switching points; (b) phase projection of α-α'. 88

6.1 Analysis of the amplitude decaying percentage error of the fourth-order RK-scheme for a simple sinusoidal motion. 97
6.2 Analysis of (a) the period elongation percentage error and (b) the phase shift percentage error of the fourth-order RK-scheme for a simple sinusoidal motion. 98
6.3 The exact motion of a rapidly time-variant system Eq.(6.1) with $x(0) = 0$ and $x'(0) = 0.1$. 101
6.4 The norm of the eigenvalues of the transition matrix of the scheme 102
6.5 Numerical results for time steps (a) $h = 0.1$, (b) $h = 0.01$, and (c) $h = 0.001$. 103
6.6 The numerical error of the scheme for $h = 0.01$. 104
6.7 Bifurcation diagram for the simplified four dimensional freeplay model. 110

6.8 The time histories of x_1 for Case 1 with (a). $h = 0.02$ and (b). $h = 0.005$. 111
6.9 The time histories of x_1 for Case 1 with (a). $h = 0.08$ and (b). $h = 0.00125$. 111
6.10 The phase paths of x_1–x_2 for Case 1 with (a). $h = 0.08$ and (b). $h = 0.00125$. 112
6.11 The time histories of x_3 for Case 1 with (a). $h = 0.08$ and (b). $h = 0.00125$. 112
6.12 The phase paths of x_3–x_4 for Case 1 with (a). $h = 0.08$ and (b). $h = 0.00125$. 113
6.13 The time histories of x_1 for Case 2 with (a). $h = 0.08$ and (b). $h = 0.02$. 113
6.14 The time histories of (a). x_1 and (b). x_3 for Case 2 with $h = 0.005$. 114
6.15 The phase paths of x_1–x_2 for Case 2 with (a). $h = 0.08$ and (b). $h = 0.02$. 114
6.16 The time histories of x_3 for Case 2 with (a). $h = 0.08$ and (b). $h = 0.02$. 115
6.17 The phase paths of x_3–x_4 for Case 2 with (a). $h = 0.08$ and (b). $h = 0.02$. 115
6.18 Time history of x_1 for Case 1 resulting from PT-method. . . . 116
6.19 Time histories of x_1 and x_3 for Case 2, result from PT-method. 116
6.20 The phase paths of x_1–x_2 and of x_3–x_4 for Case 2, result from PT-method. 117
6.21 A comparison between the RK result and the PT result. . . . 118
6.22 Switching point location errors in the RK-method for Case 1 . 119

List of Tables

3.1 Case studies for the aeroelastic system Eq.(2.2) with cubic springs 36

3.2 The frequency relationship with the bifurcation parameter $\gamma = U^*/U_L^*$ for Case 1. 38

3.3 The frequency relationship with the bifurcation parameter $\gamma = U^*/U_L^*$ for Case 2. 38

4.1 Cases studies for the freeplay model 65

4.2 Coexistence of limit cycle oscillations for the freeplay model . 69

4.3 Results of Formulation 2 for Cases 5 and 6 in Table 4.2 69

5.1 Case studies for a hysteresis model. 85

5.2 Coexistence of limit cycle cscillations for a hysteresis model. . 86

6.1 Case studies using RK-method for a freeplay model 109

6.2 Case studies using PT-method for a freeplay model 109

Chapter 1

Introduction

1.1 Background

Problems in aeroelasticity were first intuitively visualized by means of a triangle of forces by Collar[13] in 1946. As shown in Fig. 1.1., three types of

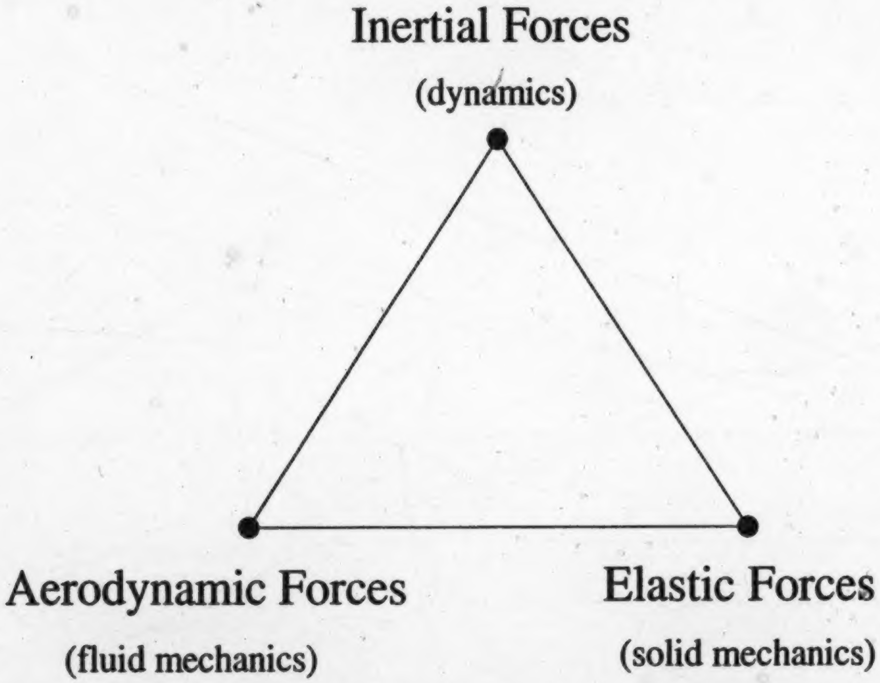

Figure 1.1: A triangle of forces for problems in aeroelasticity.

forces involved in aeroelasticity, namely, aerodynamic, elastic and inertial forces, are placed at the vertices of the triangle. Each aeroelastic phenomenon can be located on the diagram according to its relation to the three vertices. For example, while dynamic aeroelastic phenomena such as flutter involve all three types of forces, static aeroelastic phenomena such as wing divergence involve only aerodynamic and elastic forces.

Collar's idea was further employed and developed by Dowell et al.[19]. Aeroelasticity was then defined as a multi-disciplinary field concerned with those physical phenomena which involve significant mutual interaction among inertial, elastic and aerodynamic forces. Also, by pairing the vertices of the triangle, we can identify some other important technical fields: flight mechanics (i.e. stability and control) concerns dynamics and aerodynamics; structural vibration is related to dynamics and solid mechanics; static aeroelasticity involves fluid mechanics and solid mechanics. Each of these technical fields may be thought of as a special aspect of aeroelasticity.

Aeroelastic phenomena are not uncommon. They occur in everyday life: trees sway in the wind; flags and sails flap; suspension bridges and airplane wings flutter. However, attempts to develop a theory to understand them were made essentially by aeronautical engineers. Problems in aeroelasticity started did not attain the prominent role that they now play until the early stages of World War II. Prior to that time, airplane speeds were relatively low and the load requirements placed on aircraft structures by design criteria specifications produced a structure sufficiently rigid to preclude most aeroelastic phenomena. As speeds increased, however, with little or no increase in load requirements, and in the absence of rational stiffness criteria for design, aircraft designers encountered a wide variety of problems which we now classify as aeroelastic problems. A historical discussion of aeroelasticity, including its impact on aerospace vehicle design, can be found in Chapter I of Bisplinghoff and Ashley[7] and AGARD[64].

Although in the past, aeronautical problems were the focus in the field of aeroelasticity, applications are appearing at an increasing rate in other fields such as flows about bridges in civil engineering and fluid flows in flexible pipes in mechanical engineering. More details about the applications in several non-airfoil fields such as plates and shells, turbomachinery and helicopters (rotor systems) are presented in Dowell[18], Dowell et al.[19] and Dowell and Ilgamov[20].

1.2 Nonlinear Aeroelasticity

Dowell and Ilgamov[20] categorized aeroelastic models into three classes: fully linear models in which both the static equilibrium problem and the dynamic motion problem are treated by linear models, dynamically linear models in which the nonlinear static model and the dynamically linear model are used, and fully nonlinear models in which both the static and dynamic problems are nonlinear.

In the fully linear models, the deformed structure does not significantly influence its dynamic response and the steady flow field deviation does not appreciably change the unsteady, time-dependent aerodynamic forces. Moreover, the dynamic motions are sufficiently small that there are no significant nonlinear effects. As the models can be reduced to a set of linear equations, the fully linear models are widely used in most classic approaches on aeroelasticity. Within the classic works, theoretical work relies heavily on linear mathematical concepts, and experimental results are commonly interpreted by assuming that the physical model behaves in a linear manner.

For many years, fully linear models, both theoretically and experimentally, have been successful in providing approximate estimates to aeroelasticians. By studying such models, researchers established much of their understanding of aeroelastic phenomena such as divergence, flutter, control surface reversal, and gust response. These models are well presented in the now classic texts by Scanlan and Rosenbaum[73], Fung[23], Bisplinghoff et al.[8], and more recently by Forsching[22] and Dowell et al.[19].

If the deformed structure and/or the steady flow field do influence the subsequent dynamic response, a dynamically linear model has to be used. For example[18], if a plate is buckled from its initial flat configuration, its dynamic response may be significantly changed from that for the initially flat plate. Another example[33] is the dynamic aeroelastic behavior of a rotor blade which is often significantly modified by its deformed structure. Nonlinear static aeroelasticity involves nonlinear aerodynamics and nonlinear structures. Nonlinear aerodynamics has to be considered when airspeed increases to high subsonic or transonic Mach numbers. Also, flow separation and shock oscillations can introduce phenomena such as limit cycle oscillations (LCOs) which classical aeroelasticity is unable to handle. Structural nonlinearities in airfoils arise from worn hinges of control surfaces, loose control linkages, and various other sources. Aging aircraft and combat aircraft that carry heavy external stores are more likely to be influenced by effects associated with nonlinear structures. Aircraft structures often exhibit nonlinearities that affect not only the flutter speed but also the characteristic of the motion itself.

For the phenomena involving small dynamic motions, the dynamically linear models are adequate. However, a fully nonlinear model will be more appropriate if the dynamic motions are significantly large. Several examples of these models are given in Dowell and Ilgamov[20].

In this thesis, the emphasis is placed on the flutter analysis of aeroelastic systems with structural nonlinearities. In order to limit the complexity of the aeroelastic system with structural nonlinearities, we consider a dynamically linear model with linear aerodynamics but nonlinear structures, i.e., a two-dimensional airfoil oscillating in pitch and plunge using subsonic aerodynamics where approximate expressions for the force and moment are available. Extending the analysis to more than two modes is straightforward, but the algebra is considerably more complex. A detailed description of the physical and mathematical models and the structural nonlinearities is presented in the following chapter. The subsequent section gives a literature review of the work that has been done on aeroelastic systems with nonlinear structures.

1.3 A Review of Flutter Analysis on Aeroelastic Systems with Structural Nonlinearities

Although flutter is a dangerous phenomenon that may cause structural failure, it is possible for a system to approach instability without destructive results. Under the assumption of a linear model, the system will become unstable and its motion will grow exponentially with time as the magnitude of dynamic pressure or flight velocity passes a certain critical value. However, the extent to which the amplitude of oscillation grows actually depends on the nature of the stiffness characteristics of the system. If the system is nonlinear, as the stiffness characteristics change with amplitude of motion, oscillations may increase to some amplitude at which the system experiences a stable limit cycle oscillation (LCO). Thus, the efficiency of the design of aircraft wings and control surfaces may be increased by a flutter analysis technique accounting for these nonlinearities and by an understanding of their potential influence on the flutter mechanism.

An excellent review of some possible structural nonlinearities and their effects on aeroelastically induced vibration has been provided by Breitbach[9, 10]. In general, structural nonlinearities may be classified as being either distributed or concentrated. Usually, distributed structural nonlinearities are governed by elastodynamic deformations that affect the whole structure. Concentrated structural nonlinearities, on the other hand, act locally and are commonly found in control mechanisms or in the connecting parts between wings, pylons, engines or external stores. The first attempt to study the effects of these structural nonlinearities was carried out by Woolston et al.[89, 90]. For general nonlinear dynamics, some subjects such as stability, bifurcation and chaos are commonly encountered[5, 26, 66, 67, 68, 74]. These subjects are reviewed by Lee et al. [52] particularly for nonlinear aeroelasticity. In this thesis, we consider only concentrated structural nonlinearities and investigate their effects on the aeroelastic behavior of aerosurfaces. As the concentrated structural nonlinearities can be classified into three types, namely, cubic, freeplay and hysteresis, a review of each type will be given in the following subsections.

1.3.1 Cubic Springs

The effect of cubic nonlinearity in aeroelasticity was first investigated by Woolston et al.[89, 90] for a two-dimensional airfoil oscillating in pitch and plunge using an analog computer. A 2-DOF system was analyzed for hard and soft springs in the pitch degree of freedom, where the spring stiffness was represented by the sum of a linear and a cubic term. Results were given in the form of plots of initial angular displacement versus flutter velocity. For a hard spring, the flutter boundary is a straight line at the flutter speed of the linear system. The flutter amplitude, a function of velocity, is self-limited and increases as velocity is increased beyond the flutter boundary. For the soft spring, on the other hand, the flutter is divergent at any velocity above the linear flutter speed and can be induced below the linear flutter speed by making the initial displacement sufficiently large as the soft spring has a destabilizing effect.

An alternate approach was suggested by Shen[75, 76] using the well-known Kryloff and Bogoliuboff[41] method in nonlinear vibration theory. The first approximation of Kryloff and Bogoliuboff[41], also known as the describing function method or harmonic balance method, is a method of obtaining an equivalent linear system so that traditional linear aeroelastic methods of analysis can be employed. The method assumes the existence of a periodic solution dominated by the fundamental harmonic. The amplitude of oscillation in the degree of freedom which contains the nonlinearity is prescribed and the critical velocity at which the specified oscillation will be sustained is then determined. However, Shen[75, 76] did not consider the effects of initial conditions on the flutter boundary.

Further investigation was conducted by Lee and LeBlanc[51] on the effects of initial pitch displacement on the flutter boundaries, as well as the amplitudes of pitch and plunge motion of LCO for various system parameters.

Houbolt's[34] implicit finite-difference scheme was employed throughout their study. By using incompressible aerodynamics, the aeroelastic equations for a two-dimensional airfoil oscillating in pitch and plunge are written as a pair of simultaneous finite difference equations. The effect of initial conditions on nonlinear flutter was studied numerically by varying the displacement from equilibrium of the pitch angle at the start of airfoil motion. Their conclusions agreed with the limited results given by Woolston et al.[89, 90] on the behavior of the flutter boundaries for both soft and hard springs. Lee and LeBlanc[51] also investigated the effects of the airfoil/air-mass ratio, the undamped plunge/pitch natural frequency ratio, the distance between elastic axis and the center of mass of the airfoil, and various stiffnesses of the nonlinear spring on the airfoil response.

Some experiments on the existence of LCO for the 2-DOF model with cubic soft springs were performed by O'Neil et al.[70]. By comparing their results with those given by Lee and LeBlanc[51], they found that the stability boundary is sensitive to initial conditions, and the amplitude and frequency of the airfoil response depend primarily on the free-stream velocity.

Zhao and Yang[94] studied the chaotic behavior of a self-excited aerodynamic system with a cubic nonlinearity using the equivalent linearization (describing function) method and a time marching method which employed Runge-Kutta numerical integration. By using quasi-static aerodynamics in which the lift and pitching moment depend on the instantaneous pitch angle, they found that chaos would occur for velocities above the linear flutter speed.

The same techniques were used by Price et al.[72] on a similar model with aerodynamic forces obtained from a complete unsteady analysis using Wagner's function. They noticed that the difference in aerodynamics had a considerable effect on the dynamic response of the airfoil. Chaos resulting from certain system parameters was further investigated by using techniques such as power spectral analysis, phase-space plots, Poincare maps, and Lyapunov exponents. Furthermore, LCO regions were detected for velocities well below the divergent flutter boundary.

While different numerical and analytical techniques have been employed to investigate cubic nonlinearity, a series of approaches based on Duffing's equation were also developed. Cubic nonlinearities in 1-DOF mechanical and electrical systems can often by represented by Duffing's equation, which has been the subject of investigation for many years. Some classical techniques and results related to Duffing's equation can be found in Stoker[78] and Hayashi[31], and more recent studies dealing with chaotic characteristics of this equation are given by Ueda[83] and Thompson and Stewart[81].

Some numerical simulations were carried out by Jones and Lee[38] to demonstrate the sensitivity to initial conditions in the jump phenomenon in Duffing's equation, a 1-DOF system with a cubic nonlinearity. The dynamic response of coupled Duffing's equations, a 2-DOF system with cubic nonlinearities, was investigated analytically and numerically by Wong et al.[87]. Their results suggest that the amplitude-frequency curve has a much more complex structure compared to that of a 1-DOF system. The coupled Duffing's equations were further investigated by Gong et al.[25], who showed that harmonic, quasi-periodic, and chaotic motions can exist for system parameters corresponding to those commonly used to analyze aeroelastic behavior of aircraft structures. The equations studied by Wong et al.[87] and Gong et al.[25] were derived for an airfoil oscillating in pitch and plunge without aerodynamic terms to explore the dynamics of coupled Duffing's equations before introducing further complexities when aerodynamics forces are included.

For a two-dimensional airfoil with cubic nonlinearity placed in an incompressible flow, by introducing four new variables, Lee et al.[46] reformulated the aeroelastic equations to a set of eight first-order ordinary differential equations. This approach allows existing methods suitable for the study of ordinary differential equations[11, 12, 21, 24, 27, 85] to be used in the analysis. In their studies, only the harmonic solutions were considered, and the method of slowly varying amplitude was used to investigate the dynamic response of the system with an external excitation. The equilibrium points were computed, and a linear analysis was carried out to determine their stability. The results were subject to the assumptions that higher harmonics in the response are small and the amplitudes are slowly varying functions of time such that the second-order derivatives can be neglected. They also found that the amplitude-frequency response curve of a 2-DOF system has a much more complex structure compared to that of a 1-DOF system. It is worth noting that harmonic solutions may not exist for certain values of system parameters for a 2-DOF system. However, in those cases in which harmonic solutions are found, there is a good agreement between the theoretical results and numerical simulations. More examples and discussions are given in Lee et al.[47, 48] and it turns out that the technique developed in [46, 47, 48] to determine the amplitude-frequency relationship and to analyze the stability of the equilibrium points can be used for more general cases.

The method developed by Wong et al.[87] and Gong et al.[25] for coupled nonlinear mechanical systems was later extended by Lee et al.[49, 50] to analyze aeroelastic systems with cubic nonlinearity for soft and hard springs. For a soft spring, the divergence flutter boundary varies with initial conditions. For a hard spring, on the other hand, the nonlinear flutter boundary is independent of initial conditions and divergent flutter is not encountered; instead, limit-cycle oscillation occurs for velocities greater than the flutter speed. Also, a Hopf-bifurcation was observed for the hard spring. Investigation of pre- and post-Hopf-bifurcation is carried out using methods developed for studying stability near equilibrium points of nonlinear oscillating systems[6, 42, 84]. Furthermore, the amplitudes of pitch and plunge motions of LCO in post-Hopf-bifurcation are predicted using an asymptotic theory, and the frequency is estimated using several approximate methods. Their results are compared with numerical simulations using the fourth-order Runge-Kutta scheme.

1.3.2 Freeplay Springs

Bilinear or freeplay springs, another type of concentrated structural nonlinearity, have also received considerable attention in the literature. It was first considered by Woolston et al.[89, 90], who showed numerically and experimentally that, depending on the initial pitch displacement, an LCO may occur for velocities well below the linear flutter velocity. They also showed that even at a fixed airspeed, the magnitude of LCO could change dramatically as the initial pitch displacement changes. The same result was obtained by Shen[75, 76] using the harmonic balance or describing function method. Moreover, Shen discovered the significant influence of the amount of the preload on the stability boundaries.

The freeplay nonlinearity was hardly touched in the next twenty years or so until the dynamics of a missile control surface containing structural freeplay nonlinearities was investigated by Laurenson and Trn[43] in 1980. In their study, the missile control surface was exposed to a subsonic flow represented by a simplified aerodynamics. By using the describing function method, they concluded that the presence of a freeplay nonlinearity tends to cause the effective system stiffness to be less than that of a linear system. They also observed some stable LCOs with small amplitudes beyond the linear flutter speed.

One year later, McIntosh et al.[62] analyzed a 2-DOF airfoil with freeplay structural nonlinearity in both pitch and heave directions and with the aerodynamic forces being predicted from an approximation to Wagner's function. Theoretical results agree well with those from experiments in terms of both the airspeed and frequency at the stability boundaries. In addition, they concluded that the behavior of the airfoil depends on the initial pitch displacement by showing one case in which an LCO was obtained for small displacements while a divergent flutter occurred for larger displacements.

Similar to the approach used by Lee and LeBlanc[51] for the aeroelastic equations for a two-dimensional airfoil oscillating in pitch and plunge with a cubic spring, the same system with freeplay was written in finite difference form by Lee and Desrochers[44]. For freeplay with nonzero preload, three types of oscillations, namely damped motions, LCOs, and divergent motions were observed. The location of the LCO flutter boundary depends on the airfoil parameters in addition to the values of the spring preload and freeplay. Also, for some combinations of preload and freeplay, there are pockets of LCO in the damped oscillation regions. For freeplay with zero preload, however, only LCOs and divergent motions were found, and the divergent flutter boundary occurred very close to that for the linear flutter case.

The same model, but with the aerodynamics obtained using Theodorsen's function, which is strictly correct only for harmonic motion, was considered by Yang and Zhao[93]. Theoretical results were obtained using both numerical simulation in the Laplace domain and harmonic balance methods. Experimentally and theoretically, they found that with a freeplay in the pitch direction, LCOs were obtained for airspeeds below the linear flutter speed. Furthermore, from experiments, two stable LCOs of different amplitudes were detected for certain airspeeds: one is dominated by pitch motion, the other by heave motion with a higher frequency and a larger amplitude. However, Yang and Zhao did not distinguish the velocity regions where one or two LCOs occurred or the difference in initial conditions which led to the different LCOs.

Some interesting studies on the flutter characteristics of the CF-18 aircraft were carried out by Lee and Tron[45] using the describing function method. Different nonlinearities located at the CF-18 wing-fold hinge, the outboard leading-edge flap, and the outboard leading-edge-flap hinge were investigated by treating them as bilinear springs or freeplays based on ground test data. Conditions in which divergent motion or LCO occurs and the effects of structural nonlinearities on flutter characteristics were well studied.

Hauenstein et al.[29, 30] investigated experimentally and theoretically a rigid wing flexibly mounted at its root with freeplay nonlinearities in both the pitch and heave directions. In the theoretical analysis, the aerodynamic forces were approximated using an unsteady subsonic doublet lattice technique, and the resulting equations were integrated numerically. Experimentally, time histories of both the pitch and heave displacements were measured. Theoretical results agreed very well with those from experiments for one specific case, in terms of time histories, and their spectral and phase-plane plots. They concluded that chaotic motion is not obtainable with a single root nonlinearity and that the range of chaotic motion is deeply dependent on the magnitude of the freeplay region.

Tang and Dowell[79] studied the flutter instability and forced response of a nonrotating helicopter blade with a NACA–0012 airfoil and a freeplay structural nonlinearity in pitch. They considered three typical combinations of linear/nonlinear structure with a linear/nonlinear (ONERA[82]) aerodynamic model. For the model with nonlinear structure and linear aerodynamics, LCOs were obtained for velocities below the linear flutter boundary. Furthermore, the harmonic balance method that they used detected two LCOs with different amplitudes for velocities within a narrow range. In this range, chaos was also found numerically. For the model with a linear structure and nonlinear aerodynamics and with external forces, chaos was observed as well. Considering the forced oscillation of a model with both nonlinear aerodynamics and freeplay, the response could be either periodic, chaotic, or divergent, depending on the initial conditions, especially on the flapping motion initials.

A similar helicopter blade model was also considered by Tang and Dowell[80] for a freeplay torsional stiffness nonlinearity. For the aerodynamics, the two-dimensional incompressible Theordorsen aerodynamic model, or Roger's transfer function were used. An experiment carried out at Duke University's low speed wind tunnel showed good agreement between theory (via numerical simulations) and experimental result for periodic, limit cycle and chaotic motions and forced response behavior and for the effects of an initial disturbance on nonlinear flutter instability.

Using a 2-DOF typical section model coupled to an unsteady Euler equations solver, Kousen and Bendiksen[40] observed limit cycle behavior in past transonic flutter calculations. The freeplay structural nonlinearity was added to the typical section model, and its effects on the dynamic stability problem were accessed. In addition, limit cycle behavior in the swept-wing model of Isogai[36] was demonstrated and related to the observed presence of multiple flutter points in the transonic dip region. By presenting preliminary results, they showed the effects of freeplay on the observed limit cycle behavior in the transonic regime, where strong aerodynamic nonlinearities were present.

Price et al.[72] investigated a two-dimensional airfoil subject to incompressible flow with a freeplay structural nonlinearity in pitch. The resulting equations were analyzed using a finite difference technique with the particular aim of examining the sensitivity of the airfoil aeroelastic response to its initial conditions. They found that chaotic motion could exist for a single structural nonlinearity in the pitch motion as opposed to the results in[30]. However, chaos was detected only for specific airfoil parameters and was confined to small regions in the stability boundary diagram.

A significantly different approach was developed by Alighanbari and Price[1], who performed a bifurcation analysis for the same model. First, the freeplay model was approximated by a third-order rational polynomial curve, and then the integral terms resulting from the aerodynamics were removed by twice differentiating the original equations. The nonlinear equations of motion were either integrated numerically using a fourth-order Runge-Kutta method or analyzed using the AUTO[17] software package. By using both methods, regions of period-one LCOs were detected for velocities well below the linear flutter boundary and regions of period-two and period-four LCOs were observed for the velocities below the main region of period-one LCOs. Bifurcation diagrams showing both stable and unstable periodic solutions were calculated with the help of AUTO, and the types of bifurcations were assessed by evaluating the Floquet multipliers.

As the freeplay model consists of three branches of linear functions, the system can be regarded as a combination of three linear subsystems. Correspondingly, the state-space of the system can be divided into three distinctive regions. The points where the motion flow passes from one region to the other are referred to as switching points. The location of the switching points is crucial to the dynamic response as addressed by Lin and Cheng[55]. Several numerical approaches, such as linear interpolation or bisection in Lin and Cheng[55] and the adaptive time steps in Bayly and Virgin[3], have been developed to locate the switching points.

Noticing the importance of the switching points, Conner et al.[16] investigated a 3-DOF aeroelastic typical section with control surface freeplay. The effect of the freeplay on the system response was examined numerically and experimentally. The numerical method used is a standard Runge-Kutta algorithm in conjunction with Henon's method[32]. The details of the numerical integration accounting for the abrupt stiffness change were given by Conner et al.[15].

1.3.3 Hysteresis Nonlinearities

Much less literature has been found on the study of hysteresis nonlinearities. The first attempt to study such effects in aerolasticity was carried out by Woolston et al.[90, 89], who numerically determined the flutter boundaries for a two-dimensional airfoil placed in an incompressible flow. Some examples were re-examined by Shen and Hsu[77] and Shen[75, 76] using the describing function method. This method was also used by Breitbach[9, 10] to analyze aircraft structures with hysteresis.

A numerical simulation using the fourth-order Runge-Kutta time-integration scheme was carried out in a recent study by Chan[14]. Only a hysteresis nonlinearity in the pitch degree of freedom was considered, and 19 cases were carefully studied for various system parameters and freeplay constants.

The flutter boundary diagram obtained by Chan[14] is similar to that in Woolston et al.[90], but the numerical simulations give more details on the boundary curves and the existence of isolated pockets of LCOs inside the main flutter boundary. The flutter boundary shows that the oscillations become divergent for a velocity ratio larger than 1. In the LCO region, the motion seems to be a sinusoid with a dominant fundamental and possible very weak higher harmonics for some values of the velocity ratio approaching the convergent region of the flutter boundary. This shows that the assumption of a dominant frequency in the harmonic balance or describing function technique is reasonable for the motions in this LCO region. However, inside one of the LCO pockets, the characteristics of the LCO are different from those in the main LCO region. The amplitudes are smaller and the oscillation is periodic but the presence of higher harmonics is clearly noticeable, which suggests that the assumption in Shen's[75] harmonic balance analysis is not applicable and higher approximations such as the sinusoidal method described by Johnson[37] may be used.

Chan[14] then discussed the relationships between the pitch amplitude/frequency and the velocity ratio for some specific system parameters. She concluded that the pitch amplitude and frequency are independent of the initial conditions, which is not true as we will show in Chapter 5. Chan[14] also studied the effect of preload on convergent motions, LCOs, and chaos. The study shows that a hysteresis nonlinearity with small ratios of preload over freeplay for a certain set of airfoil parameters enlarges the regions of chaotic motion beyond those for the freeplay studied by Price et al.[71]. Finally, the effects of airfoil parameters (freeplay region, natural frequency ratio, preload and airfoil/air mass ratio) on flutter boundaries were discussed in great detail.

1.4 Main Contributions

In this thesis, we mainly focus on analytical techniques for the flutter analysis of a self-excited 2-DOF aeroelastic system with all three types of structural nonlinearities. Numerical simulations have also been given to compare the results with those obtained from analytical methods.

The physical model of a 2-DOF airfoil motion used in this thesis is presented in Chapter 2. The mathematical model and its non-dimensional form for the airfoil subject to a subsonic flow are then formulated. By introducing four new variables, we then transform the two-dimensional integro-differential equations into a set of eight first-order ordinary differential equations. In the last section of Chapter 2, the descriptions and the mathematical models for three classical types of concentrated structural nonlinearities are presented.

Our first contribution concerns the prediction of the amplitude and frequency of the LCO in post-Hopf bifurcation for an aeroelastic system with a cubic hard spring and without any external forcing term. As reported in Lee et al.[49, 50], for a cubic hard spring, a supercritical Hopf-bifurcation is detected and the bifurcation parameter is the velocity with the linear flutter speed as the bifurcation value. For a self-excited system, Lee et al.[50] derived an amplitude-frequency relationship by using a slowly varying amplitude method. However, the prediction of the amplitude depends on the frequency of the LCO and for a self-excited system, there is no reference frequency. Several approximation methods have been tried for the prediction of the frequency, but the results were not satisfactory except in the region close to the Hopf point. Continuing their study to overcome this limitation, we apply the center manifold theory and the principle of normal form. Consequently, a frequency prediction formula for the self-excited system is derived. The numerical simulation has been carried out by using the fourth-order Runge-Kutta method, and an excellent agreement between the numerical result and the analytical prediction is achieved. The analysis and result are summarized in Liu et al.[56, 57] and Wong et al.[88]. Details of the center manifold technique and discussions of the results are presented in Chapter 3.

Our second contribution concerns the effects of freeplay nonlinearities. As discovered by McIntosh et al.[62], Yang and Zhao[93], Lee and Tron[45], Tang and Dowell[79], Price et al.[71] and Conner et al.[16], the limited amplitude flutter is strongly dependent on the initial conditions of the airfoil. The classical analytical technique, describing function or harmonic balance (Shen[75, 76], Breitbach[9, 10], Laurenson and Trn[43], Yang and Zhao[93], Hauenstein et al.[30], Tang and Dowell[79] and Price et al.[72]) does not permit a full exploration of this effect. The time marching integration (Lee and Desrochers[44], Yang and Zhao[93], Kousen and Bendiksen[40], and Price et al.[71, 72]) takes into account the initial conditions, but does not consider the importance of switching points. Some alternative integration schemes have been used by Lin and Cheng[55] and Conner et al.[16] to locate the switching point numerically. We develop, in Chapter 4, a technique which can be used to both locate the switching point analytically and take into account the initial conditions. Two procedures using the point transformation method are presented in section

§4.3 for the aeroelastic system with a freeplay model. The results and discussions are presented in section §4.4. This study has also been summarized in Liu et al.[58, 59] and Wong et al.[88].

Our third contribution is related to the effects of hysteresis nonlinearity on flutter analysis. In a hysteresis model, the location of switching points and the initial conditions are as important as they are in a freeplay model. Since the hysteresis nonlinearity can be represented by the superposition of two-freeplays, two procedures are also developed for this model by extending our work on the freeplay model. Details of this work are presented in Chapter 5 and are also summarized in Liu et al.[60].

While time integration methods have often been used to study the response of an aeroelastic system, the importance and necessity of analytical techniques are presented in Chapter 6 in which a detailed study of the numerical error resulting from the Runge-Kutta method are reported. For a cubic model, through some standard theoretical analysis, the numerical scheme is stable, and the numerical error can be controlled within a certain accuracy for sufficiently small time steps. For a freeplay model, however, the standard analysis cannot be used to prove the stability of the numerical scheme and the numerical error cannot be estimated analytically. Furthermore, the standard time-integration scheme cannot precisely locate the switching point. A detailed study of an example of a freeplay model shows some qualitative differences between the numerical results and the analytical results obtained by using the point transformation method. Details of this examination are also presented in Chapter 6 and have been summarized in Liu et al.[61]. This forms our fourth contribution.

Finally, some conclusions and remarks are made in Chapter 7. Explanations of the symbols used in this thesis are given in Appendix A. The main result of the center manifold theory related to our application in cubic model is outlined in Appendix B.

Chapter 2

Equations for Airfoils with Structural Nonlinearities and Subsonic Aerodynamics

2.1 Introduction

An instability mechanism known as flutter is one of the most interesting aeroelastic phenomena among the potential sources of instability and vibration problems for aircraft wings. From an analytic point of view, the mutual interaction of structural motion and aerodynamic forces may lead to energy extracted by the structure from the air-flow. Once this energy is greater than that which can be dissipated via various sources of damping, flutter, which typically involves a combined bending and torsional response of the wing, will occur.

The classical approach to this phenomenon assumes linear aerodynamics and structures which reduce the problem to a solution of a set of linear equations. Although the flutter boundaries are often well predicted, linear aerodynamics usually give insufficiently accurate results when airspeed increases to high subsonic or transonic Mach numbers. Also, effects associated with nonlinear structures may arise from worn hinges of control surfaces, loose control linkages, material behavior, and various other sources. Usually, these types of structural nonlinearities can be approximated by one of the three classical structural nonlinearities: cubic, freeplay and hysteresis.

In this thesis, a two-dimensional airfoil oscillating in pitch and plunge subjected to subsonic aerodynamics but with structural nonlinearities is investigated. Extending the analysis to a three dimensional model is straightforward, but the algebra is considerably more complex.

The formulation of the coupled equations for a two-dimensional airfoil motion is given in § 2.2. It turns out to be a system of integro-differential equations with two variables. In § 2.3, a reformulation of the original system of equations is performed, so that the rich theoretical result for systems of ordinary differential equations can be applied. Finally, three classical types of concentrated structural nonlinearities, which will be further investigated in the next three chapters, are introduced in § 2.4.

2.2 A Two-degree-of-freedom Airfoil Motion

For the physical model of a two-dimensional airfoil, we choose the two-degree-of-freedom airfoil motion oscillating in pitch and plunge, which has been employed by many authors. The symbols used in this model are given in Fig. 2.1. The pitch angle about the elastic axis is denoted by α, positive with the nose up; the plunge deflection is denoted by h, positive in the downward direction. The elastic axis is located at a distance $a_h b$ from the mid-chord, while the mass center is located at a distance $x_\alpha b$ from the elastic axis. Both distances are positive when measured towards the trailing edge of the airfoil.

The aeroelastic equations of motion for linear springs have been derived by Fung[23]. For nonlinear restoring forces with subsonic aerodynamics, the coupled equations for the airfoil in non-dimensional form can be written as follows:

$$\begin{aligned} \xi'' + x_\alpha \alpha'' + 2\zeta_\xi \frac{\bar{\omega}}{U^*}\xi' + (\frac{\bar{\omega}}{U^*})^2 G(\xi) &= -\frac{1}{\pi\mu}C_L(\tau) + \frac{P(\tau)b}{mU^2} \\ \frac{x_\alpha}{r_\alpha^2}\xi'' + \alpha'' + 2\zeta_\alpha \frac{1}{U^*}\alpha' + (\frac{1}{U^*})^2 M(\alpha) &= \frac{2}{\pi\mu r_\alpha^2}C_M(\tau) + \frac{Q(\tau)}{mU^2 r_\alpha^2} \end{aligned} \tag{2.1}$$

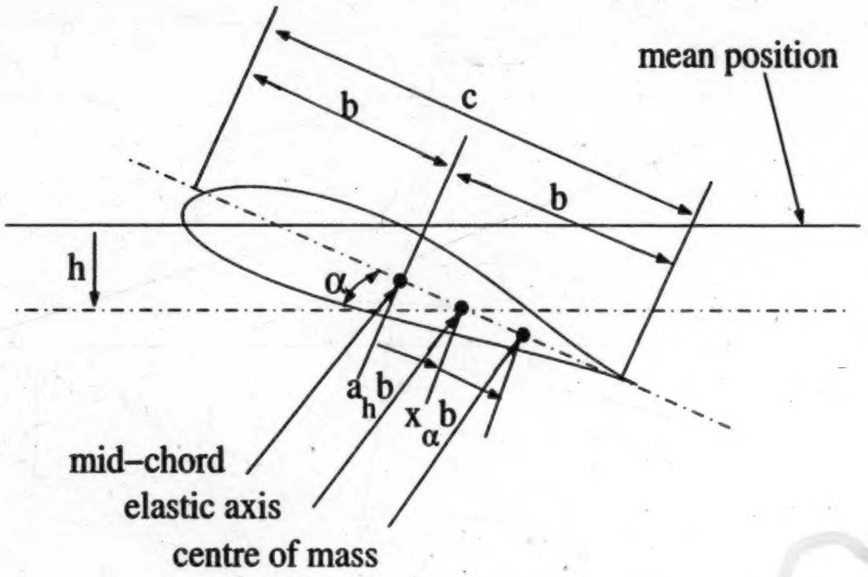

Figure 2.1: Two-degree-of-freedom airfoil motion

where $\xi = h/b$ is the non-dimensional displacement and the $'$ denotes differentiation with respect to the non-dimensional time τ defined as

$$\tau = \frac{Ut}{b}$$

U^* is a non-dimensional velocity defined as

$$U^* = \frac{U}{b\omega_\alpha}$$

and $\bar{\omega}$ is given by

$$\bar{\omega} = \frac{\omega_\xi}{\omega_\alpha}$$

where ω_ξ and ω_α are the natural frequencies of the uncoupled plunging and pitching modes respectively. ζ_ξ and ζ_α are the damping ratios, and r_α is the radius of gyration about the elastic axis. $G(\xi)$ and $M(\alpha)$ are the nonlinear plunge and pitch stiffness terms respectively. $P(\tau)$ and $Q(\tau)$ are the external applied force and moment, m is the airfoil mass per unit length and μ is the airfoil-air mass ratio. $C_L(\tau)$ and $C_M(\tau)$ are the lift and pitching moment coefficients respectively. For an incompressible flow, the expressions for $C_L(\tau)$

and $C_M(\tau)$ are given by[23]:

$$\begin{aligned}
C_L(\tau) =& \pi(\xi'' - a_h\alpha'' + \alpha') + 2\pi\{\alpha(0) + \xi'(0) + (\frac{1}{2} - a_h)\alpha'(0)\}\phi(\tau) \\
&+ 2\pi\int_0^\tau \phi(\tau-\sigma)(\alpha'(\sigma) + \xi''(\sigma) + (\frac{1}{2} - a_h)\alpha''(\sigma))d\sigma \\
C_M(\tau) =& \pi(\frac{1}{2} + a_h)\{\alpha(0) + \xi'(0) + (\frac{1}{2} - a_h)\alpha'(0)\}\phi(\tau) \\
&+ \pi(\frac{1}{2} + a_h)\int_0^\tau \phi(\tau-\sigma)\{\alpha'(\sigma) + \xi''(\sigma) + (\frac{1}{2} - a_h)\alpha''(\sigma)\}d\sigma \\
&+ \frac{\pi}{2}a_h(\xi'' - a_h\alpha'') - (\frac{1}{2} - a_h)\frac{\pi}{2}\alpha' - \frac{\pi}{16}\alpha''
\end{aligned} \tag{2.2}$$

where the Wagner function $\phi(\tau)$ is given by

$$\phi(\tau) = 1 - \psi_1 e^{-\varepsilon_1\tau} - \psi_2 e^{-\varepsilon_2\tau}$$

and the constants $\psi_1 = 0.165$, $\psi_2 = 0.335$, $\varepsilon_1 = 0.0455$, and $\varepsilon_2 = 0.3$ are obtained from Jones[39].

2.3 Model Reformulation

Due to the existence of the integral terms in (2.2), which turn the original system Eq.(2.1) into a system of integro-differential equations, it is difficult to study the dynamic behavior of the system analytically. In order to eliminate the integral terms, Lee et al.[46, 47] introduced four new variables:

$$w_1 = \int_0^\tau e^{-\varepsilon_1(\tau-\sigma)}\alpha(\sigma)d\sigma, \qquad w_2 = \int_0^\tau e^{-\varepsilon_2(\tau-\sigma)}\alpha(\sigma)d\sigma,$$

$$w_3 = \int_0^\tau e^{-\varepsilon_1(\tau-\sigma)}\xi(\sigma)d\sigma, \qquad w_4 = \int_0^\tau e^{-\varepsilon_2(\tau-\sigma)}\xi(\sigma)d\sigma.$$

Then, the system Eq.(2.1) can be rewritten in a general form containing only differential operators as:

$$
\begin{aligned}
&c_0\xi'' + c_1\alpha'' + (c_2 + 2\zeta_\xi \frac{\bar{\omega}}{U^*})\xi' + c_3\alpha' + c_4\xi \\
&\quad + c_5\alpha + c_6 w_1 + c_7 w_2 + c_8 w_3 + c_9 w_4 + (\frac{\bar{\omega}}{U^*})^2 G(\xi) = f(\tau) \\
&d_0\xi'' + d_1\alpha'' + d_2\xi' + (d_3 + 2\zeta_\alpha \frac{1}{U^*})\alpha' + d_4\xi \\
&\quad + d_5\alpha + d_6 w_1 + d_7 w_2 + d_8 w_3 + d_9 w_4 + (\frac{1}{U^*})^2 M(\alpha) = g(\tau)
\end{aligned}
\tag{2.1}
$$

The coefficients $c_0, c_1, ..., c_9, d_0, d_1, ..., d_9$ are given as follows:

$$
c_0 = 1 + \frac{1}{\mu}, \qquad c_1 = x_\alpha - \frac{a_h}{\mu}, \qquad c_2 = \frac{2}{\mu}(1 - \psi_1 - \psi_2),
$$

$$
c_3 = \frac{1}{\mu}(1 + (1 - 2a_h)(1 - \psi_1 - \psi_2)), \qquad c_4 = \frac{2}{\mu}(\epsilon_1\psi_1 + \epsilon_2\psi_2),
$$

$$
c_5 = \frac{2}{\mu}(1 - \psi_1 - \psi_2 + (\frac{1}{2} - a_h)(\epsilon_1\psi_1 + \epsilon_2\psi_2)), \qquad c_6 = \frac{2}{\mu}\epsilon_1\psi_1(1 - \epsilon_1(\frac{1}{2} - a_h)),
$$

$$
c_7 = \frac{2}{\mu}\epsilon_2\psi_2(1 - \epsilon_2(\frac{1}{2} - a_h)), \qquad c_8 = -\frac{2}{\mu}\epsilon_1^2\psi_1, \qquad c_9 = -\frac{2}{\mu}\epsilon_2^2\psi_2\ ,
$$

$$
d_0 = \frac{x_\alpha}{r_\alpha^2} - \frac{a_h}{\mu r_\alpha^2}, \qquad d_1 = 1 + \frac{1 + 8a_h^2}{8\mu r_\alpha^2}, \qquad d_2 = -\frac{1 + 2a_h}{\mu r_\alpha^2}(1 - \psi_1 - \psi_2),
$$

$$
d_3 = \frac{1 - 2a_h}{2\mu r_\alpha^2} - \frac{(1 + 2a_h)(1 - 2a_h)(1 - \psi_1 - \psi_2)}{2\mu r_\alpha^2}, \qquad d_4 = -\frac{1 + 2a_h}{\mu r_\alpha^2}(\epsilon_1\psi_1 + \epsilon_2\psi_2),
$$

$$
d_5 = -\frac{1 + 2a_h}{\mu r_\alpha^2}(1 - \psi_1 - \psi_2) - \frac{(1 + 2a_h)(1 - 2a_h)(\psi_1\epsilon_1 - \psi_2\epsilon_2)}{2\mu r_\alpha^2},
$$

$$
d_6 = -\frac{(1 + 2a_h)\psi_1\epsilon_1}{\mu r_\alpha^2}(1 - \epsilon_1(\frac{1}{2} - a_h)), \qquad d_7 = -\frac{(1 + 2a_h)\psi_2\epsilon_2}{\mu r_\alpha^2}(1 - \epsilon_2(\frac{1}{2} - a_h)),
$$

$$
d_8 = \frac{(1 + 2a_h)\psi_1\epsilon_1^2}{\mu r_\alpha^2}, \qquad d_9 = \frac{(1 + 2a_h)\psi_2\epsilon_2^2}{\mu r_\alpha^2}\ .
$$

$f(\tau)$ and $g(\tau)$ are functions depending on initial conditions, Wagner's function, and the forcing terms, namely,

$$
\begin{aligned}
f(\tau) =& \frac{2}{\mu}((\frac{1}{2} - a_h)\alpha(0) + \xi(0))(\psi_1\varepsilon_1 e^{-\varepsilon_1\tau} + \psi_2\varepsilon_2 e^{-\varepsilon_2\tau}) + \frac{P(\tau)b}{mU^2} , \\
g(\tau) =& -\frac{(1+2a_h)}{2r_\alpha^2} f(\tau) + \frac{Q(\tau)}{mU^2 r_\alpha^2} .
\end{aligned}
$$

By introducing a variable vector $X = (x_1, x_2, ..., x_8)^T$ with $x_1 = \alpha$, $x_2 = \alpha'$, $x_3 = \xi$, $x_4 = \xi'$, $x_5 = w_1$, $x_6 = w_2$, $x_7 = w_3$, and $x_8 = w_4$, the coupled equations given in Eq.(2.1) can be written as a set of eight first-order ordinary differential equations written in vector form:

$$
X' = f(X, \tau).
$$

This approach allows existing methods suitable for the study of ordinary differential equations to be used in the analysis. In this study, we assume that there is no external forcing, i.e. $Q(\tau) = P(\tau) = 0$ in Eq.(2.1). For large values of τ when transients are damped out and steady solutions are obtained, $f(\tau) = 0$ and $g(\tau) = 0$. Thus, the system can be expressed as $X' = f(X)$. In terms of vector components, Eq.(2.1) can be expressed as

$$
\begin{cases}
x_1' = x_2 \\
x_2' = a_{21}x_1 + (a_{22} - 2jc_0\zeta_\alpha \frac{1}{U^*})x_2 + a_{23}x_3 \\
\qquad +(a_{24} + 2jd_0\zeta_\xi \frac{\bar{\omega}}{U^*})x_4 + a_{25}x_5 + a_{26}x_6 + a_{27}x_7 \\
\qquad +a_{28}x_8 + j(d_0(\frac{\bar{\omega}}{U^*})^2 G(x_3) - c_0(\frac{1}{U^*})^2 M(x_1)) \\
x_3' = x_4 \\
x_4' = a_{41}x_1 + (a_{42} + 2jc_1\zeta_\alpha \frac{1}{U^*})x_2 + a_{43}x_3 \\
\qquad +(a_{44} - 2jd_1\zeta_\xi \frac{\bar{\omega}}{U^*})x_4 + a_{45}x_5 + a_{46}x_6 + a_{47}x_7 \\
\qquad +a_{48}x_8 + j(c_1(\frac{1}{U^*})^2 M(x_1) - d_1(\frac{\bar{\omega}}{U^*})^2 G(x_3)) \\
x_5' = x_1 - \varepsilon_1 x_5 \\
x_6' = x_1 - \varepsilon_2 x_6 \\
x_7' = x_3 - \varepsilon_1 x_7 \\
x_8' = x_3 - \varepsilon_2 x_8 .
\end{cases}
\tag{2.2}
$$

The expressions for j, a_{21}, ..., a_{28}, a_{41}, ..., a_{48} are given by

$$
\begin{array}{lll}
j = (c_0 d_1 - c_1 d_0)^{-1} \, , & a_{21} = j(-d_5 c_0 + c_5 d_0) \, , & a_{22} = j(-d_3 c_0 + c_3 d_0) \, , \\
a_{23} = j(-d_4 c_0 + c_4 d_0) \, , & a_{24} = j(-d_2 c_0 + c_2 d_0) \, ; & a_{25} = j(-d_6 c_0 + c_6 d_0) \, , \\
a_{26} = j(-d_7 c_0 + c_7 d_0) \, , & a_{27} = j(-d_8 c_0 + c_8 d_0) \, , & a_{28} = j(-d_9 c_0 + c_9 d_0) \, , \\
a_{41} = j(d_5 c_1 - c_5 d_1) \, , & a_{42} = j(d_3 c_1 - c_3 d_1) \, , & a_{43} = j(d_4 c_1 - c_4 d_1) \, , \\
a_{44} = j(d_2 c_1 - c_2 d_1) \, , & a_{45} = j(d_6 c_1 - c_6 d_1) \, , & a_{46} = j(d_7 c_1 - c_7 d_1) \, , \\
a_{47} = j(d_8 c_1 - c_8 d_1) \, , & a_{48} = j(d_9 c_1 - c_9 d_1) \, . &
\end{array}
$$

2.4 Structural Nonlinearities

In this thesis, we consider only concentrated nonlinearities, which can be classified roughly into three types: cubic spring, freeplay and hysteresis. The structural nonlinearities are represented by the nonlinear functions $G(x_3)$ and $M(x_1)$ in system Eq.(2.2).

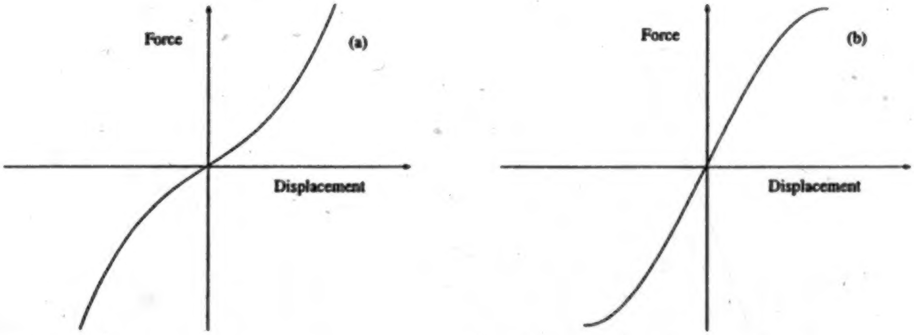

Figure 2.2: General sketch of a cubic spring: (a). cubic hard spring; (b). cubic soft spring.

2.4.1 Cubic Springs

A thin wing or propeller blade which is being twisted will most likely behave as a cubic spring. Depending on the temperature and initial conditions, the nonlinearity can be a hard or soft spring type. Sketches for both types of cubic nonlinearities are shown in Fig. 2.2. For a cubic spring, $M(x_1)$ is given by

$$M(x_1) = \beta_\alpha x_1 + \beta_{\alpha^3} x_1^3 \,, \tag{2.1}$$

where β_α and β_{α^3} are constants. When $\beta_{\alpha^3} > 0$, $M(x_1)$ represents a cubic hard spring as shown in Fig. 2.2(a), while it represents a cubic soft spring (Fig. 2.2(b)) when $\beta_{\alpha^3} < 0$.

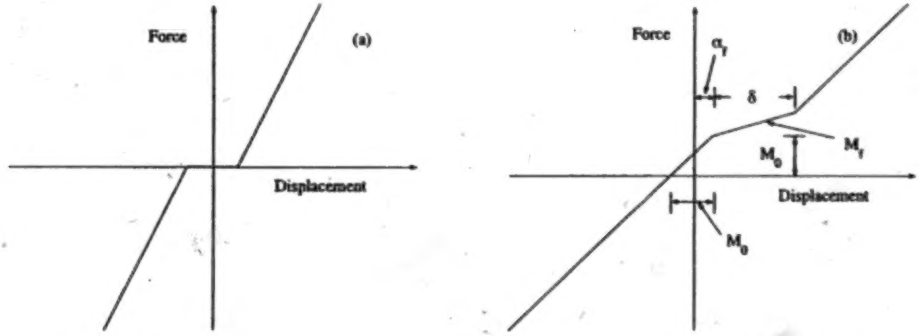

Figure 2.3: General sketch of a freeplay spring: (a). without any preload; (b). with a preload.

2.4.2 Freeplay Springs

If the main cause of nonlinearity is backlash in loose or worn control surface hinges, such as in power-operated control systems and spring-tab systems, the nonlinearity exhibits a freeplay with or without preload characteristic as shown in Fig. 2.3. For a freeplay model, $M(x_1)$ is given by

$$M(x_1) = \begin{cases} M_0 + x_1 - \alpha_f & x_1 < \alpha_f \\ M_0 + M_f(x_1 - \alpha_f) & \alpha_f \le x_1 \le \alpha_f + \delta \\ M_0 + x_1 - \alpha_f + \delta(M_f - 1) & x_1 > \alpha_f + \delta \end{cases} \tag{2.2}$$

where the preload M_0, the freeplay δ, the beginning of the freeplay α_f, and M_f are constants.

2.4.3 Hysteresis Nonlinearities

If both friction and backlash have to be considered, for example, for sweepable wings and sweepable wing-mounted stores such as on the F-111 aircraft, we

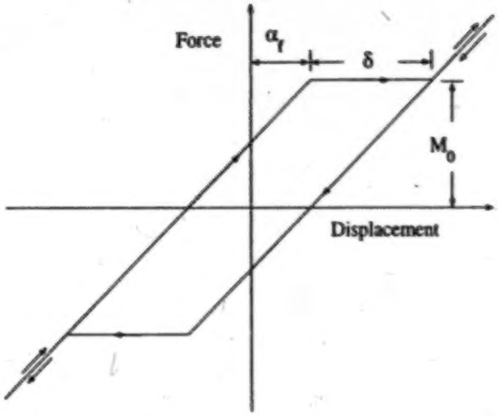

Figure 2.4: General sketch of a hysteresis spring.

have a hysteresis nonlinearity as shown in Fig. 2.4. In the mathematical model, for a hysteresis nonlinearity, $M(x_1)$ is given by

$$M(x_1) = \begin{cases} x_1 - \alpha_f + M_0 & x_1 < \alpha_f \uparrow \\ x_1 + \alpha_f - M_0 & x_1 > -\alpha_f \downarrow \\ M_0 & \alpha_f \le x_1 \le \alpha_f + \delta \uparrow \\ -M_0 & -\alpha_f - \delta \le x_1 \le -\alpha_f \downarrow \\ x_1 - \alpha_f - \delta + M_0 & x_1 > \alpha_f + \delta \uparrow \\ x_1 + \alpha_f + \delta - M_0 & x_1 < -\alpha_f - \delta \downarrow \end{cases} \tag{2.3}$$

where ↑ or ↓ denotes that the motion is increasing or decreasing in the x_1-direction. The preload M_0, the beginning of the freeplay α_f, and the freeplay δ are constants.

Here, we give the expressions for $M(x_1)$ in the pitch degree-of-freedom. Similar expressions for $G(x_3)$ in the plunge motion can be written by replacing x_1 with x_3.

The principal interest for the aeroelastician is the amplitude and frequency of the limit cycle oscillations. The next three chapters, Chapters 3, 4 and 5, include the details of the mathematical analysis to predict the amplitude and frequency of LCOs for the above three types of structural nonlinearities.

Chapter 3

Cubic Springs

3.1 Introduction

In this chapter, we concentrate on the LCOs of a 2-DOF aeroelastic system with structural nonlinearity represented by the following cubic hard spring forces:

$$M(x_1) = \beta_\alpha x_1 + \beta_{\alpha^3} x_1^3, \quad G(x_3) = \beta_\xi x_3 + \beta_{\xi^3} x_3^3. \tag{3.1}$$

When the system is subject to an external forcing term with a driving frequency ω, Lee et al.[46] derived analytical formulas that provide amplitude-frequency relationships for the pitch and plunge motion respectively. However, for a self-excited system (i.e. in the absence of external forcing term), the reference frequency ω is not known, and thus the motion cannot be determined from the amplitude-frequency relationships they derived. In [46], the frequency ω of the motion for the self-excited system was approximated by the linear frequency at the Hopf point $U^*/U_L^* = 1$, by the local frequency at a given U^*/U_L^* or by the frequency from the Jacobian matrix, but the results are not satisfactory except when the velocity U^* is very close to the linear flutter speed U_L^*. To overcome this limitation, we apply the center manifold theory of Carr[12] and the principle of normal form[85] to derive a frequency relation for the self-excited motion of a two DOF nonlinear system. Using the frequency relation together with the amplitude-frequency relationships, LCOs for the self-excited system can be predicted analytically. Numerical simulations are carried out to compare the results with those obtained from the analytical predictions.

A general procedure is discussed in § 3.2 and § 3.3 to derive the reduced system on the center manifold and the normal form for the aeroelastic system respectively. In § 3.4, the result of the amplitude-frequency relationships for the aeroelastic system is presented. The simulations for several test examples are then discussed in § 3.5, showing that the analytical prediction is in excellent agreement with the numerical result. Finally, some concluding remarks are presented in § 3.6.

3.2 The Reduced System on A Center Manifold

Following the analysis presented by Lee et al.[46], the bifurcation parameter is associated with U^*, and the bifurcation value is U_L^*, which is the value of the linear flutter speed. To study the dynamic response of the system, we introduce a perturbation parameter δ such that

$$\frac{1}{U^*} = \frac{1}{U_L^*}(1-\delta).$$

When this expression is substituted into Eq.(2.2), an autonomous system with the perturbation parameter is obtained, i.e, $X' = f(X,\delta)$. The equilibrium points are then evaluated from $f(X,\delta) = 0$. Without loss of generality, we assume the origin to be the equilibrium point. The original system Eq.(2.2) can now be rewritten as:

$$\begin{cases} X' = A \cdot X + B(\delta) \cdot X + (1-\delta)^2 F(X) \\ \delta' = 0 \end{cases} \tag{3.1}$$

The matrix A is an 8×8 Jacobian matrix evaluated at the equilibrium point and at the bifurcation value $\delta = 0$. The second and the third terms of equation Eq.(3.1) are nonlinear in X and δ. The expressions for A, $B(\delta)$ and F are given as follows:

$$A = \begin{pmatrix} A_{11} & A_{12} \\ A_{21} & A_{22} \end{pmatrix}, \qquad B = \begin{pmatrix} B_{11} & A_{21} \\ A_{21} & A_{21} \end{pmatrix},$$

with

$$A_{11} = \begin{pmatrix} 1 & 0 & 0 & 0 \\ a_{21} - b_{21} & a_{22} - b22 & a_{23} + b_{23} & a_{24} + b_{24} \\ 0 & 0 & 0 & 1 \\ a_{41} + b_{41} & a_{42} + b_{42} & a_{43} - b_{43} & a_{44} - b_{44} \end{pmatrix}, \; A_{21} = \begin{pmatrix} 0 & 0 & 0 & 0 \\ 0 & 0 & 0 & 0 \\ 0 & 0 & 0 & 0 \\ 0 & 0 & 0 & 0 \end{pmatrix},$$

$$A_{12} = \begin{pmatrix} 0 & 0 & 0 & 0 \\ a_{25} & a_{26} & a_{27} & a_{28} \\ 0 & 0 & 0 & 0 \\ a_{45} & a_{46} & a_{47} & a_{48} \end{pmatrix}, \qquad A_{22} = \begin{pmatrix} -\epsilon_1 & 0 & 0 & 0 \\ 0 & -\epsilon_2 & 0 & 0 \\ 0 & 0 & -\epsilon_1 & 0 \\ 0 & 0 & 0 & -\epsilon_2 \end{pmatrix},$$

$$B_{11} = \begin{pmatrix} 0 & 0 & 0 & 0 \\ -b_{21}(\delta^2 - 2\delta) & b_{22}\delta & b_{23}(\delta^2 - 2\delta) & -b_{24}\delta \\ 0 & 0 & 0 & 0 \\ b_{41}(\delta^2 - 2\delta) & -b_{22}\delta & -b_{43}(\delta^2 - 2\delta) & b_{44}\delta \end{pmatrix}, \qquad F = \begin{pmatrix} F_1 \\ F_2 \end{pmatrix},$$

and

$$F_1 = \begin{pmatrix} 0 \\ -b_{21}\frac{\beta_{\alpha^3}}{\beta_\alpha}x_1^3 + b_{23}\frac{\beta_{\xi^3}}{\beta_\xi}x_3^3 \\ 0 \\ b_{41}\frac{\beta_{\alpha^3}}{\beta_\alpha}x_1^3 - b_{43}\frac{\beta_{\xi^3}}{\beta_\xi}x_3^3 \end{pmatrix}, \qquad F_2 = \begin{pmatrix} 0 \\ 0 \\ 0 \\ 0 \end{pmatrix}.$$

Here, $a_{21}, a_{22}, \ldots,$ and a_{48} are identical to those presented in Chapter 2 following the aeroelastic system Eq.(2.2), and the $b_{21}, b_{22}, \ldots,$ and b_{44} are given as follows:

$$b_{21} = jc_0\left(\frac{1}{U_L^*}\right)^2\beta_\alpha, \quad b_{22} = jc_0\left(\frac{1}{U_L^*}\right)^2\zeta_\alpha, \quad b_{23} = jd_0\left(\frac{\bar{\omega}}{U_L^*}\right)^2\beta_\xi, \quad b_{24} = jd_0\left(\frac{\bar{\omega}}{U_L^*}\right)^2\zeta_\xi,$$

$$b_{41} = jc_1\left(\frac{1}{U_L^*}\right)^2\beta_\alpha, \quad b_{42} = jc_1\left(\frac{1}{U_L^*}\right)^2\zeta_\alpha, \quad b_{43} = jd_1\left(\frac{\bar{\omega}}{U_L^*}\right)^2\beta_\xi, \quad b_{44} = jd_1\left(\frac{\bar{\omega}}{U_L^*}\right)^2\zeta_\xi.$$

The matrix A has one pair of purely imaginary eigenvalues $\lambda_1 = i\omega_0$, $\bar{\lambda}_1 = -i\omega_0$, one pair of complex eigenvalues with negative real parts, $\lambda_2 = b+ic$, $\bar{\lambda}_2 = b - ic$, and four negative real eigenvalues λ_3, λ_4, λ_5, λ_6. From the center manifold theory, it is possible to reduce the dimensionality of the system. To obtain the center manifold, we first transform system Eq.(3.1) to a standard form. A transformation matrix P is obtained from the eigenvectors of A, such that $P^{-1} \cdot A \cdot P = J$, where J is the Jordan canonical form of A containing all the eigenvalues of A:

$$J = \begin{pmatrix} 0 & \omega_0 & 0 & 0 & 0 & 0 & 0 & 0 \\ -\omega_0 & 0 & 0 & 0 & 0 & 0 & 0 & 0 \\ 0 & 0 & b & c & 0 & 0 & 0 & 0 \\ 0 & 0 & -c & b & 0 & 0 & 0 & 0 \\ 0 & 0 & 0 & 0 & \lambda_3 & 0 & 0 & 0 \\ 0 & 0 & 0 & 0 & 0 & \lambda_4 & 0 & 0 \\ 0 & 0 & 0 & 0 & 0 & 0 & \lambda_5 & 0 \\ 0 & 0 & 0 & 0 & 0 & 0 & 0 & \lambda_6 \end{pmatrix}.$$

Introducing a new variable, $Y = P^{-1} \cdot X = (y_1, y_2, \ldots, y_8)^T$, system Eq.(3.1) becomes:

$$\begin{cases} Y' = J \cdot Y - P^{-1} \cdot B(\delta) \cdot P \cdot Y + (1-\delta)^2 P^{-1} \cdot F(P \cdot Y) \\ \delta' = 0 \end{cases} \tag{3.2}$$

The dynamic response of system Eq.(3.2), which is nine-dimensional, can be investigated through an invariant two-dimensional system. Defining

$$J_A = \begin{pmatrix} 0 & \omega_0 & 0 \\ -\omega_0 & 0 & 0 \\ 0 & 0 & 0 \end{pmatrix},$$

$$J_B = \begin{pmatrix} b & c & 0 & 0 & 0 & 0 \\ -c & b & 0 & 0 & 0 & 0 \\ 0 & 0 & \lambda_3 & 0 & 0 & 0 \\ 0 & 0 & 0 & \lambda_4 & 0 & 0 \\ 0 & 0 & 0 & 0 & \lambda_5 & 0 \\ 0 & 0 & 0 & 0 & 0 & \lambda_6 \end{pmatrix},$$

$Y_A = (y_1, y_2, \delta)^T$, $Y_B = (y_3, y_4, y_5, y_6, y_7, y_8)^T$, system Eq.(3.2) can be rewritten as

$$\begin{cases} Y_A' = J_A \cdot Y_A + F_A(Y_A, Y_B) \\ Y_B' = J_B \cdot Y_B + F_B(Y_A, Y_B) \end{cases} \tag{3.3}$$

where F_A and F_B are nonlinear functions of Y_A and Y_B. Here, we start from the second order terms since the first order terms have already been included in the first part associated with Y_A and Y_B. J_A has one pair of purely imaginary eigenvalues and one zero eigenvalue. All eigenvalues of J_B have negative real parts. From the center manifold theorem given by Carr[12], a center manifold H exists for Eq.(3.3), i.e. $Y_B = H(Y_A)$ such that the flow of Eq.(3.3) near the equilibrium point is governed by $Y_A' = J_A \cdot Y_A + F_A(Y_A, H(Y_A))$, which is a 3-dimensional system. Theoretically, the function H can be solved from the following functional equation

$$\frac{\partial}{\partial Y_A} H(Y_A)(J_A \cdot Y_A + F_A(Y_A, H(Y_A))) = J_B \cdot H(Y_A) + F_B(Y_A, H(Y_A)) \ . \quad (3.4)$$

However, the solution for the above equation with the exact expression of the function H is as difficult to obtain as the solution for the original system. Following another important result given by Carr[12], the center manifold H can be approximated to any desired degree of accuracy. The polynomial approximation of the center manifold H is assumed, and is denoted by $\Phi = (\phi_3, \phi_4, \phi_5, \phi_6, \phi_7, \phi_8)^T$, in which:

$$\phi_i(y_1, y_2, \delta) = h_{i1} y_1 \delta + h_{i2} y_2 \delta + h_{i3} y_1^2 + h_{i4} y_2^2 + h_{i5} \delta^2 + h_{i6} y_1 y_2 \quad (3.5)$$

$$i = 3, 4, 5, 6, 7, 8$$

where h_{31}, h_{32}, ..., h_{36}, h_{41}, ..., ..., and h_{86} are constants to be determined from using the center manifold theory. Substituting (3.5) into Eq.(3.4) and replacing $H(Y_A)$ by its polynomial approximation $\Phi(Y_A)$, we obtain

$$\frac{\partial}{\partial Y_A} \Phi(Y_A) \cdot (J_A Y_A + F_A(Y_A, \Phi(Y_A)) = J_B \cdot \Phi(Y_A) + F_B(Y_A, \Phi(Y_A)) \ .$$

Equating the coefficients associated with $y_1\delta$, $y_2\delta$, y_1^2, y_2^2, δ^2, and $y_1 y_2$, we obtain a system of 36 algebraic equations with h_{31}, h_{32}, ..., and h_{86} as variables. These equations can be solved by a standard computer program such as Maple[35] and Mathematica[86]. Extension to a higher order approximation of center manifold is straightforward, but the algebra becomes considerably more complex.

3.3 The Principle of Normal Form

Once the expression of the center manifold is obtained, the original system is reduced to a three dimensional system on the center manifold. Since the solution of the reduced system is not exactly identical to Y_A, we denote the corresponding solutions for y_1 and y_2 by u_1 and u_2 respectively. Regarding δ as a parameter, the system is reduced to two dimensions:

$$\begin{cases} u_1' = \omega_0 u_2 + g_1(u_1, u_2, \delta) \\ u_2' = -\omega_0 u_1 + g_2(u_1, u_2, \delta) \end{cases} \tag{3.1}$$

where g_1 and g_2 contain the nonlinear terms as functions of u_1, u_2 and δ. An important result in the application of the center manifold theorem is that the asymptotic behavior of the solutions near the equilibrium point and the bifurcation value of the original eight dimensional system can be studied by analyzing the reduced two dimensional system given in Eq.(3.1).

To simplify Eq.(3.1) for symbolic computations, we rewrite the system as:

$$U' = B \cdot U + F(U) \tag{3.2}$$

with

$$B = \begin{pmatrix} b_{11}(\delta) & b_{12}(\delta) \\ b_{21}(\delta) & b_{22}(\delta) \end{pmatrix}, \qquad F(U) = \begin{pmatrix} f_1(u_1, u_2, \delta) \\ f_2(u_1, u_2, \delta) \end{pmatrix},$$

where $U = (u_1, u_2)^T$. The first term $B \cdot U$ is the linear part for u_1, u_2, and the second term $F(U)$ is the nonlinear part for u_1, u_2.

Now the transformation matrices are defined as:

$$NP = \frac{1}{\sqrt{b_{12}^2 + \theta^2 + (\alpha - b_{11})^2}} \begin{pmatrix} 0 & b_{12} \\ \theta & \alpha - b_{11} \end{pmatrix}$$

and

$$NP^{-1} = \frac{\sqrt{b_{12} + \theta^2 + (\alpha - b_{11})^2}}{b_{12}\theta} \begin{pmatrix} -\alpha + b_{11} & b_{12} \\ \theta & 0 \end{pmatrix}$$

where $\alpha = \frac{1}{2}(b_{11} + b_{12})$ and $\theta = \sqrt{b_{11}b_{22} - b_{12}b_{21} - \alpha^2}$. By introducing a new variable vector $Y = NP^{-1} \cdot U = (y_1, y_2)^T$, we transform system Eq.(3.2) into the standard form:

$$Y' = J \cdot Y + NP^{-1} \cdot F(NP \cdot Y) \quad \text{with} \quad J = \begin{pmatrix} \alpha & \theta \\ -\theta & \alpha \end{pmatrix}$$

i.e.

$$\begin{cases} y_1' = \alpha y_1 + \theta y_2 + F_1(y_1, y_2, \delta) \\ y_2' = -\theta y_1 + \alpha y_2 + F_2(y_1, y_2, \delta) \end{cases} \tag{3.3}$$

where F_1 and F_2 are nonlinear terms of y_1 and y_2 , and α and θ are related to the parameter δ.

The complex form of system Eq.(3.3) can be written as:

$$Z' = \lambda Z + h(Z, \bar{Z}),$$

where $\lambda(\delta) = \alpha(\delta) + i\theta(\delta)$, and $Z = y_1 + iy_2$. $h(Z, \bar{Z})$ includes nonlinearities of Z and $\bar{Z}$.

By the principle of normal form, the near identity transformation is introduced:

$$Z = V + g(V, \bar{V})$$

where V is a new variable and g includes the second and third order nonlinearities of V and $\bar{V}$. The normal form of the system Eq.(3.3) can be expressed as:

$$V' = \lambda V + F_{21} V^2 \bar{V}$$

where F_{21} is a complex number whose value is related to δ.

Taking $a(\delta) = Re(F_{21})$ and $b(\delta) = Im(F_{21})$, we express $V = r(\tau) * e^{i\omega(\tau)}$. The normal form in polar coordinates can be expressed as:

$$\begin{cases} r' = \alpha r + ar^3 \\ \omega' = \theta + br^2 \end{cases} \tag{3.4}$$

After the coefficients α, θ, a and b are Taylor expanded at $\delta = 0$, the above system becomes:

$$\begin{cases} r' = \dot{\alpha}(0)\delta r + a(0)r^3 = r(\dot{\alpha}(0)\delta + a(0)r^2) \\ \omega' = \theta(0) + \dot{\theta}(0)\delta + b(0)r^2 = (\theta(0) + \dot{\theta}(0)\delta) + b(0)r^2 \end{cases} \tag{3.5}$$

Note that the prime denotes derivatives with respect to τ and the dot denotes derivatives with respect to δ. The stability of the fixed point and the periodic orbit can now be analyzed. Furthermore, the frequency of the limit cycle oscillations can be predicted from a frequency relation given by:

$$\omega = \omega_0 + (\dot{\theta}(0) - \frac{b(0)\dot{a}(0)}{a(0)})\delta \, . \tag{3.6}$$

The amplitude of the motion of the original system can also be predicted from the reduced system on the center manifold. However, due to errors introduced in approximating the center manifold, the predicted amplitude value may not be sufficiently accurate.

3.4 Amplitudes of Limit Cycle Oscillations

To determine the amplitudes of limit cycle oscillations associated with the pitch and plunge motions, we assume

$$\begin{cases} \xi(\tau) = a_1(\tau)cos(\omega\tau) + b_1(\tau)sin(\omega\tau), \\ \alpha(\tau) = a_2(\tau)cos(\omega\tau) + b_2(\tau)sin(\omega\tau), \\ w_i(\tau) = a_{i+2}(\tau)cos(\omega\tau) + b_{i+2}sin(\omega\tau), \quad i = 1, 2, 3, 4 \end{cases} \tag{3.1}$$

where $a_i(\tau)$ and $b_i(\tau)$, $i = 1, 2, \cdots, 6$ are slowly varying functions of τ, and ω is the angular frequency of the LCO. Let r and R denote the amplitude of ξ and α respectively, where $r = \sqrt{a_1^2 + b_1^2}$ and $R = \sqrt{a_2^2 + b_2^2}$.

Substituting Eq.(3.1) into Eq.(2.2) and matching the coefficients of $cos(\omega\tau)$ and $sin(\omega\tau)$ leads to a system of 12 first-order nonlinear differential equations in a_i and b_i, $i = 1, 2, \cdots, 6$. After considerable algebraic manipulations, the following amplitude equations are obtained:

$$\begin{cases} A = & \frac{(n_1^2 + s_1^2)}{m_1^2 + (p_1 + q_1 r^2)^2} \\ r^2 = & AR^2 \\ R^2 = & \frac{1}{q_2}(-s_2 \pm \sqrt{(p_2^2 + m_2^2)A - n_2^2}) \end{cases} \tag{3.2}$$

where m_1, n_1, $\cdots$ are functions of the system parameters and the frequency ω. The expressions of m_1, n_1, $\cdots$ in terms of system parameters and the frequency ω are given as follows:

$$
\begin{aligned}
m_1 =&(c_2 + 2\zeta_\xi \frac{\bar{\omega}}{U^*})\omega - \frac{c_8\omega}{\epsilon_1^2+\omega^2} - \frac{c_9\omega}{\epsilon_2^2+\omega^2} & n_1 &= c_3\omega - \frac{c_6\omega}{\epsilon_1^2+\omega^2} - \frac{c_7\omega}{\epsilon_2^2+\omega^2} \\
p_1 =&\frac{c_8\epsilon_1}{\epsilon_1^2+\omega^2} + \frac{c_9\epsilon_2}{\epsilon_2^2+\omega^2} + c_4 + \beta_\xi(\frac{\bar{\omega}}{U^*})^2 - c_0\omega^2 & q_1 &= \frac{3}{4}\beta_{\xi^3}(\frac{\bar{\omega}}{U^*})^2 \\
s_1 =&c_5 - c_1\omega^2 + \frac{c_6\epsilon_1}{\epsilon_1^2+\omega^2} + \frac{c_7\epsilon_2}{\epsilon_2^2+\omega^2} & p_2 &= \frac{c_8\epsilon_1}{\epsilon_1^2+\omega^2} + \frac{d_9\epsilon_2}{\epsilon_2^2+\omega^2} + d_4 - d_0\omega^2 \\
n_2 =&(d_3 + 2\zeta_\alpha \frac{1}{U^*})\omega - \frac{d_6\omega}{\epsilon_1^2+\omega^2} - \frac{d_7\omega}{\epsilon_2^2+\omega^2} & m_2 &= d_2\omega - \frac{d_8\omega}{\epsilon_1^2+\omega^2} - \frac{d_9\omega}{\epsilon_2^2+\omega^2} \\
q_2 =&\frac{3}{4}\beta_{\alpha^3}(\frac{1}{U^*})^2 & s_2 &= d_5 + \beta_\alpha(\frac{1}{U^*})^2 - d_1\omega^2 + \frac{d_6\epsilon_1}{\epsilon_1^2+\omega^2} + \frac{d_7\epsilon_2}{\epsilon_2^2+\omega^2}
\end{aligned}
$$

The detailed derivation can be found in Lee et al.[46]. Now, using the amplitude-frequency relationships given in (3.2) and the frequency relation (3.6) derived in the previous section, the solutions of limit cycle oscillations can be predicted analytically.

3.5 Case Studies and Discussion

In order to demonstrate the accuracy of the analytical formulas given in (3.6) and (3.2) in predicting the frequency and amplitude of LCOs, we consider the following examples in which the aeroelastic system given in Eq.(2.1) contains cubic restoring forces. In all cases, analytical prediction are compared with solutions obtained numerically using a fourth-order Runge-Kutta time-integration scheme applied to system Eq.(2.2).

The following parameters:

$$\mu = 100, \quad a_h = -1/2, \quad x_\alpha = 1/4, \quad \zeta_\xi = \zeta_\alpha = 0, \quad r_\alpha = 0.5\ , \qquad (3.1)$$

are used in all case studies. These system parameters are chosen from [71]. The procedure discussed in the previous section does not depend on the choice of the parameters. The nonlinear restoring forces $M(\alpha)$ and $G(\xi)$ are defined in (3.1). Now, by varying the value of $\bar{\omega}$ and the coefficients β_α, β_{α^3}, β_ξ, β_{ξ^3}, we consider the following four cases shown in Table 3.1.

Case	β_α	β_{α^3}	β_ξ	β_{ξ^3}
1	1	3	1	0
2	1	4	1	1
3	1	40	1	0.1
4	0.1	40	1	0

Table 3.1: Case studies for the aeroelastic system Eq.(2.2) with cubic springs

For Cases 1 and 4, structural nonlinearity is applied only in the pitch degree of freedom. In Cases 2 and 3, cubic restoring forces are applied in both the pitch and plunge degrees of freedom.

In Case 1, for $\bar{\omega} = 0.2$, the approximate center manifold is given by:

$$\begin{cases} \phi_3 = -2.278662600 y_1 \delta - 2.932984813 y_2 \delta \\ \phi_4 = 5.389063673 y_1 \delta - 3.395569702 y_2 \delta \\ \phi_5 = -2.576198739 y_1 \delta + 0.5470484684 y_2 \delta \\ \phi_6 = -0.03759292923 y_1 \delta + 0.05243761634 y_2 \delta \\ \phi_7 = 0.01137223245 y_1 \delta - 0.01813461435 y_2 \delta \\ \phi_8 = -7.328109745 y_1 \delta + 0.4092693894 y_2 \delta \end{cases} \tag{3.2}$$

Substituting $y_3 = \phi_3$, $y_4 = \phi_4$, $y_5 = \phi_5$, $y_6 = \phi_6$, $y_7 = \phi_7$, $y_8 = \phi_8$ into the first equation of Eq.(3.3), a governing system of equations for y_1 and y_2 is obtained. Note that by replacing y_i using the above expressions given in ϕ_i, for $i = 3, 4, 5, 6, 7, 8$, the solution for system Eq.(3.3) can be approximated by explicit functions in terms of y_1, y_2 and δ. However, y_1 and y_2 are no longer exactly identical to those defined in the original system Eq.(3.2); hence, we denote y_1 and y_2 by u_1 and u_2. Therefore,

$$\begin{cases} u_1' = -.08404421373u_2 - .005002186045\delta u_1 + .02298015261\delta u_2 \\ \qquad +.000001060912229u_1^3 - .00001078496711u_1^2u_2 + .07708383842\delta^2 u_1 \\ \qquad +.00003654575512u_1u_2^2 - .00004127944026u_2^3 - .06508466062\delta^2 u_2 \\ u_2' = .08404421392u_1 - .1034553702\delta u_1 + .3210345363\delta u_2 \\ \qquad +.00002847473453u_1^3 - .0002894669955u_1^2u_2 + .3223789845\delta^2 u_1 \\ \qquad +.0009808829109u_1u_2^2 - .001107934352u_2^3 - 1.281473950\delta^2 u_2 \end{cases} \tag{3.3}$$

Transforming this reduced system into a standard form and rewriting the standard form in complex form, we obtain the normal form after introducing the near identity transformation. After the Taylor expansions are applied to the coefficients of the normal form expressions in polar coordinates, the coefficients in Eq.(3.5) are given by:

$$\begin{cases} \omega(0) = \omega_0 = 0.08404421382 \\ \dot{\omega}(0) = -0.06321776140 \\ \dot{\alpha}(0) = 0.1580161751 \\ a(0) = -0.0002233463476 \\ b(0) = 0.00007505815011 \end{cases} \tag{3.4}$$

By analyzing system Eq.(3.5) with these results, we can verify that when $\delta < 0$, the equilibrium point is asymptotically stable, which means that for $U^* < U_L^*$ all motions will decay to zero amplitude. For $\delta > 0$, the equilibrium point becomes unstable. However, there is a stable periodic orbit with a frequency $\omega = 0.0840 - 0.0101\delta$ when $\bar{\omega} = 0.2$.

For different values of $\bar{\omega}$, and using the same procedure, we derived the corresponding frequency relation which depends on the bifurcation parameter δ (or the ratio $\gamma = U^*/U_L^*$) as shown in Table 3.2.

Numerical simulations using the Runge-Kutta scheme were carried out to compare their results with those obtained from the analytical predictions. Fig.3.1 displays the frequency and the amplitudes for pitch and plunge motions

$\bar{\omega}$	$\omega = \omega(\delta)$	$\omega = \omega(\gamma)$	U_L^*
0.2	$0.0840 - 0.0101 * \delta$	$0.0739 + 0.0101/\gamma^2$	6.28509
0.4	$0.1192 - 0.0333 * \delta$	$0.0859 + 0.0333/\gamma^2$	5.23376
0.6	$0.1730 - 0.0616 * \delta$	$0.1114 + 0.0616/\gamma^2$	4.40100
0.8	$0.2244 - 0.0823 * \delta$	$0.1421 + 0.0823/\gamma^2$	4.11454
1.0	$0.2522 - 0.0702 * \delta$	$0.1820 + 0.0702/\gamma^2$	4.33559

Table 3.2: The frequency relationship with the bifurcation parameter $\gamma = U^*/U_L^*$ for Case 1.

$\bar{\omega}$	$\omega = \omega(\delta)$	$\omega = \omega(\gamma)$	U_L^*
0.2	$0.0840 + 0.0082 * \delta$	$0.0922 - 0.0082/\gamma^2$	6.28509
0.4	$0.1192 - 0.0158 * \delta$	$0.1034 + 0.0158/\gamma^2$	5.23376
0.6	$0.1730 - 0.0554 * \delta$	$0.1176 + 0.0554/\gamma^2$	4.40100
0.8	$0.2244 - 0.0812 * \delta$	$0.1432 + 0.0812/\gamma^2$	4.11454
1.0	$0.2522 - 0.0683 * \delta$	$0.1839 + 0.0683/\gamma^2$	4.33559

Table 3.3: The frequency relationship with the bifurcation parameter $\gamma = U^*/U_L^*$ for Case 2.

that are predicted using the analytical formulas (3.6) and (3.2) with $\bar{\omega}$=0.2. This figure shows that excellent agreement in both frequencies and amplitudes of the limit cycle oscillations is obtained.

In Case 2, we consider an aeroelastic system with cubic structural nonlinearities in both pitch and plunge degrees of freedom.

For different $\bar{\omega}$'s, with the corresponding bifurcation value U_L^*, the frequency relations with the bifurcation parameter $\delta = 1 - (U_L^*/U^*)^2$ are shown in Table 3.3.

Furthermore, in Fig. 3.2, we display the frequencies and the amplitudes for pitch motions that are predicted using the analytical formulas (3.6) and (3.2) when $\bar{\omega}$=0.2. These results are compared with those from the numerical simulations, and it is shown that excellent agreement in both frequency

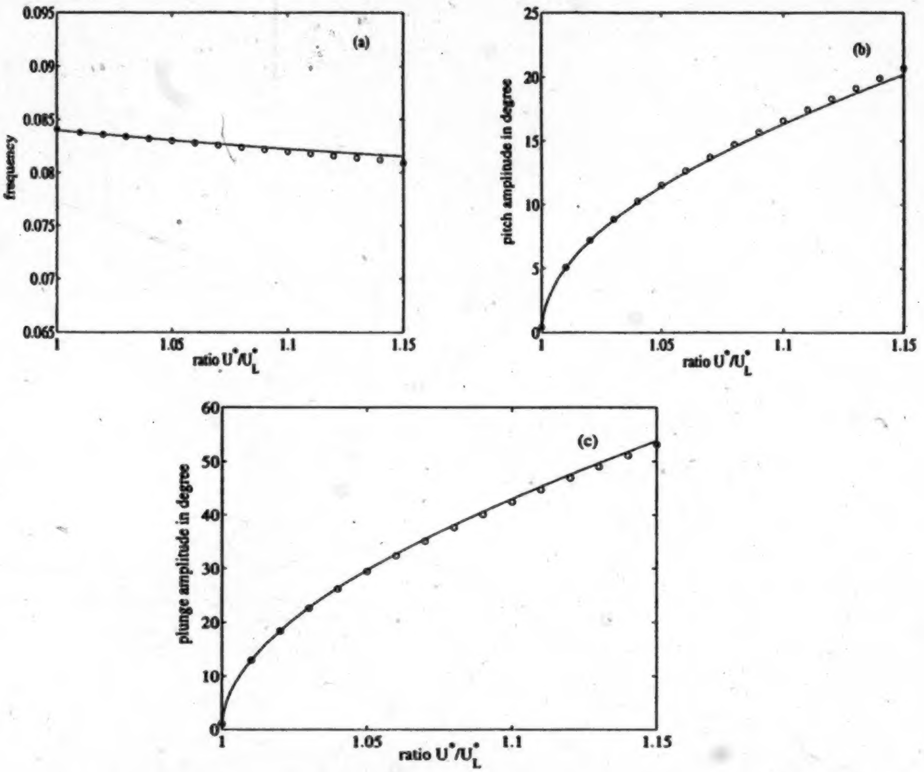

Figure 3.1: Dynamic response for Case 1. (a). frequency; (b). amplitude of pitch motion; (c). amplitude of plunge motion.

and amplitude is obtained. We see some variations in the frequencies and the amplitudes when the ratio U^*/U_L^* increases from the bifurcation point ($U^*/U_L^* = 1$). This is expected due to the limitations of the center manifold theory.

In Case 3, we investigate the aeroelastic system with a stronger nonlinear term in $M(\alpha)$ such that $\beta_{\alpha^3}/\beta_\alpha = 40$. At $\bar{\omega} = 0.2$, the frequency equation is given by $\omega = 0.0840 - 0.0101(1 - (U_L^*/U^*)^2)$. The variation of frequency ω with U^*/U_L^* is plotted in Fig. 3.3(a). Notice that the results in Fig. 3.3(a) are almost identical to those displayed in Fig. 3.1(a) for Case 1. Recall that the linear coefficients β_α equal to one for both Cases 3 and 1, but the nonlinear coefficients β_{α^3} equal to 40 and 3 for Cases 3 and 1 respectively. Although

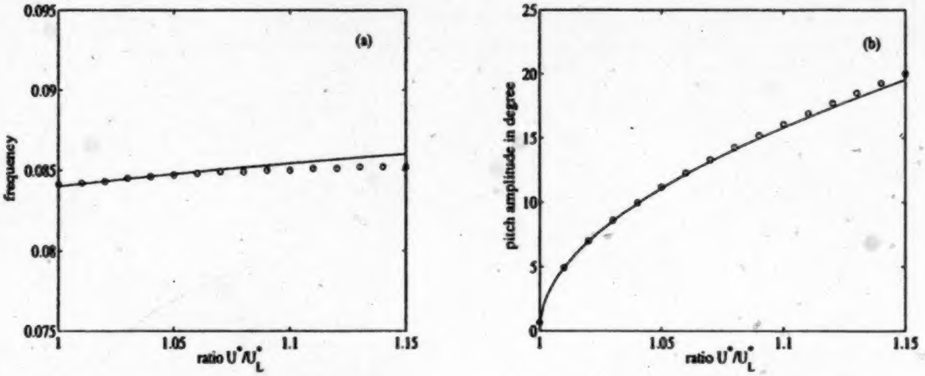

Figure 3.2: Dynamic response for Case 2. (a). frequency; (b). amplitude of pitch motion.

it may seem rather surprising to observe that the frequency relation is not sensitive to the nonlinear coefficient, a satisfactory explanation will be provided shortly. The corresponding amplitudes of pitch and plunge motions when $\bar{\omega} = 0.2$, as shown in Figs. 3.3(b) and (c), are not the same, however, as those reported in Case 1 (see Figs. 3.1(b) and (c)).

In Case 4, we consider a very strong nonlinear case in the pitch degree of freedom where $\beta_{\alpha^3}/\beta_\alpha = 400$. Our proposed procedure is applied. The frequency equation at $\bar{\omega} = 0.2$ is given by $\omega = 0.1822 - 0.0659(1 - (U_L^*/U^*)^2)$, where $U_L^* = 1.36468$. Comparisons with numerical simulations are shown in Fig.3.4.

From the results reported here, it is evident that our analytical analysis gives an accurate prediction of the frequency and amplitudes of the pitch and plunge motions of LCOs. Moreover, while numerical simulations show that the frequency variation with U^*/U_L^* is almost the same for Cases 1 and 3, an explanation is provided by using the analytical analysis. Since both linear coefficients β_α and β_ξ are identical for Cases 1 and 3, the linear flutter speed, $U^* = 6.28509$, is identical at $\bar{\omega} = 0.2$ for both cases. Now, by applying the center manifold theory and normal form method to system Eq.(2.2), we obtain

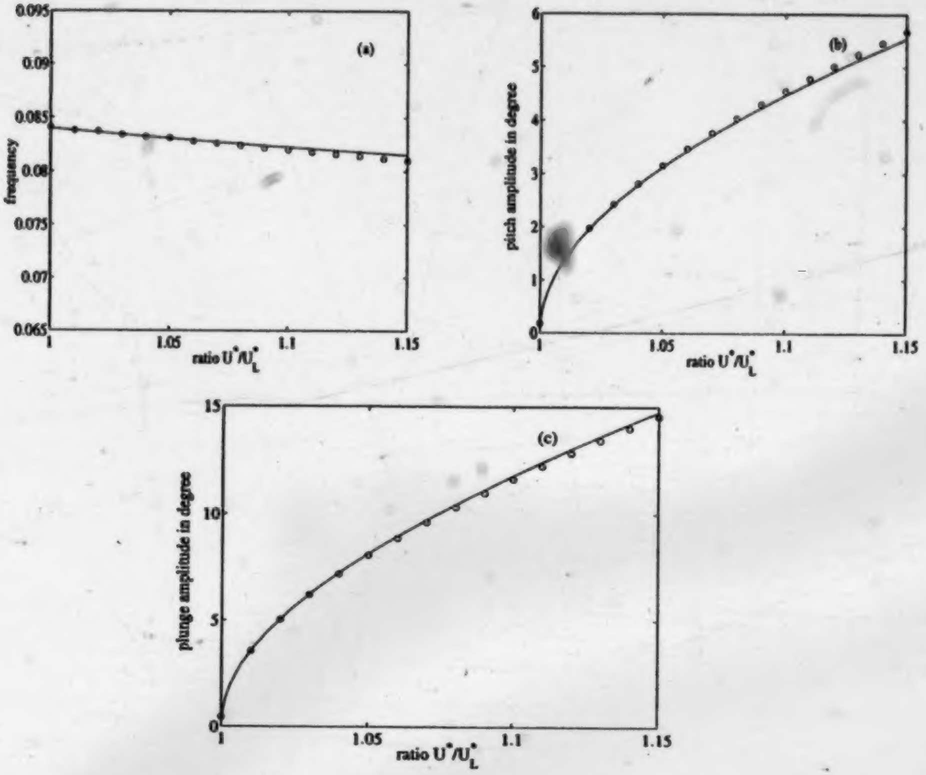

Figure 3.3: Dynamic response for Case 3. (a). frequency; (b). amplitude of pitch motion; (c). amplitude of plunge motion.

coefficients of formula (3.6) in terms of β_{α^3} and β_{ξ^3}:

$$\begin{cases} \omega_0 = 0.08404421382 \\ \dot{\theta}(0) = -0.06321776140 \\ \dot{\alpha}(0) = 0.1580161751 \\ a(0) = -0.00007444878252\beta_{\alpha^3} + 0.00006278101583\beta_{\xi^3} \\ b(0) = 0.00002501938337\beta_{\alpha^3} + 0.000006148895571\beta_{\xi^3} \end{cases} \tag{3.5}$$

Notice that the nonlinear coefficients β_{α^3} and β_{ξ^3} affect only the coefficients

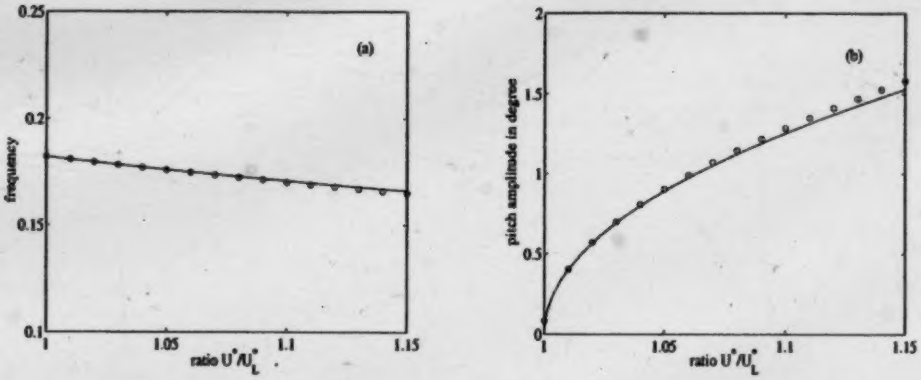

Figure 3.4: Dynamic response for Case 4. (a). frequency; (b). amplitude of pitch motion.

$a(0)$ and $b(0)$. The frequency relation in terms of β_{α^3} and β_{ξ^3} is given by

$$\begin{aligned}\omega =& 0.08404421382 + (-0.06321776140 \\ & - 0.1580161751\frac{0.00002501938337\beta_{\alpha^3} + 0.000006148895571\beta_{\xi^3}}{-0.00007444878252\beta_{\alpha^3} + 0.00006278101583\beta_{\xi^3}})\delta\end{aligned} \tag{3.6}$$

From the above formula, it is clear that when either β_{α^3} or β_{ξ^3} is zero, the other nonlinear coefficient β_{ξ^3} or β_{α^3} will not affect the resulting frequency. Hence, the frequency ω depends only on δ and is independent of β_{ξ^3} or β_{α^3}. In Case 1, $\beta_{\xi^3} = 0$, and the frequency relation is independent of the value of β_{α^3}. When both coefficients are present but with $\beta_{\alpha^3} >> \beta_{\xi^3}$ as in Case 3, it is easy to verify that the effect due to the nonlinear coefficient β_{ξ^3} can be neglected. Therefore, Case 3 can be considered to be similar to Case 1.

Unlike the frequency relation, the amplitude equations given in Eq.(3.2) indicate that the amplitude of LCOs is more sensitive to the variation in the nonlinear coefficients β_{α^3} and β_{ξ^3}. This observation is indeed confirmed by the results reported in Figs.3.2 and 3.4.

3.6 Concluding Remarks

In this chapter, we derived a frequency relation for a self-excited two-degree-of-freedom aeroelastic system with structural nonlinearities represented by cubic springs. Together with the amplitude-frequency relationships derived in [46], the limit cycle oscillations (LCOs) for the self-excited system can be predicted analytically. Our study shows that the frequency and amplitude of LCOs do not depend on the choice of initial conditions. Moreover, it has been shown that when the structural nonlinearity is applied only in one degree of freedom, or when nonlinearities appear in both pitch and plunge degrees of freedom but with one of the nonlinear coefficients much greater than the other nonlinear term, then the frequency relation is not affected by the nonlinear coefficients β_{α^3} or β_{ξ^3}. However, the corresponding amplitude of the LCO is sensitive to the variation in β_{α^3} and β_{ξ^3}. The mathematical approach presented here not only provides an accurate agreement with the numerical results obtained by using a fourth-order Runge-Kutta time-integration scheme but also leads to a better understanding of nonlinear aeroelasticity, especially near the bifurcation points. In the present work, we focus on the study of LCOs through a Hopf-bifurcation. The period doubling phenomenon in which an LCO subsequently gives rise to a two-period orbit by means of a flip-bifurcation has been detected in aeroelastic systems with cubic structural nonlinearities[52]. The phenomenon is interesting and important since it may provide a way to investigate period-two and chaotic motions. However, since the bifurcation analysis will now depend upon periodically varying parameters instead of the fixed points in a Hopf-bifurcation, a general procedure based on time-dependent center manifold theory and time-dependent normal form will be required.

Chapter 4

Freeplay Models

4.1 Introduction

In the previous chapter, we studied a self-excited two degree-of-freedom aeroelastic system with cubic restoring forces. Through the application of the center manifold theory and the principle of normal form, analytical formulas are derived which are capable of accurately predicting the frequencies and amplitudes of limit cycle oscillations. This chapter is to continue our study to develop a mathematical technique for a freeplay model.

Although it seems that the technique discussed in the previous chapter based on the center manifold theory can still be applied if we replace the freeplay model by polynomial or rational polynomial approximation, a detailed investigation carried out in § 4.2 leads to the conclusion that such an approach should not be used. The previous studies on the aeroelastic response of the freeplay model applied the describing function method or the harmonic balance method. However, the dynamic response of the system cannot be fully exploited since the analytical techniques do not take into account any initial conditions.

Time integration methods have often been used to study the response of an aeroelastic system with freeplay. It should be noted that, for a piecewise linear system such as a freeplay model, it is not straightforward to analyze the stability of the numerical schemes, because some of the eigenvalues corresponding to one of the linear sub-systems may have positive real parts. Furthermore, the standard time-integration scheme with uniform time step cannot precisely locate the switching point where the change in linear regions occurs. The importance of capturing switching points was noted by Lin and Cheng[55] and Conner et al.[16]. Lin and Cheng[55] reported an example showing that an entirely incorrect asymptotic behavior for nonlinear flutter can be predicted due to the error in capturing the switching point in the Runge-Kutta numerical scheme. More analysis of the errors introduced by numerical schemes for aeroelastic systems with structural nonlinearities will be presented in Chapter 6, which shows that significant differences between the exact motion and the numerical prediction may be observed for some cases. However, for cases discussed in this chapter, the numerical solution is considered to be accurate since a sufficiently small time step is used to integrate the aeroelastic system.

In this chapter, we introduce a mathematical technique based on the point transformation method[2]. Two formulations are developed to investigate the nonlinear aeroelastic model with a freeplay nonlinearity. One attractive feature of the present approach compared to a numerical time-integration scheme is that the formulations track the system behavior to the exact point where the change in linear sub-domains occurs. Moreover, the solution corresponding to each linear region is determined analytically. It will be demonstrated that the formulations developed are efficient and effective. Not only can they accurately predict the amplitude and frequency of the LCOs, but also they are capable of detecting complex nonlinear aeroelastic behavior such as periodic motion with harmonics, period doubling, chaotic motion and the coexistence of stable LCOs.

Some investigation is first carried out in § 4.2 to compare the original system with the systems associated with the rational polynomial approximations for the freeplay stiffness. Then, the idea of the point transformation technique and two formulations for the aeroelastic system with the freeplay model are developed in § 4.3. By using this point transformation technique, several examples are then investigated and the results are presented in § 4.4. Finally, the advantages and disadvantages of these two formulations are addressed in section § 4.5.

4.2 Rational Polynomial Approximations for Freeplay Springs

The freeplay model, which is defined by a piecewise linear function given in (2.2), is continuous but not differentiable. Since the existence of the center manifold requires the nonlinear function to be at least C^2 continuous, i.e. the second derivative exists and is continuous, the center manifold theory does not apply for the aeroelastic system with a freeplay model. Consequently, the procedure developed in Chapter 3 cannot be used to investigate the freeplay model.

Motivated by using an approximation for the nonlinear function as suggested in [1], we replaced the piecewise linear function by a third-order rational polynomial, which is C^∞ continuous on the interval $[-15^o, 15^o]$. Although it seems that the center manifold method can now be applied to system Eq.(2.2) with $M(x_1)$ being replaced by the rational polynomial approximation, this approach should not be used for the following two reasons.

First, it is important to note that one feature of the freeplay nonlinearity is the existence of switching points where changes in linear sub-domains occur. Since a slight change in the system parameters could affect the nonlinear aeroelastic behavior considerably, replacing a freeplay by a numerical approximation, which eliminates the switching points, would cause the location of the bifurcation point to be no longer exact.

For example, consider system Eq.(2.2) with the system parameters given by $\mu = 100$, $a_h = -1/2$, $x_\alpha = 1/4$, $r_\alpha = 0.5$, $\zeta_\xi = \zeta_\alpha = 0$, and with $G(x_3) = x_3$, the freeplay stiffness $M(x_1)$ given by (2.2), where $\alpha_f = M_0 = 0.25^o$, $M_f = 0$, and $\delta = 0.5^o$. Two rational polynomials $R_1(x_1)$ and $R_2(x_1)$ are constructed to approximate the piecewise linear function,

$$R_1(x_1) = \frac{c_1 + x_1(c_2 + x_1(c_3 + c_4x_1))}{1 + x_1(c_5 + x_1(c_6 + c_7x_1))}, \qquad R_2(x_1) = \frac{a_1x_1 + a_2x_1^2 + a_3x_1^3}{1 + b_1x_1 + b_2x_1^2},$$

where $c_1 = 0.0021$, $c_2 = 0.9277$, $c_3 = -134.7957$, $c_4 = 5954.619$, $c_5 = -121.2787$, $c_6 = 6414.885$, $c_7 = 1064.4611$ for $R_1(x)$, and $a_1 = 0.948815$, $a_2 = -129.93$, $a_3 = 5462.32$, $b_1 = -112.41$, $b_2 = 5732.43$ for $R_2(x)$. From

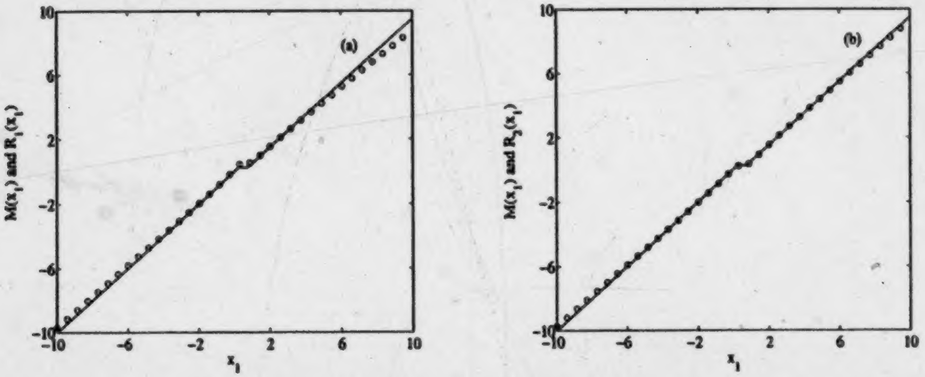

Figure 4.1: The original freeplay model and its approximations, (a). with $R_1(x_1)$; (b). with $R_2(x_1)$. Solid line: $M(x_1)$; open circle: approximated values of $R_1(x_1)$ or $R_2(x_1)$.

Fig. 4.1, where the solid line denotes the original model and the open circle denotes the approximated value, both $R_1(x_1)$ and $R_2(x_1)$ seem to provide a good approximation to the original piecewise linear function $M(x_1)$ for $x_1 \in [-10^o, 10^o]$. However, different qualitative dynamical response are resulted when the nonlinear term is represented by $R_1(x_1)$ or $R_2(x_1)$. For instance, when $U^*/U_L^* = 0.96$, $x_1(0) = 0.13$, and with other initial conditions set to zeroes, the system with $R_1(x_1)$ leads to a divergent motion in Fig. 4.2(a), while the dynamic response of the system with $R_2(x_1)$ gives a periodic motion in Fig. 4.2(b).

Second, since initial conditions play an important role in the dynamic response of aeroelastic systems with freeplay for some range of airfoil parameters, the center manifold method, which does not take into account any information due to initial conditions, would not be expected to provide a good predic-

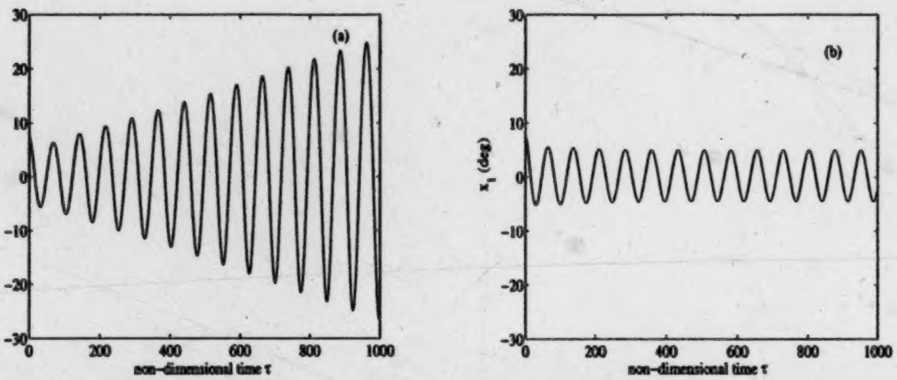

Figure 4.2: The system response when the freeplay model is replaced by $R_1(x_1)$: divergent motion (a), and by $R_2(x_1)$: periodic motion (b).

tion for a freeplay a model. Examples of different nonlinear system behaviors yielded by the same system parameters but with different initial conditions can be found in § 4.4. Hence, the center manifold method should not be used in the present study.

4.3 The Point Transformation Method

Consider the eight dimensional system given in Eq.(2.2) for a freeplay stiffness in pitch and a linear spring in plunge, where $M(x_1)$ is given by (2.2) and $G(x_3) = \beta x_3$. According to the three linear branches of the piecewise linear function for a freeplay model, the phase space $X \in R^8$ can be divided into three regions, $R_i (i = 1, 2, 3)$, each of which corresponds to a linear system:

$$\begin{array}{lll} X' = AX + F_1 & \text{in} & R_1 = \{X \in R^8 | x_1 < \alpha_f\} \\ X' = BX + F_2 & \text{in} & R_2 = \{X \in R^8 | \alpha_f < x_1 < \alpha_f + \delta\} \\ X' = AX + F_3 & \text{in} & R_3 = \{X \in R^8 | x_1 > \alpha_f + \delta\} \end{array}$$

Here A and B are 8 by 8 constant matrices, and F_1, F_2 and F_3 are 8 by 1 constant vectors. The elements of A, B and $F_i (i = 1, 2, 3, 4)$ are determined by the system parameters of the coupled aeroelastic equations, and they are given by

$$A = \begin{pmatrix} A_1 & A_2 \\ A_3 & A_4 \end{pmatrix}, \qquad B = \begin{pmatrix} B_1 & A_2 \\ A_3 & A_4 \end{pmatrix},$$

and $F_1 = (M_0 - \alpha_f)F$, $F_2 = (M_0 - M_f\alpha_f)F$ and $F_3 = (M_0 - \alpha_f + \delta_0(M_f - 1))F$. The elements of the 4 by 4 block matrices, $A_i (i = 1, 2, 3, 4)$, B_1 and the vector F are defined as:

$$A_1 = \begin{pmatrix} 0 & 1 & 0 & 0 \\ a_{21} - jc_0(\frac{1}{U^*})^2 & a_{22} & a_{23} + jd_0\beta(\frac{\bar{\omega}}{U^*})^2 & a_{24} \\ 0 & 0 & 0 & 1 \\ a_{41} + jc_1(\frac{1}{U^*})^2 & a_{42} & a_{43} - jd_1\beta(\frac{\bar{\omega}}{U^*})^2 & a_{44} \end{pmatrix}$$

$$A_2 = \begin{pmatrix} 0 & 0 & 0 & 0 \\ a_{25} & a_{26} & a_{27} & a_{28} \\ 0 & 0 & 0 & 0 \\ a_{45} & a_{46} & a_{47} & a_{48} \end{pmatrix}$$

$$A_3 = \begin{pmatrix} 1 & 0 & 0 & 0 \\ 1 & 0 & 0 & 0 \\ 0 & 0 & 1 & 0 \\ 0 & 0 & 1 & 0 \end{pmatrix}$$

$$A_4 = \begin{pmatrix} -\epsilon_1 & 0 & 0 & 0 \\ 0 & -\epsilon_2 & 0 & 0 \\ 0 & 0 & -\epsilon_1 & 0 \\ 0 & 0 & 0 & -\epsilon_2 \end{pmatrix}$$

$$B_1 = \begin{pmatrix} 0 & 1 & 0 & 0 \\ a_{21} - jc_0M_f(\frac{1}{U^*})^2 & a_{22} & a_{23} + jd_0\beta(\frac{\bar{\omega}}{U^*})^2 & a_{24} \\ 0 & 0 & 0 & 1 \\ a_{41} + jc_1M_f(\frac{1}{U^*})^2 & a_{42} & a_{43} - jd_1\beta(\frac{\bar{\omega}}{U^*})^2 & a_{44} \end{pmatrix}$$

$$F = \begin{pmatrix} 0 \\ -jc_0(\frac{1}{U^*})^2 \\ 0 \\ jc_1(\frac{1}{U^*})^2 \\ 0 \\ 0 \\ 0 \\ 0 \end{pmatrix}$$

Now we consider a freeplay model shown in Fig. 4.3. Let the $Z - Y$ plane represent the eight dimensional phase space, where $Z = \{x_1\}$ and $Y = \{x_2, x_3, x_4, x_5, x_6, x_7, x_8\}$. The $Z - Y$ phase space is now divided into three regions R_1, R_2 and R_3 according to the sub-spaces $Z = \alpha_f$ and $Z = \alpha_f + \delta$ as shown in Fig. 4.4(a). The system response can then be predicted by following a general phase path.

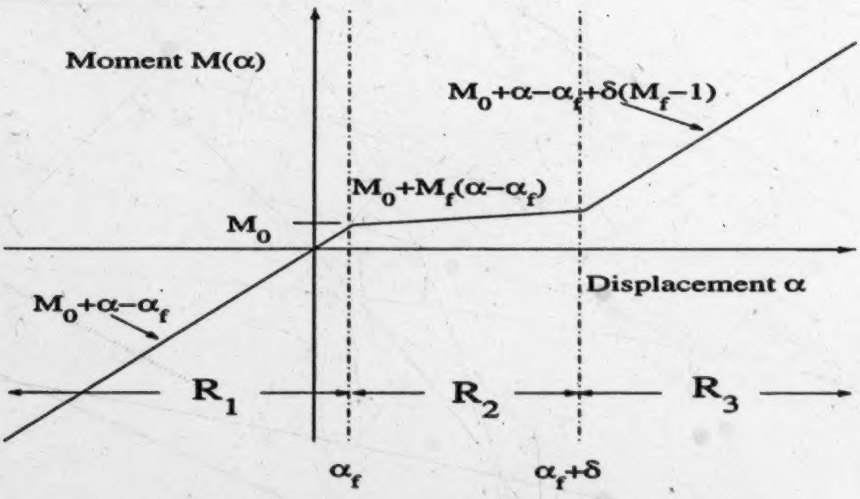

Figure 4.3: General sketch of a freeplay model.

Assuming that a motion initially starts at a point X_0 as shown in Fig.4.4(a), the trajectory begins in R_1 and passes through R_2 into R_3. Then it returns through R_2 back into R_1. Let X_1 and X_2 be the points through which the trajectory enters R_2 and R_3 respectively. Let X_3 and X_4 be the points through

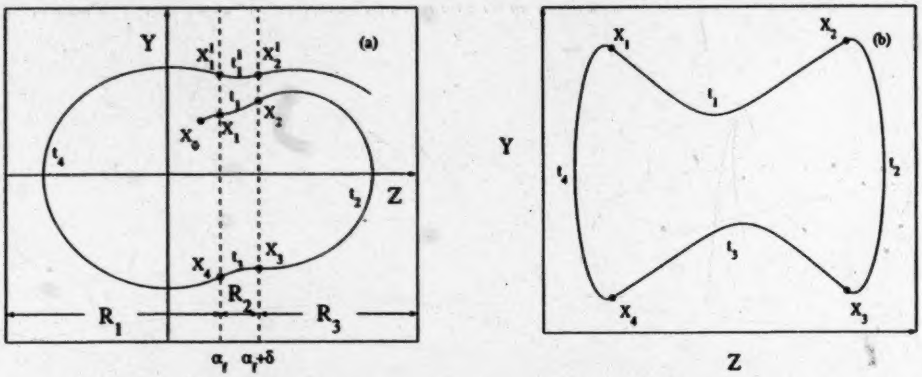

Figure 4.4: General trajectory of system (2.2) with a freeplay stiffness in pitch.

which the trajectory leaves R_3 and R_2 respectively. These points (X_1, X_2, X_3 and X_4) are called switching points, since they locate the places where the linear systems change. Let t_1 be the travelling time of the trajectory (from X_1 to X_2) in region R_2. Similarly, let t_2, t_3 and t_4 be the travelling times of the trajectory in regions R_3, R_2 and R_1 respectively. The above process of the point transformation is then repeated. When a steady-state is reached, the trajectory may consist of only four switching points X_1, X_2, X_3, X_4 and four travelling times t_1, t_2, t_3 and t_4 as illustrated in Fig.4.4(b).

It should be noted that the system of equations in each region is strictly linear. Hence the exact solutions in R_1, R_2 and R_3 can be expressed analytically. Using the analytical solutions in different regions, we can determine the maximum and minimum values of α corresponding to $\alpha' = 0$. Moreover, based on the information provided by the switching points, travelling times and the maximum and minimum amplitudes for α, we can predict the type of steady-state motion for the aeroelastic system. For instance, when the transients have diminished, we may observe a repetition of the switching points X_1, X_2, X_3, X_4 and the corresponding travelling times t_1, t_2, t_3, t_4 covering the entire region as shown in Fig. 4.4(b). Then the steady-state motion is classified as a limit cycle oscillation (LCO) with one frequency. The existence of one frequency component is further confirmed by only one maximum and one minimum value for α. The frequency can be determined by $f = 1/T$, where T

denotes the period which is the sum of the travelling times (i.e., $T = \sum_{i=1}^{4} t_i$). The resulting LCO is of period-one, and the trajectory illustrated in Fig. 4.4(b) has one complete loop covering the three regions R_1, R_2 and R_3.

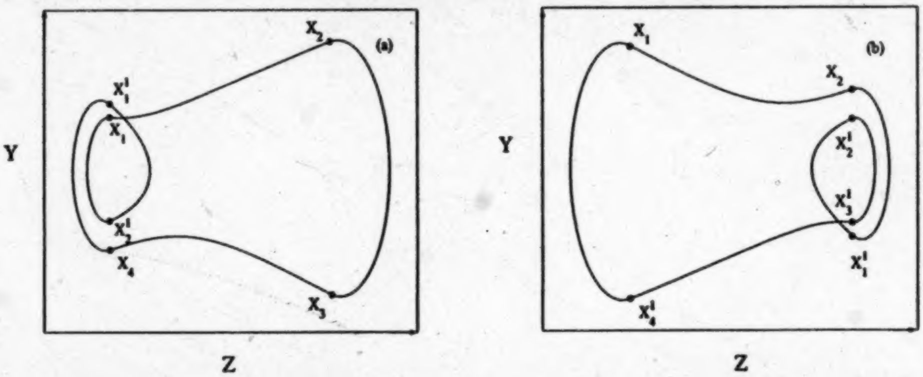

Figure 4.5: Trajectories for system Eq.(2.2) with a freeplay stiffness in pitch: period-one with harmonics where (a) the smaller loop covers R_1 and R_2; (b) the smaller loop covers R_2 and R_3.

The point transformation method is capable of predicting more general periodic motions. Note that it is not necessary that the switching points appear in the sequence as shown in Fig. 4.4(b). For example, the steady-state trajectory displayed in Fig. 4.5(a) which contains six switching points. The additional two points X_1^1 and X_2^1 are introduced after completing the sequence discussed previously. In this case, a complete loop consists of six points, X_1, X_2, X_3, X_4, X_1^1, X_2^1, and six corresponding travelling times, t_1, t_2, t_3, t_4, t_1^1, t_2^1. Unlike the trajectory shown in Fig. 4.4(b), the complete loop covering the entire region also contains a smaller loop covering two regions R_1 and R_2. The smaller loop is defined as the one covering only one or two regions. The resulting LCO is of period-one, since we observe only one complete loop covering the entire region. However, the presence of a smaller loop indicates that the LCO has a harmonic component. Since the LCO is of period-one, the frequency is estimated by $f = 1/T$ where $T = \sum_{i=1}^{4} t_i + \sum_{i=1}^{2} t_i^1$. The typical feature of an LCO with harmonics can be verified by four values for α when $\alpha' = 0$. Recall that for a period-one LCO with one frequency, only two values of α corresponding to $\alpha' = 0$ exist. Fig. 4.5(b) illustrates a similar situation, but with the two extra switching points X_2^1 and X_3^1 due to the presence of a smaller loop covering regions R_2 and R_3.

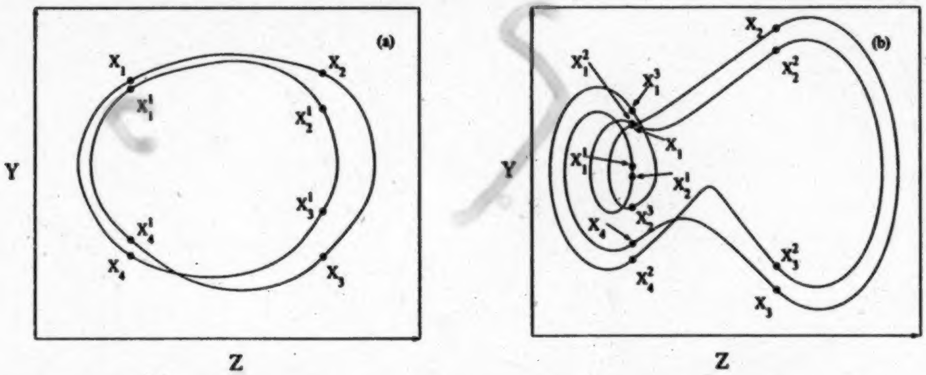

Figure 4.6: Trajectories for system Eq.(2.2) with a freeplay stiffness in pitch: period-two LCO (a) without harmonics and (b) with harmonics where two smaller loops cover R_1 and R_2.

The predicted limit cycle oscillations discussed in Fig. 4.4 and 4.5 are of period-one, since the point transformation confirms the presence of only one complete loop covering the entire region. If however, a complete loop covers the entire region n times, the LCO is classified as a period-n LCO, and the frequency is given by $f = 1/T$ where the period T is the sum of the travelling times. For example, Figs. 4.6(a) and (b) display period-two LCOs. Fig. 4.6(a) corresponds to a simple period-two LCO, and the trajectory contains 8 switching points and 8 travelling times in a complete loop. In Fig. 4.6(b), a complete loop contains two smaller loops, indicating that the period-two LCO has harmonic components. If the sequence of switching points does not repeat after a sufficiently long time, the motion may be classified as chaos.

In summary, the point transformation method can be used to detect a general period-n limit cycle oscillation for an aeroelastic system with freeplay. Moreover, it can predict the presence of harmonic components and is also capable of determining the frequency and the maximum and minimum amplitudes of an LCO.

In the following sections, we present two formulations based on the above discussion. Then the formulations developed will be applied to predict the nonlinear aeroelastic behavior for a freeplay model.

4.3.1 Formulation 1

This formulation begins with a given set of initial conditions X_0. First, the travelling times are determined by solving a nonlinear equation. Then, the switching points are calculated by the multiplication of a known matrix by a known vector, which will be further explained after the formulation is presented. If the round-off error can be neglected, the formulation will produce the exact solution for the aeroelastic system. The detailed procedure is given as following.

Step 0. Set the initial vector $X_0 = (x_{01}, x_{02}, x_{03}, \dots, x_{08})^T$. Let $i = 1$ for $\alpha_f < x_{01} < \alpha_f + \delta$ and $x_{02} > 0$, $i = 2$ for $x_{01} > \alpha_f + \delta$, $i = 3$ for $\alpha_f < x_{01} < \alpha_f + \delta$ and $x_{02} < 0$, and $i = 4$ for $x_{01} < \alpha_f$. Set $X_i = X_0$, and go to step i.

Step 1. Solve the nonlinear equations $\alpha_f + \delta = \{e^{Bt}X_1 + \mathcal{B}(t)F_2\}|_{(1)}$ and $\alpha_f = \{e^{Bt}X_1 + \mathcal{B}(t)F_2\}|_{(1)}$ separately for t. Here, $\{V\}|_{(n)}$ denotes the nth element of the vector V. Let the smallest positive solutions corresponding to the first and second equations be t^* and t^{**} respectively. If $t^* < t^{**}$, let $t_1 = t^*$, compute X_2 by $X_2 = e^{Bt_1}X_1 + \mathcal{B}(t_1)F_2$, and go to step 2. If $t^{**} < t^*$, let $t_3 = t^{**}$, compute X_4 by $X_4 = e^{Bt_3}X_1 + \mathcal{B}(t_3)F_2$, and go to step 4.

Step 2. First, solve $\{e^{At}X_2 + \mathcal{A}(t)F_3\}|_{(2)} = 0$ for t, assign the smallest positive value to t_u, and compute the maximum amplitude by $\alpha_{max} = \{e^{At_u}X_2 + \mathcal{A}(t_u)F_3\}|_{(1)}$. Then, solve $\alpha_f + \delta = \{e^{At}X_2 + \mathcal{A}(t)F_3\}|_{(1)}$ for t, assign the smallest positive value to t_2, and compute X_3 by $X_3 = e^{At_2}X_2 + \mathcal{A}(t_2)F_3$. Go to step 3.

Step 3. Similar to Step 1, solve the nonlinear equations $\alpha_f = \{e^{Bt}X_3 + \mathcal{B}(t)F_2\}|_{(1)}$ and $\alpha_f + \delta = \{e^{Bt}X_3 + \mathcal{B}(t)F_2\}|_{(1)}$ separately for t. Let the smallest positive solutions corresponding to the first and second nonlinear equations be t^* and t^{**} respectively. If $t^* < t^{**}$, let $t_3 = t^*$, compute X_4 by $X_4 =$

$e^{Bt_3}X_3 + \mathcal{B}(t_3)F_2$, and go to step 4. If $t^{**} < t^{*}$, let $t_1 = t^{**}$, compute X_2 by $X_2 = e^{Bt_1}X_3 + \mathcal{B}(t_1)F_2$, and go to step 2.

Step 4. Similar to Step 2, first solve $\{e^{At}X_4 + \mathcal{A}(t)F_1\}|_{(2)} = 0$ for t, assign the smallest positive value to t_l, and compute the minimum amplitude by $\alpha_{min} = \{e^{At_l}X_4 + \mathcal{A}(t_l)F_1\}|_{(1)}$. Then, solve $\alpha_f = \{e^{At}X_4 + \mathcal{A}(t)F_1\}|_{(1)}$ for t, assign the smallest positive value to t_4, and compute X_1 by $X_1 = e^{At_4}X_4 + \mathcal{A}(t_4)F_1$. Go to step 1.

The matrices $\mathcal{A}(t)$ and $\mathcal{B}(t)$ are given by $\mathcal{A}(t) = \int_0^t e^{A(t-\tau)}d\tau$ and $\mathcal{B}(t) = \int_0^t e^{B(t-\tau)}d\tau$. Jordan Canonical forms of A and B are introduced to help computing the matrices e^{At}, e^{Bt}, $e^{A(t-\tau)}$ and $e^{B(t-\tau)}$. Let the matrices A and B be decomposed such that $A = PJ_AP^{-1}$ and $B = QJ_BQ^{-1}$, where J_A and J_B are the Jordan Canonical forms of A and B:

$$J_A = \begin{pmatrix} a & b & 0 & 0 & 0 & 0 & 0 & 0 \\ -b & a & 0 & 0 & 0 & 0 & 0 & 0 \\ 0 & 0 & c & d & 0 & 0 & 0 & 0 \\ 0 & 0 & -d & c & 0 & 0 & 0 & 0 \\ 0 & 0 & 0 & 0 & \lambda_{a_1} & 0 & 0 & 0 \\ 0 & 0 & 0 & 0 & 0 & \lambda_{a_2} & 0 & 0 \\ 0 & 0 & 0 & 0 & 0 & 0 & \lambda_{a_3} & 0 \\ 0 & 0 & 0 & 0 & 0 & 0 & 0 & \lambda_{a_4} \end{pmatrix},$$

and

$$J_B = \begin{pmatrix} e & f & 0 & 0 & 0 & 0 & 0 & 0 \\ -f & e & 0 & 0 & 0 & 0 & 0 & 0 \\ 0 & 0 & \lambda_{b_1} & 0 & 0 & 0 & 0 & 0 \\ 0 & 0 & 0 & \lambda_{b_2} & 0 & 0 & 0 & 0 \\ 0 & 0 & 0 & 0 & \lambda_{b_3} & 0 & 0 & 0 \\ 0 & 0 & 0 & 0 & 0 & \lambda_{b_4} & 0 & 0 \\ 0 & 0 & 0 & 0 & 0 & 0 & \lambda_{b_5} & 0 \\ 0 & 0 & 0 & 0 & 0 & 0 & 0 & \lambda_{b_6} \end{pmatrix},$$

where $\{a \pm bi,\ c \pm di,\ \lambda_{a_1},\ \lambda_{a_2},\ \lambda_{a_3},\ \lambda_{a_4}\}$ and $\{e \pm fi,\ \lambda_{b_1},\ \lambda_{b_2},\ \lambda_{b_3},\ \lambda_{b_4},\ \lambda_{b_5},\ \lambda_{b_6}\}$ are eigenvalues of A and B, respectively. Thus, e^{At} and e^{Bt} can be computed by $e^{At} = P\bar{J}_A P^{-1}$ and $e^{Bt} = P\bar{J}_B P^{-1}$, where $\bar{J}_A$ is

$$\begin{pmatrix} e^{at}cos(bt) & e^{at}sin(bt) & 0 & 0 & 0 & 0 & 0 & 0 \\ -e^{at}sin(bt) & e^{at}cos(bt) & 0 & 0 & 0 & 0 & 0 & 0 \\ 0 & 0 & e^{ct}cos(dt) & e^{ct}sin(dt) & 0 & 0 & 0 & 0 \\ 0 & 0 & -e^{ct}sin(dt) & e^{ct}cos(dt) & 0 & 0 & 0 & 0 \\ 0 & 0 & 0 & 0 & e^{\lambda_{a_1}t} & 0 & 0 & 0 \\ 0 & 0 & 0 & 0 & 0 & e^{\lambda_{a_2}t} & 0 & 0 \\ 0 & 0 & 0 & 0 & 0 & 0 & e^{\lambda_{a_3}t} & 0 \\ 0 & 0 & 0 & 0 & 0 & 0 & 0 & e^{\lambda_{a_4}t} \end{pmatrix},$$

and $\bar{J}_B$ is

$$\begin{pmatrix} e^{et}cos(ft) & e^{et}sin(ft) & 0 & 0 & 0 & 0 & 0 & 0 \\ -e^{et}sin(ft) & e^{et}cos(ft) & 0 & 0 & 0 & 0 & 0 & 0 \\ 0 & 0 & e^{\lambda_{b_1}t} & 0 & 0 & 0 & 0 & 0 \\ 0 & 0 & 0 & e^{\lambda_{b_2}t} & 0 & 0 & 0 & 0 \\ 0 & 0 & 0 & 0 & e^{\lambda_{b_3}t} & 0 & 0 & 0 \\ 0 & 0 & 0 & 0 & 0 & e^{\lambda_{b_4}t} & 0 & 0 \\ 0 & 0 & 0 & 0 & 0 & 0 & e^{\lambda_{b_5}t} & 0 \\ 0 & 0 & 0 & 0 & 0 & 0 & 0 & e^{\lambda_{b_6}t} \end{pmatrix}.$$

The matrix $\mathcal{A}(t)$ can be computed by $\mathcal{A}(t) = P\bar{A}P^{-1}$, where $\bar{A}$ is

$$\begin{pmatrix} v(a,b,t) & s(a,b,t) & 0 & 0 & 0 & 0 & 0 & 0 \\ -s(a,b,t) & v(a,b,t) & 0 & 0 & 0 & 0 & 0 & 0 \\ 0 & 0 & v(c,d,t) & s(c,d,t) & 0 & 0 & 0 & 0 \\ 0 & 0 & -s(c,d,t) & v(c,d,t) & 0 & 0 & 0 & 0 \\ 0 & 0 & 0 & 0 & l(\lambda_{a_1},t) & 0 & 0 & 0 \\ 0 & 0 & 0 & 0 & 0 & l(\lambda_{a_2},t) & 0 & 0 \\ 0 & 0 & 0 & 0 & 0 & 0 & l(\lambda_{a_3},t) & 0 \\ 0 & 0 & 0 & 0 & 0 & 0 & 0 & l(\lambda_{a_4},t) \end{pmatrix},$$

and the matrix $\mathcal{B}(t)$ can be computed by $\mathcal{B}(t) = Q\bar{B}Q^{-1}$, where $\bar{B}$ is

$$\begin{pmatrix} v(e,f,t) & s(e,f,t) & 0 & 0 & 0 & 0 & 0 & 0 \\ -s(e,f,t) & v(e,f,t) & 0 & 0 & 0 & 0 & 0 & 0 \\ 0 & 0 & l(\lambda_{b_1},t) & 0 & 0 & 0 & 0 & 0 \\ 0 & 0 & 0 & l(\lambda_{b_2},t) & 0 & 0 & 0 & 0 \\ 0 & 0 & 0 & 0 & l(\lambda_{b_3},t) & 0 & 0 & 0 \\ 0 & 0 & 0 & 0 & 0 & l(\lambda_{b_4},t) & 0 & 0 \\ 0 & 0 & 0 & 0 & 0 & 0 & l(\lambda_{b_5},t) & 0 \\ 0 & 0 & 0 & 0 & 0 & 0 & 0 & l(\lambda_{b_6},t) \end{pmatrix},$$

where the functions $v : R^3 \rightarrow R$, $s : R^3 \rightarrow R$, and $l : R^2 \rightarrow R$ are given by

$$v(a,b,t) = \int_0^t e^{a(t-\tau)} cos(b(t-\tau))d\tau = \frac{-a + ae^{at}cos(bt) + be^{at}sin(bt)}{a^2+b^2},$$

$$s(a,b,t) = \int_0^t e^{a(t-\tau)} sin(b(t-\tau))d\tau = \frac{b - be^{at}cos(bt) + ae^{at}sin(bt)}{a^2+b^2},$$

$$l(\lambda,t) = \int_0^t e^{\lambda(t-\tau)}d\tau = \begin{cases} \frac{e^{\lambda t}-1}{\lambda} & \lambda \neq 0 \\ t & \lambda = 0\,. \end{cases}$$

In the formulation, the travelling time t is first determined by solving a nonlinear equation $f(t) = 0$, where $f(t)$ involves either $e^{at}cos(bt+\phi_1)$, $e^{ct}cos(dt+\phi_2)$, $e^{\lambda_{a_1}t}$, $e^{\lambda_{a_2}t}$, $e^{\lambda_{a_3}t}$ and $e^{\lambda_{a_4}t}$, or $e^{et}cos(ft+\psi)$, $e^{\lambda_{b_1}t}$, $e^{\lambda_{b_2}t}$, $e^{\lambda_{b_3}t}$, $e^{\lambda_{b_4}t}$, $e^{\lambda_{b_5}t}$ and $e^{\lambda_{b_6}t}$. By analyzing the monotone intervals of the terms associated with $e^{at}cos(bt+\phi_1)$, $e^{ct}cos(dt+\phi_2)$ and $e^{et}cos(ft+\psi)$, it is easy to find the smallest positive solution to the equation $f(t) = 0$. Then, the new state $X_i (i = 1,2,3,4)$ are computed from a known matrix by a known vector multiplications. For example, in Step 1, once the travelling time t_1 is determined, the new state vector X_2 can be updated from X_1 according to $X_2 = e^{Bt_1}X_1 + \mathcal{B}(t_1)F_2$. Recall that X_1 and F_2 are vectors, e^{Bt_1} and $\mathcal{B}(t_1)$ can be computed by the above procedures. Hence, X_2 is determined by performing linear algebraic operations. If no positive solution for $f(t) = 0$ can be found in any of the steps discussed above, the motion either diverges if the linear system has at least one eigenvalue with a positive real part, or it converges to the equilibrium in that region if the real parts of all eigenvalues of the linear system are negative. If the values of the switching points or the amplitudes of α become unbounded, then the motion is divergent.

4.3.2 Formulation 2

If only the steady-state solution of an aeroelastic model is of interest, the following alternative formulation is proposed so that the travelling times and the switching points of an LCO can be determined directly without going through the transient state. However, we must first assume the specified type of the investigated motion. For example, for a period-one LCO, let the four switching points be

$$X_1 = \begin{pmatrix} \alpha_f \\ s_1 \end{pmatrix} \quad X_2 = \begin{pmatrix} \alpha_f + \delta \\ s_2 \end{pmatrix} \quad X_3 = \begin{pmatrix} \alpha_f + \delta \\ s_3 \end{pmatrix} \quad X_4 = \begin{pmatrix} \alpha_f \\ s_4 \end{pmatrix}$$

where s_1, s_2, s_3 and s_4 are seven-dimensional variable vectors representing the switching points in the subspace $\{X \in R^8 | x_1 = \alpha_f\}$ or $\{X \in R^8 | x_1 = \alpha_f + \delta\}$. Let $t_i (i = 1, 2, 3, 4)$ denote the corresponding travelling times. Then t_i and $s_i (i = 1, 2, 3, 4)$ can be determined by solving the following system of nonlinear equations

$$\begin{cases} X_2 = e^{Bt_1} X_1 + \mathcal{B}(t_1) F_2 \\ X_3 = e^{At_2} X_2 + \mathcal{A}(t_2) F_3 \\ X_4 = e^{Bt_3} X_3 + \mathcal{B}(t_3) F_2 \\ X_1 = e^{At_4} X_4 + \mathcal{A}(t_4) F_1 \ . \end{cases} \tag{4.1}$$

Note that Eq.(4.1) is thirty-two dimensional since $X_i (i = 1, 2, 3, 4)$ are eight-dimensional vectors. The period of this period-one LCO is given by the sum of the total travelling time $T = \sum_{i=1}^{4} t_i$, and the frequency f is calculated by $f = 1/T$. The amplitudes α_{max} and α_{min} are given by

$$\begin{cases} \text{solve } \{e^{At_u} X_2 + \mathcal{A}(t_u) F_3\}|_{(2)} = 0 \text{ for } t_u \\ \text{set } \alpha_{max} = \{e^{At_u} X_2 + \mathcal{A}(t_u) F_3\}|_{(1)} \\ \text{solve } \{e^{At_l} X_4 + \mathcal{A}(t_l) F_1\}|_{(2)} = 0 \text{ for } t_l \\ \text{set } \alpha_{min} = \{e^{At_l} X_4 + \mathcal{A}(t_l) F_1\}|_{(1)} \ , \end{cases} \tag{4.2}$$

where X_2 and X_4 are solutions to Eq.(4.1).

To determine the frequency of an LCO, only the values of $t_i (i = 1, 2, 3, 4)$ are of interest. With some algebra, the thirty-two dimensional system Eq.(4.1) can be further reduced to a four-dimensional system with variables $t_i (i = 1, 2, 3, 4)$

$$\begin{cases} \alpha_f = \{H_1(t_1, t_2, t_3, t_4)G_1(t_1, t_2, t_3, t_4)\}|_{(1)} \\ \alpha_f + \delta = \{H_2(t_1, t_2, t_3, t_4)G_2(t_1, t_2, t_3, t_4)\}|_{(1)} \\ \alpha_f + \delta = \{H_3(t_1, t_2, t_3, t_4)G_3(t_1, t_2, t_3, t_4)\}|_{(1)} \\ \alpha_f = \{H_4(t_1, t_2, t_3, t_4)G_4(t_1, t_2, t_3, t_4)\}|_{(1)} , \end{cases} \tag{4.3}$$

Here $H_i (i = 1, 2, 3, 4)$ are the 8 by 8 matrix functions of $t_i (i = 1, 2, 3, 4)$, and the expressions are given as:

$$\begin{aligned} H_1(t_1, t_2, t_3, t_4) &= (I - e^{At_4}e^{Bt_3}e^{At_2}e^{Bt_1})^{-1} \\ H_2(t_1, t_2, t_3, t_4) &= (I - e^{Bt_1}e^{At_4}e^{Bt_3}e^{At_2})^{-1} \\ H_3(t_1, t_2, t_3, t_4) &= (I - e^{At_2}e^{Bt_1}e^{At_4}e^{Bt_3})^{-1} \\ H_4(t_1, t_2, t_3, t_4) &= (I - e^{Bt_3}e^{At_2}e^{Bt_1}e^{At_4})^{-1} \end{aligned}$$

where I denotes the identity 8 by 8 matrix, and $G_i (i = 1, 2, 3, 4)$ are 8 by 1 vector functions of $t_i (i = 1, 2, 3, 4)$, and the expressions are given as:

$$\begin{aligned} G_1(t_1, t_2, t_3, t_4) &= e^{At_4}e^{Bt_3}e^{At_2}B(t_1)F_2 + e^{At_4}e^{Bt_3}A(t_2)F_3 \\ &\quad + e^{At_4}B(t_3)F_2 + A(t_4)F_1 \\ G_2(t_1, t_2, t_3, t_4) &= e^{Bt_1}e^{At_4}e^{Bt_3}A(t_2)F_3 + e^{Bt_1}e^{At_4}B(t_3)F_2 \\ &\quad + e^{Bt_1}A(t_4)F_1 + B(t_1)F_2 \\ G_3(t_1, t_2, t_3, t_4) &= e^{At_2}e^{Bt_1}e^{At_4}B(t_3)F_2 + e^{At_2}e^{Bt_1}A(t_4)F_1 \\ &\quad + e^{At_2}B(t_1)F_2 + A(t_2)F_3 \\ G_4(t_1, t_2, t_3, t_4) &= e^{Bt_3}e^{At_2}e^{Bt_1}A(t_4)F_1 + e^{Bt_3}e^{At_2}B(t_1)F_2 \\ &\quad + e^{Bt_3}A(t_2)F_3 + B(t_3)F_2 . \end{aligned}$$

The frequency of the period-one LCO motion can then be determined by $f = 1/\sum_{i=1}^{4} t_i$, and the four switching points are given by $X_i = H_i(t_1, t_2, t_3, t_4)$

$G_i(t_1, t_2, t_3, t_4)$ with $i = 1, 2, 3, 4$. The amplitudes α_{max} and α_{min} are given by Eq.(4.2).

For a period-one LCO with harmonics, assuming that the small loop in the state space covers regions R_1 and R_2, there exist six switching points instead of four as in the simple period-one motion. By adding two more switching points

$$X_5 = \begin{pmatrix} \alpha_f \\ s_5 \end{pmatrix} \quad \text{and} \quad X_6 = \begin{pmatrix} \alpha_f \\ s_6 \end{pmatrix},$$

where s_5 and s_6 are seven-dimensional vectors representing the switching points in the subspace $\{X \in R^8 | x_1 = \alpha_f\}$, Eq.(4.1) is then rewritten as

$$\begin{cases} X_2 = e^{Bt_1} X_1 + \mathcal{B}(t_1) F_2 \\ X_3 = e^{At_2} X_2 + \mathcal{A}(t_2) F_3 \\ X_4 = e^{Bt_3} X_3 + \mathcal{B}(t_3) F_2 \\ X_5 = e^{At_4} X_4 + \mathcal{A}(t_4) F_1 \\ X_6 = e^{Bt_5} X_5 + \mathcal{B}(t_5) F_2 \\ X_1 = e^{At_6} X_6 + \mathcal{A}(t_6) F_1 \, . \end{cases} \tag{4.4}$$

Consequently, the frequency is given by $f = 1/\sum_{i=1}^{6} t_i$. Since the motion contains four values of amplitude exist for α when $\alpha' = 0$, the following additional formulas

$$\begin{cases} \text{solve } \{e^{At_m} X_5^1 + \mathcal{B}(t_m) F_2\}|_{(2)} = 0 \text{ for } t_m \\ \alpha_{max} = \{e^{At_m} X_5^1 + \mathcal{B}(t_m) F_2\}|_{(1)} \\ \text{solve } \{e^{At_n} X_6^1 + \mathcal{A}(t_n) F_1\}|_{(2)} = 0 \text{ for } t_n \\ \alpha_{min} = \{e^{At_n} X_6^1 + \mathcal{A}(t_n) F_1\}|_{(1)} \end{cases} \tag{4.5}$$

are included to Eq.(4.2) to compute the LCO amplitudes.

Generally speaking, for a period-n LCO or a period-n LCO with harmonics, Eqs.(4.1) and (4.2) or Eqs.(4.4) and (4.5) have to be modified to determine the corresponding travelling times and the amplitudes.

Although Formulation 1 starts with a given set of initial conditions, it is not a time-integration scheme since the solution to each linear subsystem is determined analytically. The formulation given in §3.1 is capable of detecting any type of steady-state motion including convergent, divergent, period-n, period-n with harmonics, and chaotic motions. Under the same system parameters, starting from different initial conditions, the trajectory may converge to different LCOs, which indicates the coexistence of the LCOs of the original system Eq.(2.2).

When Formulation 2 is applied, only the steady-state behavior is detected since no information with respect to the transients is used. This is very efficient if only the steady-state solution is of interest. However, the formulations given in Eqs.(4.1) and (4.2) (or Eqs.(4.4) and (4.5)) are valid only for detecting a period-one LCO (or a period-one LCO with harmonics). For other types of motion, the formulation has to be modified correspondingly. Note that only the positive solutions of $t_i (i = 1,2,3,4)$ to Eq.(4.1) (or Eq.(4.4) are valid since the variables $t_i (i = 1,2,3,4)$ represent the travelling times. Also note that one valid solution of Eq.(4.1) (or Eq.(4.4) corresponds to one period-one LCO (or one period-one LCO with harmonics) of the original system Eq.(2.2). However, there may be other valid solutions to Eq.(4.1) (or Eq.(4.4), indicating the coexistence of period-one LCOs (or of period-one LCOs with harmonics). Furthermore, under the same system parameters, we may have valid solutions to Eq.(4.1) (or Eq.(4.4) and to some other similar nonlinear equation systems corresponding to other types of LCOs. However, Formulation 2 cannot be used to predict convergent, divergent or chaotic motions.

4.4 Results and Discussions

In this section, we present the applications of the point transformation formulations developed in this paper.

To demonstrate the effectiveness of the point transformation method, Formulations 1 and 2 are applied to a freeplay model. The system parameters under consideration are the same as those given in (3.1). The nonlinear restoring force $M(x_1)$ is given by (2.2) with $M_0 = 0$, $\delta = 0.5^o$, $M_f = 0$, and $\alpha_f = 0.25^o$, and the plunge is linear with $G(x_3) = x_3$.

The linear flutter speed $U_L^* = 6.2851$ is determined by solving the aeroelastic system for $M_0 = \delta = \alpha_f = 0$. For $U^* > U_L^*$, some of the eigenvalues in regions R_1, R_2 and R_3 have positive real parts. Thus, the solution is divergent. As U^* decreases below U_L^*, the real parts of all eigenvalues of systems in R_1 and R_3 are negative, but some eigenvalues of the system in R_2 may have positive real parts. Hence, for $U^* < U_L^*$, the aeroelastic system admits various nonlinear behaviors. When all eigenvalues of the system in region R_2 have negative real parts, a damped oscillation results, and the solution converges to its equilibrium point after the transients die out. However, when some of the eigenvalues of the system in R_2 have positive real parts, the solution could become a fixed point, a limit cycle oscillation or a chaotic motion.

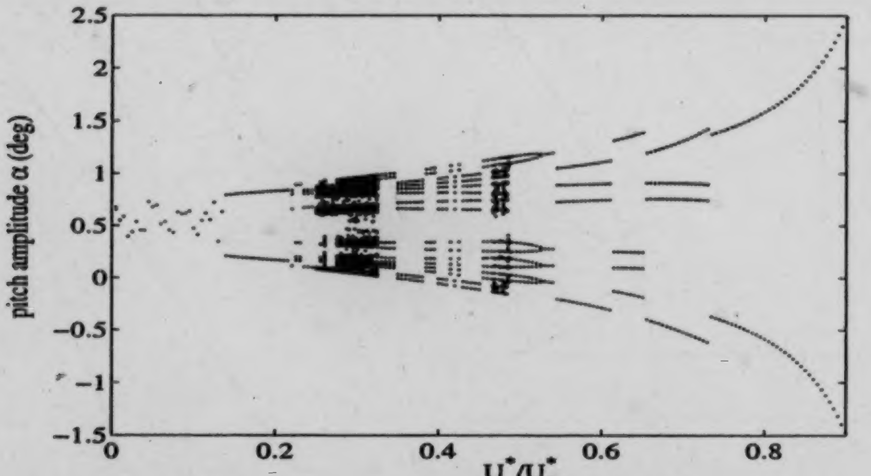

Figure 4.7: Bifurcation diagram for $\alpha(0) = 3^o$ and $\alpha'(0) = \xi(0) = \xi'(0) = 0$.

Numerous simulations over a wide range of velocities $0 < U^*/U_L^* < 1$ have been performed using Formulation 1. Note that the nonlinear aeroelastic response for the freeplay model depends strongly on the initial conditions. In this study, the value of $\alpha(0)$ is selected to be in the range of $\pm 5^o$ so that the steady-state solution for pitch and plunge are small enough for linear aerodynamics to be valid. For the results presented in this section, we report those using a non-zero value for $x_1(0)$ (i.e., $\alpha(0)$), and other values $x_i(0)$ for

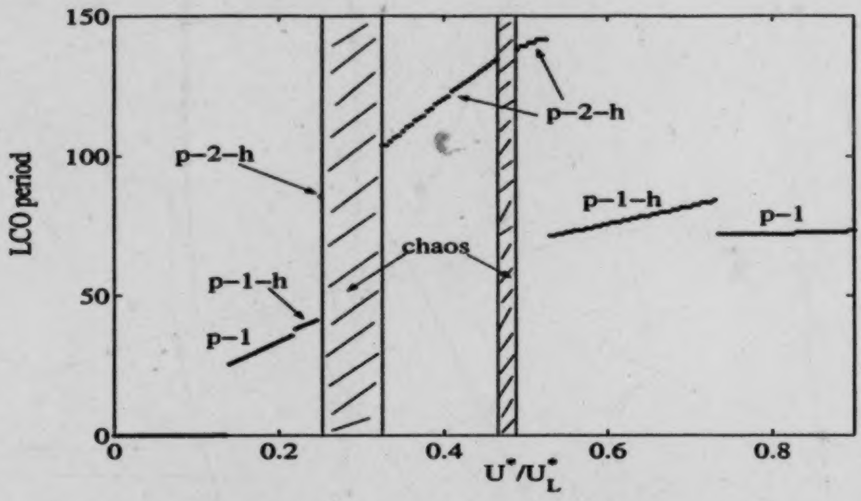

Figure 4.8: Period diagram for $\alpha(0) = 3^o$ and $\alpha'(0) = \xi(0) = \xi'(0) = 0$.

$i = 2, 3, ..., 8$ are set to zero. To illustrate the complex nonlinear system behaviors, we display a bifurcation diagram and a period diagram in Figs. 4.7 and 4.8. The results reported are obtained using Formulation 1, and they correspond to the choice of $\alpha(0) = 3^o$. In these two figures, the horizontal axis is the bifurcation parameter U^*/U^*_L. The vertical axis is the maximum and minimum values of the pitch angle when $\alpha' = 0$ in Fig. 4.7. In Fig. 4.8, we present the values of the LCO's period, and the classification of the steady-state solution is also described where p-n denotes a period-n LCO and p-n-h denotes a period-n LCO with harmonics.

For $0 < U^*/U^*_L \leq 0.13$, a single point is shown in the bifurcation diagram, which indicates that the solution converges to an equilibrium point. Since zero travelling time is determined by Formulation 1, this corresponds to a zero value for the period shown in Fig. 4.8. For example, when $U^* = 0.07U^*_L$, no positive solution for the travelling time can be found in Step 3 of Formulation 1. The zero time implies that the solution will not pass through the regions R_1 and R_3. Since the real parts of all eigenvalues of the system in R_2 are negative, the solution converges to the equilibrium point in R_2. For $0.14 \leq U^*/U^*_L \leq 0.215$, two amplitudes of α corresponding to the maximum and minimum of pitch

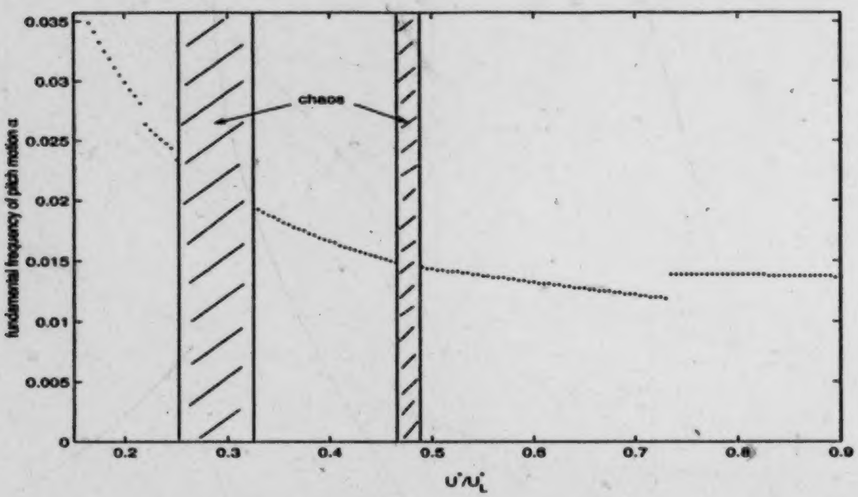

Figure 4.9: Frequency diagram for $\alpha(0) = 3^o$ and $\alpha'(0) = \xi(0) = \xi'(0) = 0$.

when $\alpha' = 0$ are shown in Fig. 4.7. This indicates that the solution is an LCO with period-one. It has one frequency with the period given in Fig. 4.8. For $0.216 \leq U^*/U_L^* \leq 0.245$, four amplitudes of α when $\alpha' = 0$ are shown in Fig. 4.7, and four switching points are detected by both formulations. Thus, the solution is a period-one LCO with harmonics, and the period, which is the same amount as the total travelling time, is shown in the corresponding period diagram. Note that there exists a small jump in the value of the LCO period when the solutions change from simple period-one to period-one with harmonics. Increasing U^* slightly to $U^* = 0.25U_L^*$, we observe a large jump in the period and eight values of α when $\alpha' = 0$ for the steady-state. Note that the period is almost double, indicating the appearance of a period doubling phenomenon. The solution becomes a period-two LCO with harmonics. The type of motion remains unchanged for $0.25 \leq U^*/U_L^* \leq 0.529$ except for two intervals when $0.252 \leq U^*/U_L^* < 0.325$ and $0.466 \leq U^*/U_L^* \leq 0.488$, where the solution becomes chaotic as shown in Fig. 4.7. A large number of amplitudes of α when $\alpha' = 0$ are detected in the chaotic regions, and they appear to lie along a vertical line in the bifurcation diagram. As U^* increases to $0.53U_L^*$, a large drop with a factor of two in the period occurs, and the solutions change

Case	U^*/U_L^*	Type of Motion	T	α_{max}	α_{min}
1	0.20	p-1	33.4464	0.8311	0.1689
2	0.22	p-1-h	37.9893	0.8872	0.1653
3	0.2510	p-2-h	83.5829	0.9063	0.1567
4	0.3	chaotic			

Table 4.1: Cases studies for the freeplay model

from period-two with harmonics to period-one with harmonics. A further small reduction in amplitude for pitch appears when $U^*/U_L^* = 0.732$, and the solution becomes a simple period-one LCO.

In order to illustrate the equivalence of both Formulations 1 and 2, four typical cases are selected for a more detailed examination. The results corresponding to the choice of initial condition $\alpha(0) = 3^o$ are presented in Table 4.1 and in Figs. 4.10–4.13. In Table 4.1, T represents the period, and α_{max} and α_{min} denote the absolute maximum and minimum values of pitch. The solutions obtained from both formulations are essentially identical, and they are in good agreement with the numerical solution obtained by the Runge-Kutta time-integration scheme. The results obtained from the point transformation method are denoted by filled circles in the figures, and the numerical solutions from the time-integration scheme are illustrated by solid lines. It should be noted that the time-step is usually chosen so that the time-integration method provides a stable numerical solution. Since for an aeroelastic system with freeplay, some of the eigenvalues of the system in region R_2 may have positive real parts, it is difficult to perform the standard stability analysis. In numerical simulations, the time-step Δt is chosen to be sufficiently small in order to ensure that a good accuracy is achieved. Here, Δt can only be selected numerically when the solution computed by Δt is essentially the same as those obtained using $\Delta t/2$. We found that the choice of Δt depends strongly on the bifurcation parameter. For the freeplay model presented in Table 4.1, the result by using $\Delta t = 0.3$ is found to be a good numerical solution for $U^* = 0.2U_L^*$.

As U^* increases to $0.25U_L^*$, a much smaller time-step $\Delta t = 0.0125$ must be used to obtain an accurate solution. The choice of Δt becomes more critical as the solution approaches chaos. Hence, solving an aeroelastic system using a numerical method becomes very time-consuming because a large number of computing steps per cycle is required especially when U^* nears the chaotic regions. Moreover, the appropriate value for Δt can be determined only through a sequence of numerical computations using Δt, $\Delta t/2$, $\Delta t/4$, ..., etc..

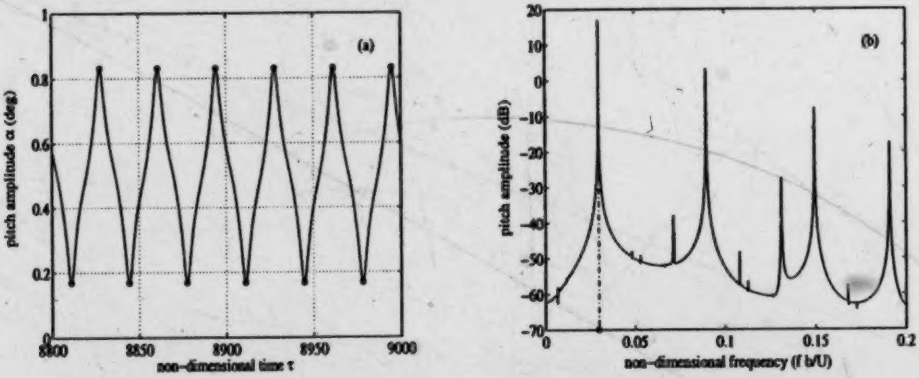

Figure 4.10: The time history (a) and power spectral density (b) of pitch motion for Case 1 in Table 4.1. Solid line: Runge-Kutta time-integration result; filled circle: point transformation result.

For Case 1, using Formulation 1 starting with $\alpha(0) = 3^o$, an LCO is detected after eight cycles. Four switching points and four travelling times are recorded, and they are similar to those displayed in Fig. 4.4(b). Since two amplitudes of α corresponding to $\alpha' = 0$ are determined(Fig.4.10), we conclude that the LCO is period-one with the frequency given by the nondimensional $f = 1/T = 0.0299$. The predicted frequency is in excellent agreement with that determined from the power spectral density (PSD) plot based on the time history of the numerical solution (Fig. 4.10(b)). When Formulation 2 is applied, the same amplitudes and frequency are obtained directly without the transient stage. As U^* increases to $0.22U_L^*$, six switching points and travelling times are recorded, and they are similar to those shown in Fig. 4.5(a). The existence of a smaller loop covering regions R_1 and R_2 indicates that the LCO has harmonics. Four amplitudes of α when $\alpha' = 0$ are detected, and they are in good agreement with the numerical solution (Fig. 4.11(a)). The frequency

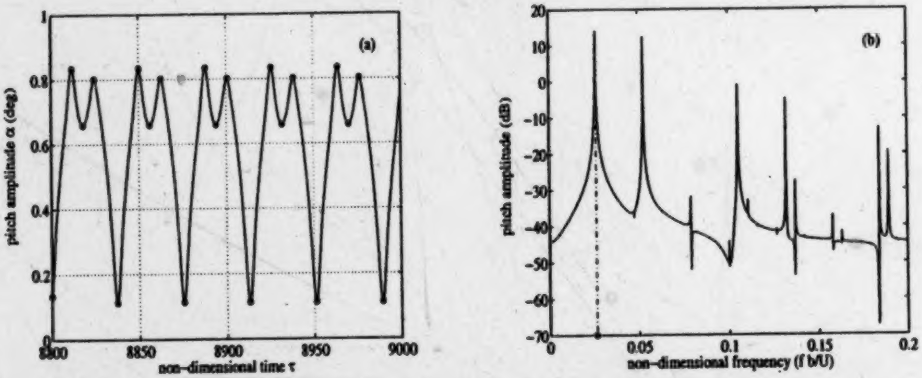

Figure 4.11: The time history (a) and power spectral density (b) of pitch motion for Case 2 in Table 4.1. Solid line: Runge-Kutta time-integration result; filled circle: point transformation result.

$f = 1/T = 0.0263$ agrees well with the first dominant frequency reported from the PSD plot shown in Fig. 4.11(b). The point transformation method confirms the existence of the harmonic components, but it is unable to predict the value of the harmonics which appears at $2f = 0.0526$ as shown in the PSD plot.

For Case 3, the period $T = 83.58$, which is almost double the period $T = 37.98$ reported for Case 2. Both formulations 1 and 2 indicate twelve switching points and eight amplitudes of α when $\alpha' = 0$. Moreover, the switching points displayed in the phase plane are similar to those shown in Fig. 4.6(b), where the complete loop covers the entire region twice, and it also contains two smaller loops covering regions R_1 and R_2. Hence, the resulting LCO is of period-two with harmonics. Fig. 4.12 shows the pitch amplitudes corresponding to $\alpha' = 0$ and the predicted frequency of the LCO.

When $U^* = 0.3U_L^*$, the values of switching points, travelling times, and the amplitudes of α obtained using Formulation 1 do not settle down to a repeated sequence even after a sufficiently long time when $\tau > 15,000$. The switching points appear to be on a vertical line in the phase space of $\alpha - \alpha'$ as shown in

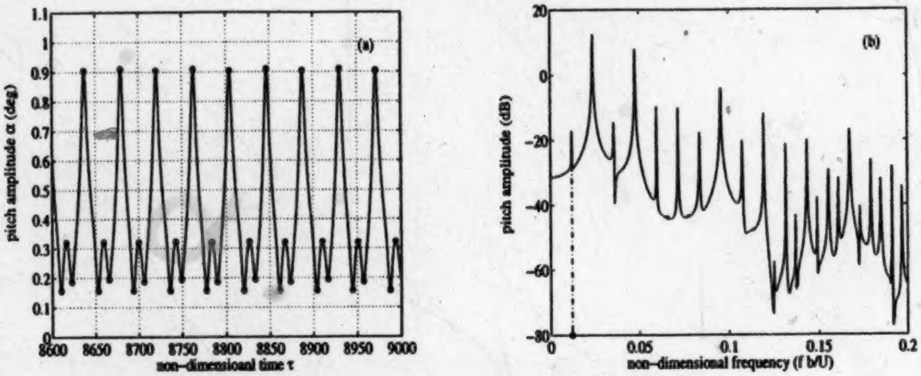

Figure 4.12: The time history (a) and power spectral density (b) of pitch motion for Case 3 in Table 4.1. Solid line: Runge-Kutta time-integration result; filled circle: point transformation result.

Fig. 4.13(a). The amplitudes of α when $\alpha' = 0$ also lie on a vertical line in the bifurcation diagram shown in Fig. 4.7. This suggests that the motion is chaotic. The chaos is confirmed from the phase trajectory of $\alpha - \alpha'$(Fig. 4.13(b)) resulting from the numerical time-integration scheme, and a typical "two-well potential" trajectory is observed. It is also worthwhile to note that the locations of the two inner loops are near the subspaces corresponding to $\alpha = 0.25^o$ and $\alpha = 0.75^o$. The PSD spectrum (Fig. 4.13(c)) from the numerical solution also confirms the existence of broadband frequency components, an indication of chaos. The particular case was also investigated by Price et al.[71], and they concluded that the motion is indeed chaotic.

One of the important features of the freeplay model is that the aeroelastic system admits the coexistence of stable LCOs. Table 4.2 reports the cases with the speed ratio $U^*/U_L^* = 0.2161, 0.22$ and 0.7. Starting with various initial conditions for $\alpha(0)$, different LCOs are predicted by Formulation 1. For example, for $U^* = 0.2161U_L^*$ and $\alpha(0) = 0.3^o$, the LCO converges to a period-one LCO with harmonics, where the frequency is given by $f = 0.0266$. Changing the initial condition to $\alpha(0) = 3^o$, the solution becomes a simple period-one LCO, and the frequency is given by $f = 0.0281$. For $U^* = 0.22U_L^*$, the solutions corresponding to the initials $\alpha(0) = \pm 3^o$ are of the same type,

Case	U^*/U_L^*	$x_1(0)$	Motion Type	T	α_{max}	α_{min}
1	0.2161	0.3	p-1-h	37.5344	0.8341	0.1149
2	0.2161	3	p-1	35.6384	0.8403	0.1597
3	0.22	-3	p-1-h	37.9893	0.8347	0.1128
4	0.22	3	p-1-h	37.9893	0.8872	0.1653
5	0.7	-0.5	p-1-h	81.9875	1.5179	0.2451
6	0.7	-5	p-1	72.05	1.2973	-0.2973

Table 4.2: Coexistence of limit cycle oscillations for the freeplay model

	t_1	t_2	t_3	t_4
initial guess	10	30	10	30
final solution	8.85644138	20.57834338	7.86033041	44.68989101
initial guess	5	20	10	20
final solution	20.18151269	21.03447205	10.70421369	22.42792629

Table 4.3: Results of Formulation 2 for Cases 5 and 6 in Table 4.2

namely period-one LCO with harmonics. Although the periods are identical, the amplitudes of α for $\alpha' = 0$ are different. The point transformation method confirms that the locations of the six switching points are actually different, and they are similar to those shown in Fig. 4.5(a) and (b). Note that the smaller loop covers regions R_1 and R_2 for Case 3 and regions R_2 and R_3 for Case 4. For $U^* = 0.7U_L^*$, four switching points are found by the point transformation method when $\alpha(0) = -0.5^o$ and -5.0^o.

However, the number of amplitudes of α when $\alpha' = 0$ are found to be four and two as shown in Fig.4.14(a) and (c), corresponding to the above initial conditions. This gives an indication of the existence of harmonic components for Case 5. The phase trajectory constructed from the numerical time-integration solution confirms the existence of a smaller loop as shown in Figs. 4.14(b) and (d). However, since the smaller loop exists only in the region R_1, no extra switching point is found in the point transformation method.

Although no explicit information concerning the initial condition is required in Formulation 2, the coexistence of stable LCOs can be determined by solving different sets of nonlinear equations or by changing the initial guess values to solve the same set of nonlinear equations. For $U^*/U_L^* = 0.2161$, solving Eq. (4.1) or (4.3) gives the LCO in Case 2, and the solution of Eq. (4.4) leads to the LCO in Case 1. Similarly, when $U^*/U_L^* = 0.22$, solving Eq. (4.4) gives the LCO in Case 3. In order to determine the motion type for Case 4, a different set of nonlinear equations has to be developed, since the switching points are now in a different sequence. Cases 5 and 6 correspond to two different types of LCOs, but both have four switching points, X_1, X_2, X_3

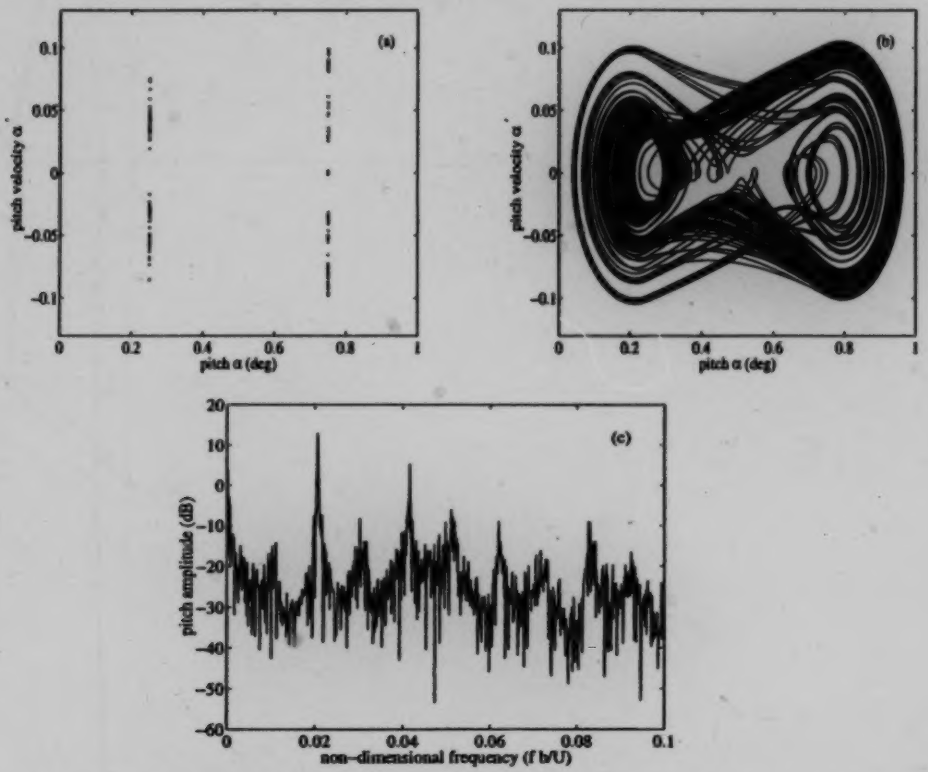

Figure 4.13: Chaotic motion of Case 4 in Table 4.1: (a) the switching points by using point transformation method; (b) the phase path by using Runge-Kutta time-integration; (c) the PSD plot.

and X_4. The switching points and travelling times are determined by solving the same nonlinear equations Eq. (4.1) in Formulation 2 but with different initial guess values. Table 4.3 reports the values of the initial guess which are

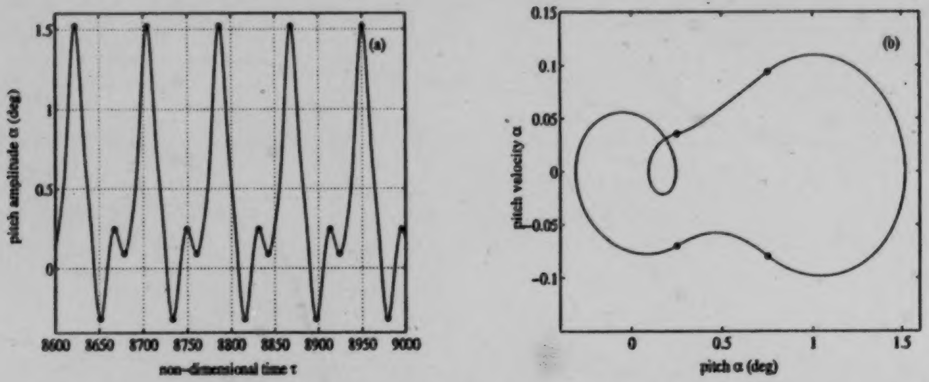

Figure 4.14: The time history (a) and phase path (b) for Case 5 in Table 4.2. Solid line: Runge-Kutta time-integration result; filled circle: point transformation result.

used for solving Eq. (4.1) in which other initial starting values $s_i (i = 1, 2, 3, 4)$ are set to zero. The corresponding solution for t_1, t_2, t_3 and t_4 are presented in Table 4.3. These results confirm the coexistence of two stable LCOs with two different periods, namely $T = 82$ and $T = 72$ for Cases 5 and 6 respectively.

4.5 Concluding Remarks

A mathematical technique based on the point transformation method has been developed to investigate the dynamic response of a self-excited two-degree-of-freedom aeroelastic system with structural nonlinearity represented by a freeplay stiffness. The method provides an accurate prediction since the switching points where the changes in linear sub-domains occur are located exactly, and the solution in each sub-domain is determined analytically. Two formulations are developed, and they have been applied to investigate the nonlinear aeroelastic behavior of a freeplay model. The results of the present study show that both formulations can accurately predict the frequency and amplitude of LCOs. Moreover, the formulations are also capable of detecting complex nonlinear behavior such as periodic motions with harmonics, period doubling, chaotic motions and the coexistence of stable limit cycles. Formulation 2 is particularly attractive since it can detect the presence of a particular type of LCO directly without considering the transients. From the illustrative examples presented in this paper, it is clearly demonstrated that analytic predictions are in excellent agreement with those resulting from a numerical time-integration scheme. The point transformation formulations are developed for an aeroelastic system with a structural nonlinearity in the pitch degree of freedom. However, the analysis can readily be extended to include nonlinearities in both degrees of freedom.

Chapter 5

Hysteresis Nonlinearities

5.1 Introduction

This chapter extends the point transformation technique developed in the previous chapter for freeplay models to investigate the dynamic response of the aeroelastic system with a hysteresis model. Since a hysteresis nonlinearity can be represented by a superposition of two freeplays, the location of switching points and the initial conditions are as important as they are in a freeplay model. As a piecewise linear system, a hysteresis model can also be analyzed by the point transformation method. Unlike a freeplay model with only three linear subsystems, a hysteresis model consists of six linear subsystems governing six regions in its state space. However, because of the special characteristics of a symmetric hysteresis model, at most four switching points are actually needed. Two formulations of the point transformation method are now developed for a hysteresis model by extending the formulations given in Chapter 4 for a freeplay model. Applications of these formulations to several examples are carried out to study the nonlinear behavior of the model, whose results confirm most of Chan's[14] numerical solutions. Furthermore, the point transformation technique not only detects the existence of the period-one, period-two, and period-four LCOs with harmonics components, but it is also capable to predict the amplitudes and frequencies of these motions. This point transformation method with the attractive features such as taking into account the initial conditions and locating the switching points exactly is the most suitable analytical method for investigating the aeroelastic response of systems containing piecewise linear restoring forces.

Similar to a numerical scheme for a freeplay model, the time-integration scheme for the hysteresis model cannot be proven stable since some of the eigenvalues corresponding to the linear subsystems may have positive real parts. Furthermore, the scheme in general cannot precisely locate the switching points where the change in linear regions occurs. However, for the cases reported in this paper, the numerical solutions obtained by using Runge-Kutta method are sufficiently accurate since the time steps are chosen to be sufficiently small. Thus, in the result and discussion section, the numerical results are used to cross check the predictions obtained by the point transformation method.

This chapter is organized as follows. First, the general implementation and two formulations of the point transformation method are developed for a hysteresis model in § 5.2. Then, these two formulations are applied to several examples of a hysteresis model and the corresponding discussion of the results are carried out in § 5.3. Finally, some concluding remarks are given in § 5.4.

5.2 The Point Transformation Method

A hysteresis model is a piecewise linear system whose state space consists of six linear regions, each of which is governed by a linear subsystem. The point transformation method, which is suitable for all piecewise linear systems, can be applied to this model.

Consider a hysteresis model given by (2.3). As x_1 increases, the system follows the upper branch of the hysteresis:

$$M(x_1) = \begin{cases} x_1 - \alpha_f + M_0 & x_1 < \alpha_f \\ M_0 & \alpha_f \leq x_1 \leq \alpha_f + \delta \\ x_1 - \alpha_f - \delta + M_0 & x_1 > \alpha_f + \delta \, . \end{cases}$$

On the other hand, as x_1 decreases, the system follows the lower branch of the hysteresis:

$$M(x_1) = \begin{cases} x_1 + \alpha_f + \delta - M_0 & x_1 < -\alpha_f - \delta \\ -M_0 & -\alpha_f - \delta \leq x_1 \leq -\alpha_f \\ x_1 + \alpha_f - M_0 & x_1 > -\alpha_f \ . \end{cases}$$

Thus, a hysteresis can be treated as two freeplays following specified directions. For the symmetric hysteresis nonlinearity as shown in Fig. 2.4, we have $x_1 - \alpha_f + M_0 = x_1 + \alpha_f + \delta - M_0$ and $x_1 - \alpha_f - \delta + M_0 = x_1 + \alpha_f - M_0$. For this hysteresis model, as x_1 increases, the state space consists of three linear regions $IR_i (i = 1, 2, 3)$, each of which corresponds to a linear subsystem:

$$\begin{aligned} IR_1 = \{X \in R^8 \mid x_1 < \alpha_f\} : &\qquad X' = AX + F_1 \\ IR_2 = \{X \in R^8 \mid \alpha_f \leq x_1 \leq \alpha_f + \delta\} : &\qquad X' = CX + F_4 \\ IR_3 = \{X \in R^8 \mid x_1 > \alpha_f + \delta\} : &\qquad X' = AX - F_1 \ . \end{aligned}$$

Similarly, as x_1 decreases, the three linear regions $DR_i (i = 1, 2, 3)$ of the state space are given by

$$\begin{aligned} DR_1 = \{X \in R^8 \mid x_1 < -\alpha_f - \delta\} : &\qquad X' = AX + F_1 \\ DR_2 = \{X \in R^8 \mid -\alpha_f - \delta \leq x_1 \leq -\alpha_f\} : &\qquad X' = CX - F_4 \\ DR_3 = \{X \in R^8 \mid x_1 > -\alpha_f\} : &\qquad X' = AX - F_1 \ . \end{aligned}$$

Here A and C are 8 by 8 constant matrices, and F_1 and F_4 are 8 by 1 constant vectors. The elements of A, C and F_i, $i = 1, 4$ are determined from the system parameters of the coupled aeroelastic equations, and they are given by

$$A = \begin{pmatrix} A_1 & A_2 \\ A_3 & A_4 \end{pmatrix}, \qquad C = \begin{pmatrix} C_1 & A_2 \\ A_3 & A_4 \end{pmatrix},$$

and $F_1 = (M_0 - \alpha_f)F$, $F_4 = M_0 F$, where the elements of the 4 by 4 block matrices for A_1, A_2, A_3, A_4 and the 8 by 1 vector F are defined in Chapter 4, and C_1 is given as follows

$$C_1 = \begin{pmatrix} 0 & 1 & 0 & 0 \\ a_{21} & a_{22} & a_{23} + jd_0\beta(\frac{\bar{\omega}}{U^*})^2 & a_{24} \\ 0 & 0 & 0 & 1 \\ a_{41} & a_{42} & a_{43} - jd_1\beta(\frac{\bar{\omega}}{U^*})^2 & a_{44} \end{pmatrix}.$$

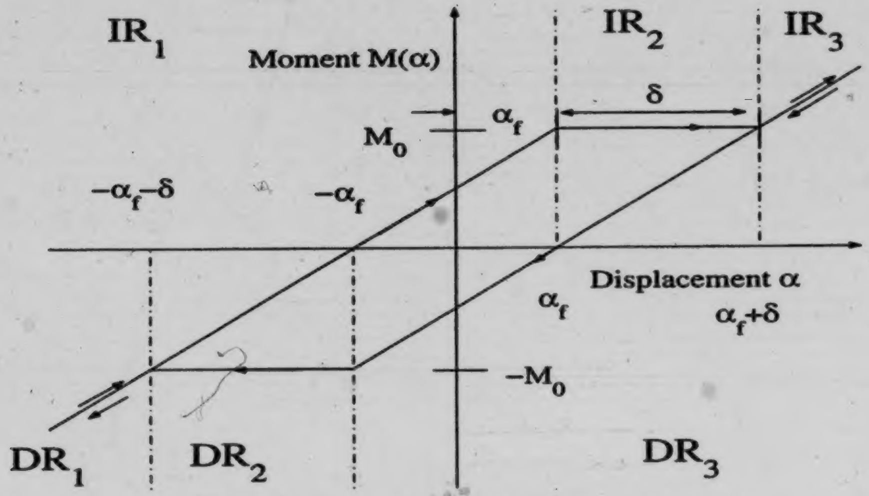

Figure 5.1: General sketch of a freeplay spring.

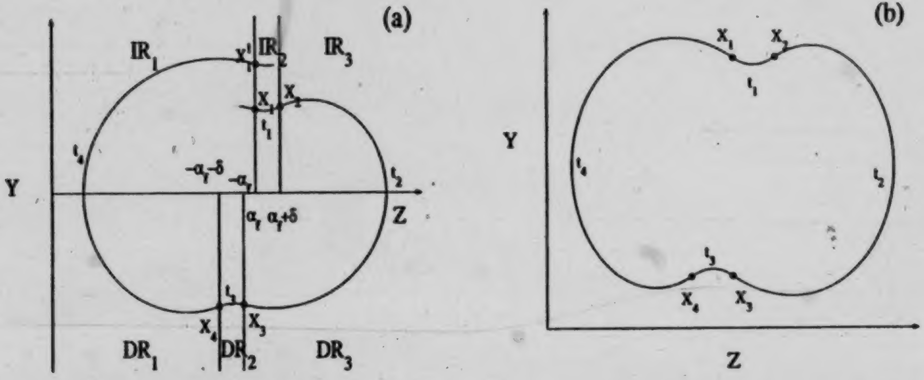

Figure 5.2: General trajectory (a) and a period-one LCO (b) of the aeroelastic system Eq.(2) with hysteresis structure. Filled circles: switching points.

Let the $Z - Y$ plane represent the eight dimensional state space with $Z = \{x_1\}$ and $Y = \{x_2, x_3, x_4, x_5, x_6, x_7, x_8\}$. Then the $Z - Y$ plane is divided by the sub-spaces $Z = -\alpha_f$, $Z = -\alpha_f - \delta$, $Z = \alpha_f$ and $Z = \alpha_f + \delta$ into six regions IR_1, IR_2, IR_3, DR_1, DR_2, and DR_3 as shown in Fig. 5.1. From the general idea of the point transformation method, similar to the discussion for a freeplay model presented in Chapter 4, six switching points should be identified since there are six regions. However, from the following discussion for a general trajectory as illustrated in Fig. 5.2(a), in fact only four of them are important and needed to be identified. When the system follows the upper branch of the hysteresis, its trajectory begins in IR_1 and passes through IR_2 into IR_3. As the value of x_1 changes from increasing to decreasing, the trajectory enters DR_3. The system then follows the lower branch of the hysteresis, correspondingly its trajectory returns through DR_2 into DR_1. Now, as the value of x_1 changes from decreasing to increasing, the trajectory re-enters IR_1. Let X_1 and X_2 be the points through which the trajectory enters IR_2 and IR_3 respectively. Let X_3 and X_4 be the points through which the trajectory leaves DR_3 and DR_2 respectively. These points (X_1, X_2, X_3 and X_4) are the switching points that needed to be identified, since they locate the places where the linear systems change. Notice that there is no need to locate the point where the trajectory passes from IR_3 to DR_3, since the linear systems in these two regions are the same. For the same reason, there is no need to identify the point where the trajectory passes from DR_1 to IR_1. Let t_1 be the travelling time of the trajectory (from X_1 to X_2) in region IR_2. Similarly, let t_2, t_3 and t_4 be the travelling times of the trajectory in regions $IR_3(DR_3)$, DR_2 and $DR_1(IR_1)$ respectively. The above procedure is then repeated, resulting in a set of new switching points X_1^1, X_2^1, X_3^1, X_4^1 and new values for the corresponding travelling times t_1^1, t_2^1, t_3^1, t_4^1. When the transients have diminished, we may observe a repetition of the switching points X_1, X_2, X_3, X_4 and the corresponding travelling times t_1, t_2, t_3, t_4 covering the entire region as shown in Fig. 5.2(b). Then the steady-state motion is classified as a period-one limit cycle oscillation (LCO). The frequency for this LCO can be determined by $f = 1/T$, where the period T is estimated by the sum of the travelling times (i.e., $T = t_1 + t_2 + t_3 + t_4$).

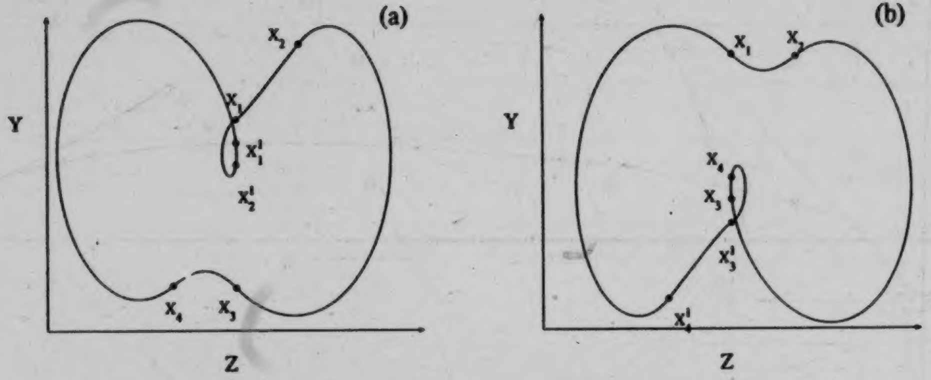

Figure 5.3: General trajectories for period-one with harmonics: (a) the smaller loop covers IR_1 and IR_2; (b) the smaller loop covers DR_1 and DR_2. Filled circles: switching points.

It is not necessary that the switching points and travelling times appear in the sequence as shown in Fig. 5.2(b). For example, the steady-state phase plane displayed in Fig. 5.3(a) contains six switching points. The additional two points X_1^1 and X_2^1 are introduced after completing the sequence as discussed in the previous paragraph. In this case, a complete loop in the phase-plane consists of six points X_1, X_2, X_3, X_4, X_1^1, X_2^1 and six corresponding travelling times t_1, t_2, t_3, t_4, t_1^1, t_2^1. Unlike the trajectory shown in Fig. 5.2(b), a complete loop covering the entire region for this case also contains a smaller loop covering the two regions IR_1 and IR_2. The smaller loop is defined as the one that covers only one or two regions. The resulting LCO is of period-one, since we observe only one complete loop covering the entire region. However, the presence of a smaller loop indicates that the LCO has a harmonic component. Since the LCO is of period-one, the frequency is estimated by $f = 1/T$ with $T = t_1 + t_2 + t_3 + t_4 + t_1^1 + t_2^1$. The typical feature of LCO with harmonics can be verified by the appearance of four values for α when $\alpha' = 0$. Fig. 5.3(b) shows a trajectory of period-one with harmonics, in which the smaller loop covers DR_2 and DR_3.

The point transformation method can be generalized in a straightforward manner to predict a period-n LCO or period-n LCO with harmonics(e.g. a

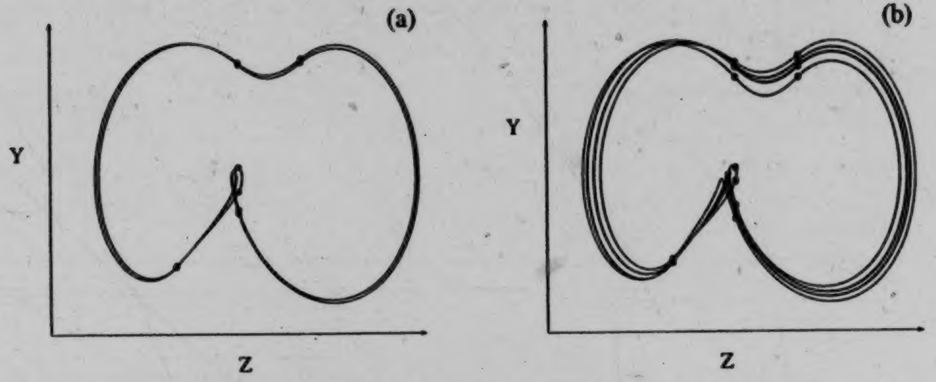

Figure 5.4: Trajectories for a period-two with harmonics (a) and a period-four with harmonics (b) LCOs. Filled circles: switching points.

period-two LCO with harmonics as shown in Fig. 5.4(a) and a period-four LCO with harmonics as shown in Fig. 5.4(b)), and the values of the frequency and maximum and minimum amplitudes can be estimated as well. If however, after a sufficiently long time, the sequence of switching points still does not repeat, it may indicate that the motion is chaotic.

Based on the above discussion of applying the point transformation to the aeroelastic system with the hysteresis stiffness, we present two approaches in the following subsections.

5.2.1 Formulation 1

Starting from the initial point of a trajectory, this formulation is developed to determine the travelling times and the switching points in each region. First, the travelling times are determined by solving a nonlinear equation. Then the switching points are calculated by the multiplication of a known matrix by a known vector. If the round-off error can be neglected, the formulation will produce the exact solution for the aeroelastic system. The detailed procedure is given as follows.

Step 0. Set the initial point $X_0 = (x_{01}, x_{02}, x_{03}, ..., x_{08})^T$. If $x_{02} > 0$, set $i = 1$ for $\alpha_f \le x_{01} \le \alpha_f + \delta$, $i = 2$ for $x_{01} > \alpha_f + \delta$ and $i = 4$ for $x_{01} < \alpha_f$; otherwise set $i = 2$ for $x_{01} > -\alpha_f$, $i = 3$ for $-\alpha_f - \delta \le x_{01} \le -\alpha_f$ and $i = 4$

for $x_{01} < -\alpha_f - \delta$. Set $X_i = X_0$, and go to step i.

Step 1. Solve nonlinear equations $\alpha_f + \delta = \{e^{Ct}X_1 + \mathcal{C}(t)F_2\}|_{(1)}$ and $\alpha_f = \{e^{Ct}X_1 + \mathcal{C}(t)F_2\}|_{(1)}$ separately for t. Here, $\{V\}|_{(n)}$ denotes the nth element of the vector V. Let the smallest positive solutions corresponding to the first and second equations be t^* and t^{**} respectively. If $t^* < t^{**}$, let $t_1 = t^*$, compute X_2 by $X_2 = e^{Ct_1}X_1 + \mathcal{C}(t_1)F_2$, and go to step 2. If $t^{**} < t^*$, let $t_3 = t^{**}$, compute X_4 by $X_4 = e^{Ct_3}X_1 + \mathcal{C}(t_3)F_2$, and go to step 4.

Step 2. First solve the nonlinear equation $\{e^{At}X_2 - \mathcal{A}(t)F_1\}|_{(2)} = 0$ for t, assign the smallest positive solution to t_u, and compute the maximum amplitude by $\alpha_{max} = \{e^{At_u}X_2 - \mathcal{A}(t_u)F_1\}|_{(1)}$. Then solve the nonlinear equation $-\alpha_f = \{e^{At}X_2 - \mathcal{A}(t)F_1\}|_{(1)}$ for t, assign the smallest positive solution to t_2, and compute X_3 by $X_3 = e^{At_2}X_2 - \mathcal{A}(t_2)F_1$. Go to step 3.

Step 3. Similar to Step 1, solve $\alpha_f = \{e^{Ct}X_3 + \mathcal{C}(t)F_2\}|_{(1)}$ and $\alpha_f + \delta = \{e^{Ct}X_3 + \mathcal{C}(t)F_2\}|_{(1)}$ separately for t. Let the smallest positive solutions corresponding to the first and second nonlinear equations be t^* and t^{**} respectively. If $t^* < t^{**}$, let $t_3 = t^*$, compute X_4 by $X_4 = e^{Ct_3}X_3 + \mathcal{C}(t_3)F_2$, and go to step 4. If $t^{**} < t^*$, let $t_1 = t^{**}$, compute X_2 by $X_2 = e^{Ct_1}X_3 + \mathcal{C}(t_1)F_2$, and go to step 2.

Step 4. Similarly to Step 2, first solve the nonlinear equation $\{e^{At}X_4 + \mathcal{A}(t)F_1\}|_{(2)} = 0$ for t, assign the smallest positive solution to t_l, and compute the minimum amplitude by $\alpha_{min} = \{e^{At_l}X_4 + \mathcal{A}(t_l)F_1\}|_{(1)}$. Then solve the nonlinear equation $\alpha_f = \{e^{At}X_4 + \mathcal{A}(t)F_1\}|_{(1)}$ for t, assign the smallest positive solution to t_4, and compute X_1 by $X_1 = e^{At_4}X_4 + \mathcal{A}(t_4)F_1$. Go to step 1.

The computations of e^{At} and $\mathcal{A}(t)$ can be found in Chapter 4. $\mathcal{C}(t)$ is defined as $\mathcal{C}(t) = \int_0^t e^{C(t-\tau)}d\tau$. For various U^*, the matrix C may have one pair of complex and six distinct real eigenvalues, or two pairs of complex and four real eigenvalues. For the former case, the computations of e^{Ct} and $\mathcal{C}(t)$ are similar to those for e^{At} and $\mathcal{A}(t)$, while for the latter case, they are similar to those for e^{Bt} and $\mathcal{B}(t)$ discussed in Chapter 4. In fact, there are a number of ways to evaluate an exponential of a matrix, and nineteen different methods are discussed by Moler and Van Loan[65]. Using the closed form for these computations yields an analytical formulation.

If no positive solution for the nonlinear equation can be found, the motion either diverges if the linear system has at least one positive real part eigenvalue, or converges to the equilibrium if the real parts of all the eigenvalues of the linear system are negative. When all transients are diminished and a repetition in the values of the switching points is observed, the correspond motion is an LCO. The amplitude and the period of the LCO can be predicted analytically. If after a sufficiently long time the repetition of the switching points can not be found and the values of the switching points remain bounded, the motion may be classified as chaotic.

5.2.2 Formulation 2

This formulation applies only after transients die out and LCO appears. For example, for a period-one LCO, the four switching points can be written as (notice that the switching points are different from those corresponding to a freeplay model):

$$X_1 = \begin{pmatrix} \alpha_f \\ s_1 \end{pmatrix} \quad X_2 = \begin{pmatrix} \alpha_f + \delta \\ s_2 \end{pmatrix} \quad X_3 = \begin{pmatrix} -\alpha_f \\ s_3 \end{pmatrix} \quad X_4 = \begin{pmatrix} -\alpha_f - \delta \\ s_4 \end{pmatrix}$$

where s_1, s_2, s_3 and s_4 are seven dimensional variable vectors representing the switching points in the subspace $\{X \in R^8 | x_1 = \alpha_f\}$, $\{X \in R^8 | x_1 = \alpha_f + \delta\}$, $\{X \in R^8 | x_1 = -\alpha_f\}$ and $\{X \in R^8 | x_1 = -\alpha_f - \delta\}$. Let $t_i (i = 1, 2, 3, 4)$ denote the corresponding travelling times. Then, t_i and $s_i (i = 1, 2, 3, 4)$ can be determined directly by solving the following system of nonlinear equations

$$\begin{cases} X_2 = e^{Ct_1} X_1 + C(t_1) F_4 \\ X_3 = e^{At_2} X_2 - A(t_2) F_1 \\ X_4 = e^{Ct_3} X_3 - C(t_3) F_4 \\ X_1 = e^{At_4} X_4 + A(t_4) F_1 \, . \end{cases} \tag{5.1}$$

Similar to a freeplay model, Eq.(5.1) can be reduced to a four dimensional system with only the travelling times t_1, t_2, t_3 and t_4 as variables:

$$\left\{\begin{aligned} \alpha_f &= \{H_1(t_1,t_2,t_3,t_4)G_1(t_1,t_2,t_3,t_4)\}|_{(1)} \\ \alpha_f+\delta &= \{H_2(t_1,t_2,t_3,t_4)G_2(t_1,t_2,t_3,t_4)\}|_{(1)} \\ -\alpha_f &= \{H_3(t_1,t_2,t_3,t_4)G_3(t_1,t_2,t_3,t_4)\}|_{(1)} \\ -\alpha_f-\delta &= \{H_4(t_1,t_2,t_3,t_4)G_4(t_1,t_2,t_3,t_4)\}|_{(1)} \,, \end{aligned}\right. \tag{5.2}$$

where H_i ($i = 1,2,3,4$) are 8 by 8 matrix functions of t_1, t_2, t_3 and t_4, G_i ($i = 1,2,3,4$) are 8 by 1 vector functions of t_1, t_2, t_3 and t_4. However, the expressions for H_i and G_i are different from those for a freeplay model and they are defined as

$$\begin{aligned} H_1(t_1,t_2,t_3,t_4) &= (I-e^{At_4}e^{Ct_3}e^{At_2}e^{Ct_1})^{-1} \\ H_2(t_1,t_2,t_3,t_4) &= (I-e^{Ct_1}e^{At_4}e^{Ct_3}e^{At_2})^{-1} \\ H_3(t_1,t_2,t_3,t_4) &= (I-e^{At_2}e^{Ct_1}e^{At_4}e^{Ct_3})^{-1} \\ H_4(t_1,t_2,t_3,t_4) &= (I-e^{Ct_3}e^{At_2}e^{Ct_1}e^{At_4})^{-1} \end{aligned}$$

where I denotes the identity 8 by 8 matrix.

$$\begin{aligned} G_1(t_1,t_2,t_3,t_4) =& e^{At_4}e^{Ct_3}e^{At_2}C(t_1)F_4 - e^{At_4}e^{Ct_3}A(t_2)F_1 \\ & - e^{At_4}C(t_3)F_4 + A(t_4)F_1 \\ G_2(t_1,t_2,t_3,t_4) =& - e^{Ct_1}e^{At_4}e^{Ct_3}A(t_2)F_1 - e^{Ct_1}e^{At_4}C(t_3)F_4 \\ & + e^{Ct_1}A(t_4)F_1 + C(t_1)F_4 \\ G_3(t_1,t_2,t_3,t_4) =& - e^{At_2}e^{Ct_1}e^{At_4}C(t_3)F_4 + e^{At_2}e^{Ct_1}A(t_4)F_1 \\ & + e^{At_2}C(t_1)F_4 - A(t_2)F_1 \\ G_4(t_1,t_2,t_3,t_4) =& e^{Ct_3}e^{At_2}e^{Ct_1}A(t_4)F_1 + e^{Ct_3}e^{At_2}C(t_1)F_4 \\ & - e^{Ct_3}A(t_2)F_1 - C(t_3)F_4 \,. \end{aligned}$$

The period is then given by $T = t_1+t_2+t_3+t_3$ and the frequency $f = 1/T$.

The amplitudes α_{max} and α_{min} of this period-one motion are given by

$$\begin{cases} \text{solve } \{e^{At_u}X_2 - \mathcal{A}(t_u)F_1\}|_{(2)} = 0 \text{ for } t_u \\ \alpha_{max} = \{e^{At_u}X_2 - \mathcal{A}(t_u)F_1\}|_{(1)} \\ \text{solve } \{e^{At_l}X_4 + \mathcal{A}(t_l)F_1\}|_{(2)} = 0 \text{ for } t_l \\ \alpha_{min} = \{e^{At_l}X_4 + \mathcal{A}(t_l)F_1\}|_{(1)} \ , \end{cases} \tag{5.3}$$

where $X_2 = H_2(t_1, t_2, t_3, t_4)G_2(t_1, t_2, t_3, t_4)$ and $X_4 = H_4(t_1, t_2, t_3, t_4)G_4(t_1, t_2, t_3, t_4)$. Similar formulations can be derived for other types of LCOs,

Formulation 1 requires initial conditions to compute the switching points. It should be noted that this formulation is not a time-integration numerical scheme and the solution of each linear subsystem is determined analytically. The general formulation given in §3.1 can be used to detect any type of motion including period-n, period-n with harmonics, and chaotic motions. Under the same system parameters, starting from different initial conditions, the trajectory may converge to different LCOs, which indicates the coexistence of the LCOs of the original system Eq.(2.2).

When Formulation 2 is applied, only the steady-state behavior is detected since no information with respect to the transient is recorded. This approach is more efficient if only the steady-state solution is of interest. However, the formulations given in Eqs.(5.2) and (5.3) are valid only for detecting a period-one motion. In order to detect other types of system motions, the formulation must be modified accordingly. Note that only the positive solutions (i.e. $t_i > 0$, $i = 1, 2, 3, 4$) to Eq.(5.2) are valid since the variables represent the travelling times. Also notice that one valid solution of Eq.(5.2) only implies that the original aeroelastic system Eq.(2.2) exhibits a period-one LCO. However, there may be more than one valid solutions to Eq.(5.2), indicating the coexistence of stable LCOs. Formulation 2 is not able to predict chaotic motion.

5.3 Case Studies and Discussions

Applications of Formulations 1 and 2 are made to system Eq.(2.2) with the system parameters: $\mu = 100$, $a_h = -1/2$, $x_\alpha = 1/4$, $\zeta_\xi = \zeta_\alpha = 0$, $r_\alpha = 0.5$, and $\bar{\omega} = 0.2$. The pitch angle is hysteresis with $M(x_1)$ defined in (2.3) in which $M_0 = 0.5^\circ$ or 0.02°, $\delta = 1.0^\circ$, and $\alpha_f = M_0 - 0.5\delta$. The plunge is linear with $G(x_3) = x_3$. The formulations presented in the previous section do not depend on the choice of parameters. The system parameters and the hysteresis constants discussed in this section are chosen so that the point transformation results can be compared with the numerical time-integration solutions reported by Chan[14].

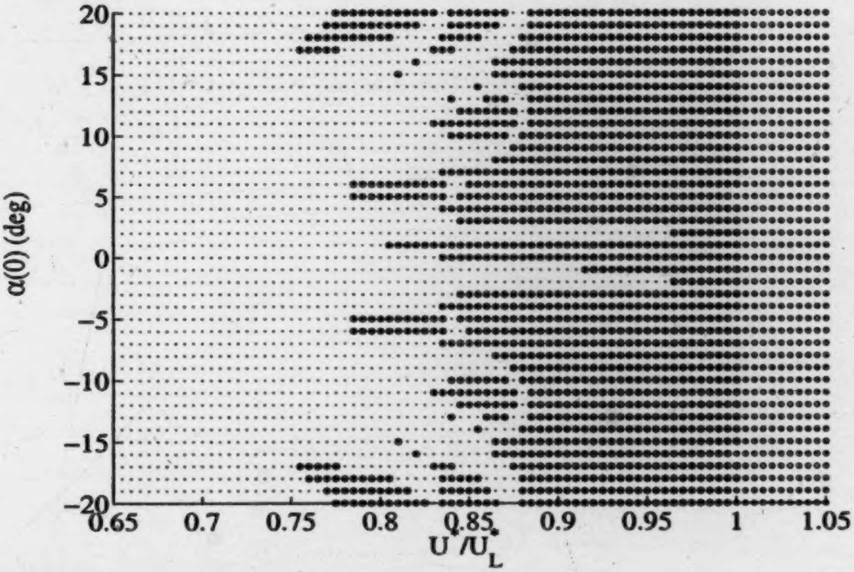

Figure 5.5: The flutter boundary diagram of an aeroelastic system with a hysteresis model. Filled dot: damped motion, star: LCO, open circle: divergent motion.

The flutter boundary diagram shown in Fig. 5.5 indicates several isolated pockets of LCOs inside the main flutter boundary, and this observation is similar to that reported by Chan[14]. For velocity ratios (U^*/U_L^*) greater than 1, since the linear subsystems in all six regions have positive real parts,

Case	U^*/U^*_L	M_0	$x_1(0)$	Motion Type	T	α_{max}	α_{min}
1	0.80	0.5^o	1^o	p-1-h	98.6429	2.6826^o	-2.4182^o
2	0.8097	0.5^o	1^o	p-1-h	99.0333	2.8342^o	-2.4640^o
3	0.8098	0.5^o	1^o	p-2-h	200.6	2.8614^o	-2.2844^o
4	0.81085	0.5^o	1^o	p-4-h	386.35	2.8646^o	-2.4241^o
5	0.2	0.02^o	3^o	chaotic			

Table 5.1: Case studies for a hysteresis model.

the system motions are divergent. As U^* decreases below U^*_L, the real parts of all eigenvalues of systems in IR_1, IR_3, DR_1, and DR_3 are negative, but some eigenvalues of the systems in IR_2 and DR_2 may have positive real parts, which results in various nonlinear behavior: damped motion, LCO or chaotic motion. In the main LCO region, the point transformation method detects a pattern of four distinct switching points and two values of maximum and minimum values of α when $\alpha' = 0$ for the steady-state, indicating a simple sinusoidal motion with a dominant frequency. For the motions on the inside LCO pockets, the harmonic components are detected and period-one, period-two and period-four LCOs are detected for various velocity ratios and initial conditions.

Several cases are selected for detailed discussion with results shown in Tables 5.1 and 5.2. Table 5.1 includes cases of various LCOs and the period doubling phenomena leading to a chaotic motion, while Table 5.2 shows the coexistence of two distinct LCOs under the same system parameters but with different initial conditions. The initial values other than $x_1(0)$ are set to zero for cases reported in Tables 5.1 and 5.2, and $M_0 = 0.5^o$ for cases in Table 5.2. Notice that in Tables 5.1 and 5.2, "p-n" denotes "period-n motion", "p-n-h" denotes "period-n with harmonics motion", T represents the period, and α_{max} and α_{min} denote the absolute maximum and minimum values of the pitch angle. The results obtained by using Formulation 1 presented in § 2.1 agree with those obtained by using Formulation 2, except for Case 5 in Table 5.1 since

Case	U^*/U_L^*	$x_1(0)$	Motion Type	T	α_{max}	α_{min}
1	0.80	1^o	p-1-h	98.6429	2.6826^o	-2.4182^o
2	0.80	5^o	p-1-h	98.6429	2.4182^o	-2.6826^o

Table 5.2: Coexistence of limit cycle oscillations for a hysteresis model.

Formulation 2 cannot be used to predict chaos. Besides the tables, the results are also shown in Figs. 5.3–5.9. Similar to the figures for a freeplay model reported in Chapter 4, the filled circles denote the predicted results obtained by using the formulations, and the solid lines represent the numerical solutions obtained by using the fourth-order Runge-Kutta time-integration scheme.

For Case 1 in Table 5.1, starting with $\alpha(0) = 1^o$ and using Formulation 1, an LCO is detected after seven cycles. Four different switching points and the corresponding four travelling times are detected. From our discussion presented in section § 2, this LCO is of period-one. However, four different values

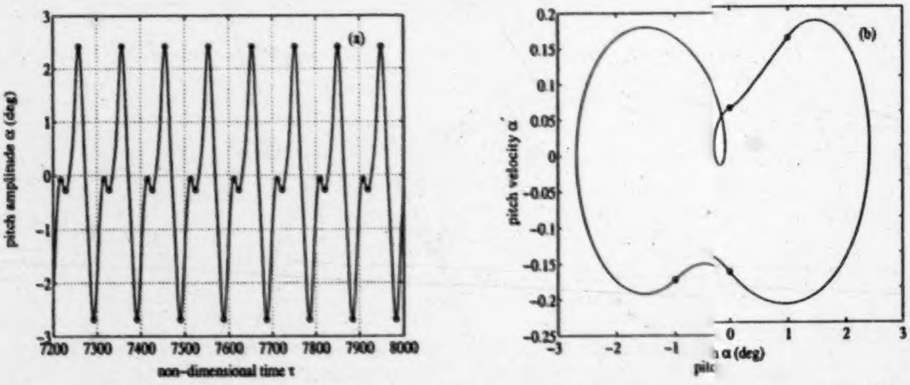

Figure 5.6: Case 1 in Table 5.1: (a) time history; (b) trajectory of α-α'. Solid line: numerical result, filled circles: point transformation method.

of α when $\alpha' = 0$ are detected. These maximum and minimum amplitudes of α are in good agreement with the time history obtained by using the fourth-order Runge-Kutta scheme as shown in Fig.5.6(a). These four values of α when $\alpha' = 0$ indicate the existence of a harmonic component. The trajectory of α - α' and the switching points are displayed in Fig.5.6(b). From the trajectory, we know that the complete loop covers the entire region once, and there is a smaller loop in region IR_1, indicating the existence of an harmonic component. Hence, the LCO of Case 1 is of period-one with harmonics. The frequency estimated by $f = 1/T = 1/98.6433 = 0.0101$ can be verified by the power spectral density (PSD) plot from the time history.

In Case 2, six switching points, six travelling times and four different values of α when $\alpha' = 0$ are recorded after the transients diminished. The location of the switching points and the trajectory of α-α' are similar to those shown in Fig.5.3(a). As discussed in § 2, this LCO is classified as period-one with harmonics. The frequency $f = 1/T = 1/99.0333 = 0.0101$ agrees well with the dominant frequency reported from the PSD plot shown in Fig.5.7(b). The numerical solution and the maximum and minimum amplitudes of α when $\alpha' = 0$ are displayed in Fig.5.7(a).

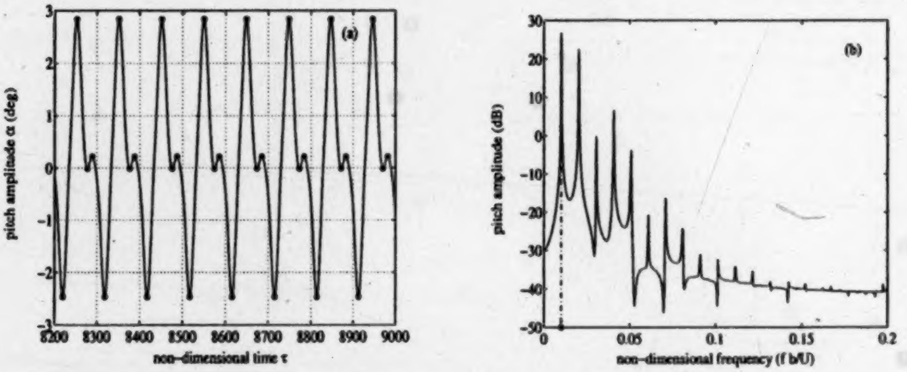

Figure 5.7: Case 2 in Table 5.1: (a) time history. (b) PSD plot. Solid line: numerical result, filled circles: point transformation method.

The total travelling time, $T = 200.6$, in Case 3, is almost double the value $T = 99.0333$ reported for Case 2. Both Formulations 1 and 2 indicate ten switching points and eight amplitudes of α when $\alpha' = 0$. Moreover, the switching points displayed in the trajectory are similar to those shown in Fig.5.4(a), where the complete loop covers the entire region twice, and it also contains smaller loops covering regions DR_1 and DR_2. Hence, the resulting LCO is of period-two with harmonics. When the value of U^* increases to

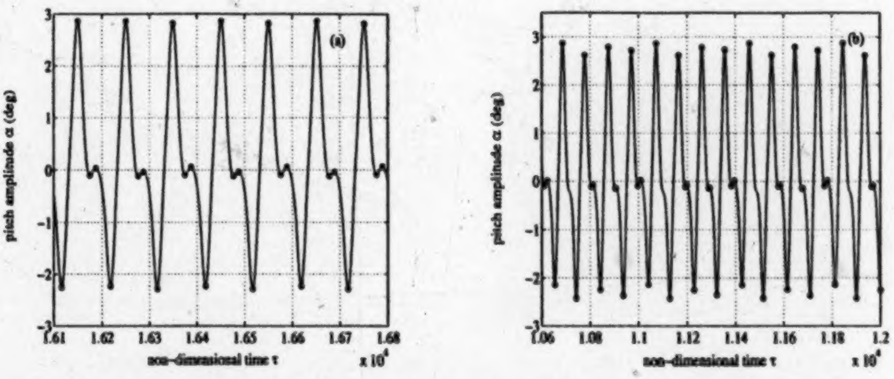

Figure 5.8: Time histories for Cases 3 and 4 in Table 5.1: (a) Case 3; (b) Case 4. Solid line: numerical result, filled circles: point transformation method.

$0.81085U_L^*$, a period-four with harmonic motion is found. Eighteen switching points and fourteen amplitudes of α when $\alpha' = 0$ are found by using both formulations. The location of the switching points and the trajectory of $\alpha - \alpha'$ are similar to Fig.5.4(b). Figs.5.8(a) and (b) present the pitch amplitudes corresponding to $\alpha' = 0$ for Cases 3 and 4, respectively.

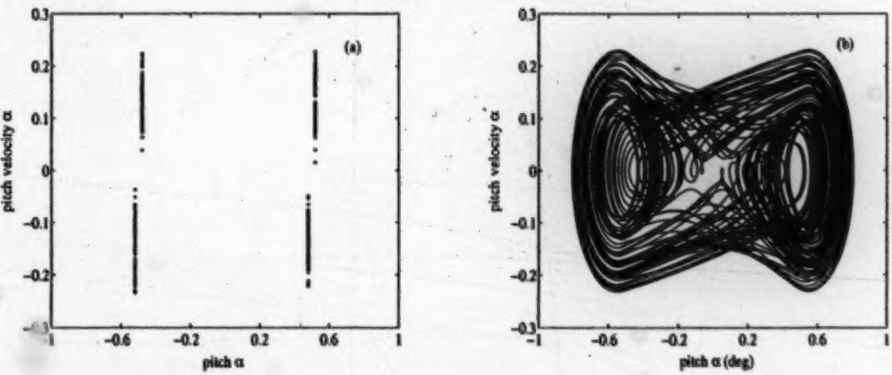

Figure 5.9: Case 5 in Table 5.1: (a) switching points; (b) phase projection of α-α'.

By decreasing the value of M_0, a chaotic motion(Case 5) is detected. For this case, the values of switching points, travelling times and the amplitudes of α obtained using Formulation 1 do not settle down to a repeated sequence even after a very long time $\tau > 15,000$. The values of the switching points appear to be on four vertical lines in the state space as shown in Fig. 5.9(a). Notice that there are only two vertical lines corresponding to a chaotic motion in a typical freeplay model. This suggests that the motion is chaotic. The chaos is confirmed from the trajectory of α-α' (Fig. 5.9(b)). The trajectory results from the numerical scheme, and a typical "two-well potential" trajectory is observed. The PSD plot from the numerical solution is similar to Fig. 4.13(c) in Chapter 4 and also confirms the existence of broadband frequency components, an indication of chaos. This case has been carefully studied in [14].

Table 5.2 demonstrates the coexistence of stable limit cycles which correspond to $U^*/U_L^* = 0.80$. Using Formulation 1, starting from $\alpha(0) = 1°$ and $5°$, the motions converge to two different period-one LCO with harmonics. The trajectories of α-α' and the switching points for Case 1 are displayed in Fig.5.6(b). For Case 2, the trajectory of α-α' and the switching points are similar to Fig.5.6(b) with a smaller loop in region DR_3. There are two sets of valid solutions to Eq.(5.2), namely $\{t_1 = 6.31,\ t_2 = 55.54,\ t_3 = 10.96,\ t_4 = 25.84\}$ and $\{t_1 = 10.96,\ t_2 = 25.84,\ t_3 = 6.31,\ t_4 = 55.54\}$, which correspond to Cases 1 and 2 respectively.

5.4 Concluding Remarks

A mathematical technique based on the point transformation method is introduced to investigate the dynamical response for a self-excited two-degree-of-freedom aeroelastic system with structural nonlinearity represented by a hysteresis stiffness. The method provides an accurate result since the solutions for the corresponding linear subsystems are determined accurately by using analytical techniques and the switching points where the change in linear regions occur are located exactly. Two formulations are developed, and they can be applied to predict the frequency and amplitude of LCOs. Moreover, the formulations are also capable of detecting complex aeroelastic behaviors such as the periodic motion with harmonics, period doubling, chaotic motions and the coexistence of stable limit cycles. The effectiveness of the proposed method has been demonstrated by verifying that the formulations can be used to predict the complex nonlinear behaviors of an aeroelastic system with hysteresis nonlinearity. The point transformation technique can also be extended for hysteresis stiffnesses in both degree of freedom.

Chapter 6

Error Analysis of RK's Discretizations of Aeroelastic Systems

6.1 Introduction

In the previous three chapters, analytical techniques were developed and applied to aeroelastic systems with structural nonlinearities. However, the solution of system Eq.(2.2) can also be obtained by numerical time-integration methods since the aeroelastic system has been reformulated into an initial value ODE problem in Chapter 2. Naturally, a question arises: why do we need the theoretical prediction when the numerical result can be obtained? Answering this question is the task of this chapter.

Some reasons are obvious. For example, for the aeroelastic system with cubic springs investigated in Chapter 3, the amplitudes and frequencies of the LCOs can be deduced directly from the analytical prediction formulas (3.6) and (3.2). When using a numerical method, we have to plug in the system parameters and the initial conditions first to obtain a time history and then apply Fourier Transforms or similar techniques to analyze the numerical solutions. Moreover, while the effects on the amplitudes and frequencies due to the change in the system parameters can be easily determined from the prediction formulas, such information cannot be achieved from a numerical approach. On the other hand, some other reasons need more efforts to reveal. For example, as we will show shortly, errors of the numerical schemes for some systems may be quite large and in some cases the behaviors of the numerical results and the analytical solutions may completely contradict to each other.

It was pointed out as early as in 1860 by George Boole that, for nonlinear differential equations, a surprisingly big difference exists between Differential Calculus and Difference Calculus. Yamaguti and Matano[92], Maeda[63] and Yamaguti and Maeda[91] showed that under certain conditions, while the orbit of the differential equation $\frac{dy}{dx} = f(y)$ is asymptotically stable, its Euler's discretization produces, for some time step h, a dynamical system which is chaotic in the sense of Li and Yorke[54]. Yamaguti and Matano's work[92] was generalized by Hata[28] to systems of differential equations. They all revealed that a stable equilibrium point in the original autonomous ordinary differential equation(s) could turn into a source of chaos in the corresponding difference equation(s).

This chapter mainly concentrates on errors of the fourth-order Runge-Kutta method (RK-method) since the method is commonly used to solve most engineering problems. Before we carry out the accuracy analysis, we have to analyze the stability, which is the most important step for the analysis of a numerical scheme. The definition for the stability we used is the A-stability, the most often referred in numerical analysis literature(e.g.[21]). Simply put, a method is stable if it produces a bounded solution when the solution of the differential equation is bounded; otherwise, it is unstable. A method that is stable for some, but not all, values of the parameter is conditionally stable; one that is stable for all values of the parameter is said to be unconditionally stable; one that is not stable for any value of the parameter is called unconditionally unstable. The error we discussed in this chapter is the global error. We calculate the error by either estimating the difference of the solutions to the consistent equation with that to the original equation, or comparing directly the numerical result with the exact solution to the original equation.

In § 6.2, the errors of the RK-schemes are analytically estimated for a simple sinusoidal motion. It shows that, although the scheme is conditionally stable for this equation, it introduces amplitude decaying and period elongation errors. For the more complicated aeroelastic system with cubic springs, the scheme is conditionally stable and introduces the amplitude and period errors as well. The stability of the numerical scheme for a rapidly time-variant system is analyzed in § 6.3 and significant differences between numerical and analytical results are observed. In a case when the scheme changes from being stable to being unstable, the numerical solution becomes divergent for any given time step, while the exact solution is convergent. For piecewise linear systems, such as freeplay and hysteresis models, the numerical results from RK-scheme are compared against the analytical solutions obtained from the PT-method in § 6.4. We find that the numerical scheme may lead to chaos, while the analytical solution is actually a fixed point and vice versa. Finally, some concluding remarks are given in § 6.5.

6.2 A Simple Sinusoidal Motion and Aeroelastic Systems with Cubic Springs

A simple sinusoidal motion is the simplest oscillation problem with a known frequency and analytical solution. It is interesting to see that the fourth-order RK-scheme may cause stability and accuracy concerns for this problem. In this section, we provide theoretical analyses for both the stability and accuracy of the scheme. The analytical technique derived in this section can be used to estimate the numerical error for a simple sinusoidal motion, and can be extended to high-dimensional systems such as the system of dynamic equilibrium equations discussed by Bathe and Wilson[4]. Although the sinusoidal motion has also been studied in [4], their study concentrated on the central difference method, the Houbolt method, the Wilson θ method and the Newmark integration procedure and the accuracy analysis was only based on numerical observations. In this section, more subtle and more detailed analysis for errors is carried out for the fourth-order RK-scheme. This section also reveals the fact that the accuracy of numerical results rely heavily on the ratio h/T, where T is the period of the motion.

The equation for a simple sinusoidal motion is given by

$$y''(t) + \omega^2 y(t) = 0 \,, \tag{6.1}$$

which can be rewritten in a form of the first-order ODE system

$$\begin{cases} y_1' = y_2 \\ y_2' = -\omega^2 y_1 \end{cases} \,, \tag{6.2}$$

with $y_1 = y$ and $y_2 = y'$. Then, the fourth-order RK's discretization of Eq.(6.2) is

$$\begin{cases} y_1^{n+1} = y_1^n + h y_2^n - \frac{1}{2}h^2\omega^2 y_1^n - \frac{1}{6}h^3\omega^2 y_2^n + \frac{1}{24}h^4\omega^4 y_1^n \\ y_2^{n+1} = y_2^n - \omega^2 h y_1^n - \frac{1}{2}h^2\omega^2 y_2^n + \frac{1}{6}h^3\omega^4 y_1^n + \frac{1}{24}h^4\omega^4 y_2^n \,, \end{cases} \tag{6.3}$$

where h is the time step, and y_1^{n+1} and y_2^{n+1} denote the numerical values of y_1 and y_2 at $t = (n+1)h$. The matrix form of the above scheme is

$$Y_{n+1} = RY_n \,, \tag{6.4}$$

where Y_{n+1}, Y_n and R are given by

$$Y_{n+1} = \begin{pmatrix} y_1^{n+1} \\ y_2^{n+1} \end{pmatrix} , \qquad Y_n = \begin{pmatrix} y_1^n \\ y_2^n \end{pmatrix} ,$$

and

$$R = \begin{pmatrix} 1 - \frac{1}{2}\omega^2 h^2 + \frac{1}{24}h^4\omega^4 & h - \frac{1}{6}h^3\omega^2 \\ -\omega^2 h + \frac{1}{6}h^3\omega^4 & 1 - \frac{1}{2}\omega^2 h^2 + \frac{1}{24}h^4\omega^4 \end{pmatrix} .$$

Thus, the stability of the scheme (6.3) can be determined by the norms of the eigenvalues of R. More specifically, if at least one of them is greater than 1, the scheme is unstable; otherwise, it is stable. For this case, the eigenvalues of R are

$$\lambda_{1,2} = (1 - \frac{1}{2}\omega^2 h^2 + \frac{1}{24}\omega^4 h^4) \pm i\omega(h - \frac{1}{6}\omega^2 h^3) \,,$$

with the norm

$$\|\lambda_{1,2}\| = 1 - \frac{1}{72}(2\pi)^6 r^6 + \frac{1}{576}(2\pi)^8 r^8 \,, \quad r = \frac{h}{T} \,,$$

less than 1 if $\frac{h}{T} \leq \frac{\sqrt{2}}{\pi}$. Hence, the scheme Eq.(6.3) is conditionally stable and is stable provided $h/T \leq 0.4501$.

In order to analytically estimate the errors of the numerical results, we derive a consistent equation which includes only the leading terms of errors in the damping and frequency terms of the discretization Eq.(6.3). Using Taylor expansion theory, we obtain the desired consistent equation:

$$y''(t) + \frac{1}{72}\omega^6 h^5 y'(t) + (\omega^2 - \frac{1}{60}\omega^6 h^4)y(t) = 0 , \tag{6.5}$$

where $\frac{1}{72}\omega^6 h^5$ is the leading term for amplitude (damping) error and $-\frac{1}{60}\omega^6 h^4$ is the leading term for frequency (period) error.

Now, given the initial conditions $y(0) = y_1^0$ and $y'(0) = y_2^0$, the exact solution to the original equation Eq.(6.1) is

$$y(t) = Asin(\omega t + \phi) , \tag{6.6}$$

with the amplitude A, period T and phase shift ϕ given by

$$\begin{cases} A = \sqrt{(y_1^0)^2 + (\frac{y_2^0}{\omega})^2} \\ T = \frac{2\pi}{\omega} \\ \phi = tan^{-1}(\frac{y_1^0}{y_2^0}\omega) . \end{cases} \tag{6.7}$$

On the other hand, the numerical solution to Eq.(6.1), i.e. the solution to the consistent equation Eq.(6.5) can be written as

$$y(t) = ANsin(\beta t + \phi N) , \tag{6.8}$$

where the amplitude AN, period TN, and phase shift ϕN are given by

$$\begin{cases} AN = e^{\alpha t}\sqrt{(y_1^0)^2 + (\frac{y_2^0 - y_1^0\alpha}{\beta})^2} \\ TN = \frac{2\pi}{\beta} \\ \phi N = tan^{-1}(\frac{y_1^0}{y_2^0 - y_1^0\alpha}\beta) , \end{cases} \tag{6.9}$$

with

$$\begin{cases} \alpha = -\frac{64\pi^6}{144}r^5 \\ \beta = \omega\sqrt{1 - \frac{16\pi^4}{60}r^4 - \frac{1024\pi^{10}}{10368}r^{10}} \\ r = \frac{h}{T} . \end{cases} \tag{6.10}$$

From (6.9), we have the amplitude decaying error since α is always negative, the amplitude AN converges to zero as t approaches to infinity. This also suggests that the RK-scheme may not lead to accurate solution for long time computations. Furthermore, the speed of the amplitude decaying depends on the value of α, which depends on the ratio h/T. The larger the ratio h/T is, the faster the decaying speed is. For the period error, as the frequency β of the solution to the consistent equation is smaller than that of the original motion, the period obtained from the numerical scheme is enlarged, indicating period elongation error. Similarly, as ϕN is different from ϕ, the phase shift error is also introduced. Therefore, the relative errors, AD (amplitude), TD (period) and ϕD (phase shift), of the scheme (6.3) for the sinusoidal motion with the initials $y(0) = y_0$ and $y'(0) = y_1$ can be defined by

$$\begin{cases} AD = \frac{|A-AN|}{A} \\ TD = \frac{|TN-T|}{T} \\ \phi D = \frac{|\phi-\phi N|}{\phi} \, . \end{cases} \tag{6.11}$$

In order to demonstrate the magnitude of errors of the RK-scheme for the simple sinusoidal motion, we consider a specific case with $\omega = 2\pi$, $y_1^0 = 1$ and $y_2^0 = 0$. From (6.7), (6.9) and (6.11), the relative errors for amplitude (AD), period(TD) and phase shift (ϕD) can be computed by

$$\begin{cases} AD = \left|1 - e^{\alpha t}\sqrt{1 + (\frac{\alpha}{\beta})^2}\right| \\ TD = \left|\frac{2\pi}{\beta} - 1\right| \\ \phi D = \left|\frac{\frac{\pi}{2} - \tan^{-1}(-\frac{\beta}{\alpha})}{\frac{\pi}{2}}\right| \, . \end{cases} \tag{6.12}$$

First, the amplitude decaying percentage (AD) versus the logarithm of time based on 10 ($log_{10}t$) is plotted in Fig. 6.1 for different time steps. These results are obtained by using the formula (6.12) with the values of α and β given by (6.10). From Fig. 6.1, when $h/T \leq 0.01$, the amplitude from RK-scheme agrees well with that of the original solution for the time t up to $t = 10^5$. As h/T increases, the time when the amplitude decaying error becomes unacceptable

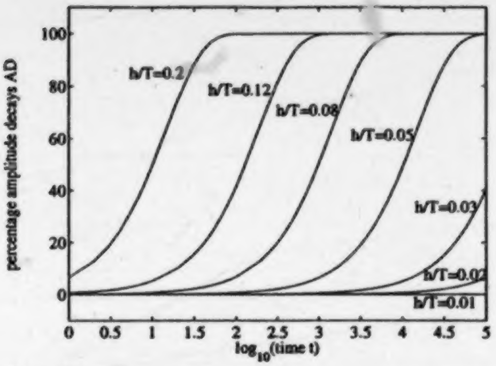

Figure 6.1: Analysis of the amplitude decaying percentage error of the fourth-order RK-scheme for a simple sinusoidal motion.

decreases dramatically. When $h/T \geq 0.2$, the numerical scheme leads to a totally different solution–a fixed point–as the amplitude dies out very quickly to zero at time $t = 100$.

Next, the period elongation percentage and the phase shift percentage errors are plotted against the ratio h/T in Fig. 6.2, since these errors are independent of time t. Compared to the amplitude error, these two types of errors are not so sensitive to the ratio. From Fig. 6.2(a), the period error can be neglected for $h/T \leq 0.02$. Although the phase shift error as shown in Fig. 6.2(b), which has not been addressed by other researchers, is very small, it does come into effect when $h/T \geq 0.04$.

The above analysis suggests that the ratio h/T plays an important role in the stability and accuracy of the numerical scheme. The larger h/T is, the larger the numerical errors (in amplitude, period and phase shift errors) are. On the other hand, the smaller h/T we use, the more accurate numerical solution we have.

In fact, the stability and accuracy analyses carried out in the above are also suitable for other systems, such as a general system of equations $M\ddot{U}(t) + C\dot{U}(t) + KU(t) = R(t)$ with the matrices M, C and K and the vectors U and R defined in [4].

For aeroelastic systems with cubic springs, which is in eight-dimension and

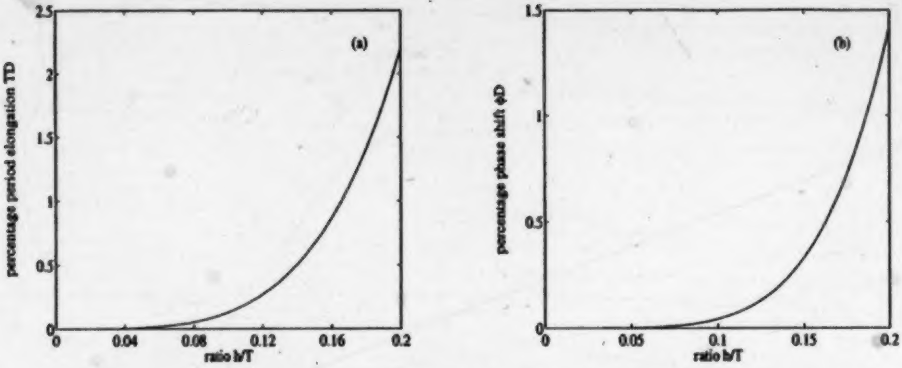

Figure 6.2: Analysis of (a) the period elongation percentage error and (b) the phase shift percentage error of the fourth-order RK-scheme for a simple sinusoidal motion.

includes cubic nonlinear terms, the analyses for stability and accuracy of the scheme are more complicated.

The original system Eq.(2.2) with cubic stiffness can be written as

$$X' = AX + FX^3 , \tag{6.13}$$

where A and F are coefficient matrices, $X = (x_1, x_2, ..., x_8)^T$ and $X^3 = (x_1^3, x_2^3, ..., x_8^3)^T$. The fourth-order RK's discretization of Eq.(6.13) can be simply expressed as

$$X_{n+1} = RX_n + f(A, F, h, X_n^3) , \tag{6.14}$$

where X_{n+1} and X_n are the numerical values of the vector variable X at time $t = (n+1)h$ and $t = nh$ respectively, X_n^3 is the numerical value of X^3 at $t = nh$,

$$R = I + hA + \frac{1}{2!}h^2A^2 + \frac{1}{3!}h^3A^3 + \frac{1}{4!}h^4A^4 .$$

and f is a nonlinear function of A, F, h and X_n^3. The stability of the scheme Eq.(6.14) can then be determined by the norms of the eigenvalues of R. For example, in Case 1 with $\delta = 0.01$ reported in Chapter 3, the scheme is stable provided $h/T < 0.12$, where $T = 74.8462$. Compared to $h/T < 0.4501$ for the sinusoidal motion, the stability condition of scheme (6.14) is much stronger.

For the accuracy, the analytical error estimates similar to (6.11) cannot be obtained by using the above accuracy analysis derived for a sinusoidal motion. However, we expect similar errors for this system since it is a nonlinear dynamic system in eight-dimension. Taking Case 1 with $\delta = 0.01$ discussed in Chapter 3 as an example, when $h/T = 0.05$ the amplitude error is 0.9486%, 77 times less than that for the sinusoidal motion with the same value of h/T and the same computation time $t = 10^4$, while the period error, 0.8675%, is 25 times larger than that for the sinusoidal motion with the same h/T. Similar to the scheme for the sinusoidal motion, it leads to more accurate numerical results when using smaller time steps. However, it should be pointed out that there is no reference frequency in the self-excited system and T is unknown before the numerical computation is carried out.

6.3 A Rapidly Time-Variant System

For the simple sinusoidal motion and the aeroelastic system with cubic springs, when h/T is sufficiently small, the numerical error will be acceptable for a finite time interval. However, there are some cases in which even with small value for h/T, the numerical result may not be reliable. A rapidly time-variant system investigated in this section provides such an example that, no matter how small the time step h is, the numerical solution always turns out to be divergent while the original motion is convergent.

The rapidly time-variant system is a linear time-variant system with exponential variation in stiffness term:

$$x''(t) + e^t x(t) = 0 . \tag{6.1}$$

This system arises from many engineering problems such as flexible link manipulators and tethered satellites[69].

The analytical solution to Eq.(6.1) can be obtained by the variable substitution method. Similar to the discussion in Li[53], by a substitution

$$\tau = 2\sqrt{e^t} , \tag{6.2}$$

Eq.(6.1) is then transformed into Bessel's equation of order 0:

$$\tau^2 x''(\tau) + \tau x'(\tau) + (\tau^2 - 0^2)x(\tau) = 0 \,. \tag{6.3}$$

Thus, a general solution to the original system Eq.(6.1) can be written as:

$$x(t) = c_1 J_0(2\sqrt{e^t}) + c_2 Y_0(2\sqrt{e^t}) \,, \tag{6.4}$$

where c_1 and c_2 are determined by the initial conditions and J_0 and Y_0 are Bessel's functions of the first and the second kind of order 0. As the limits of both $J_0(2\sqrt{e^t})$ and $Y_0(2\sqrt{e^t})$ are zero as time t approaches to infinity, for all nonzero initial conditions the motion converges to zero as t approaches to infinity.

Fig. 6.3 shows a typical motion of this rapidly time-variant system with the initial conditions $x(0) = 0$ and $x'(0) = 0.1$. The amplitude decays from about 0.075 at the beginning to almost zero at time $t = 20$, which confirms the theoretical assertion that the asymptotic behavior of the motion is zero. Furthermore, from the graph, we also observe that the period T of the cycles decreases rapidly to zero as t increases. Hence, for any given fixed time step h, h/T increases rapidly as t increases. Therefore, the numerical scheme will not be able to catch sufficient points sooner or later for a cycle, which suggests the possible failure of the scheme. To demonstrate this point in detail, the fourth-order RK-scheme is then again derived and the stability of the scheme is theoretically analyzed.

To derive the RK-scheme, the original system Eq.(6.1) is written in a form of the first-order ODE system

$$\dot{X} = A(t)X \tag{6.5}$$

with $X = (x, x')^T$ and

$$A(t) = \begin{pmatrix} 0 & 1 \\ -e^t & 0 \end{pmatrix} .$$

Then, the fourth-order RK-scheme, similar to (6.4), can be written into a simple form:

$$X_{n+1} = B(n,h)X_n \,, \tag{6.6}$$

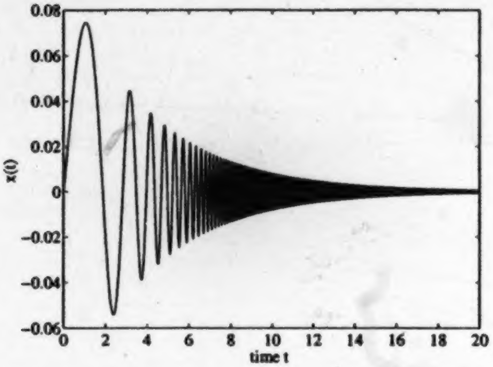

Figure 6.3: The exact motion of a rapidly time-variant system Eq.(6.1) with $x(0) = 0$ and $x'(0) = 0.1$.

where X_{n+1} and X_n are the numerical values of X at time $t = (n+1)h$ and $t = nh$ respectively, and $B(n,h)$ is a time- and step-related matrix:

$$\begin{pmatrix} a & b \\ c & d \end{pmatrix},$$

with a, b, c and d are functions of n and h:

$$\begin{aligned}
a =& 1 - \frac{1}{6}h^2e^{nh} - \frac{1}{3}h^2e^{nh+\frac{1}{2}h} + \frac{1}{24}h^4e^{2nh+\frac{1}{2}h} \\
b =& h - \frac{1}{6}h^3e^{nh+\frac{1}{2}h} \\
c =& -\frac{1}{6}he^{nh} - \frac{2}{3}he^{nh+\frac{1}{2}h} + \frac{1}{12}h^3e^{2nh+\frac{1}{2}h} - \frac{1}{6}he^{nh+h} + \frac{1}{12}h^3e^{2nh+\frac{3}{2}h} \\
d =& 1 - \frac{1}{3}h^2e^{nh+\frac{1}{2}h} - \frac{1}{6}h^2e^{nh+h} + \frac{1}{24}h^4e^{2nh+\frac{3}{2}h}\,.
\end{aligned}$$

Let

$$\lambda_1 = \frac{1}{2}(a+d) + \frac{1}{2}\sqrt{(a+d)^2 - 4(ad-bc)}$$

and

$$\lambda_2 = \frac{1}{2}(a+d) - \frac{1}{2}\sqrt{(a+d)^2 - 4(ad-bc)}$$

be the eigenvalues of $B(n,h)$. Then, the stability of the scheme (6.6) is determined by $\|\lambda_1\|$ and $\|\lambda_2\|$, which depend on the computation time $t = nh$. Fig. 6.4 displays $\|\lambda_1\|$ against the time $t = nh$ for time steps $h = 0.1$, 0.01, and 0.001. The corresponding plots exhibit the same pattern as they all begin with

1 then decrease to 0.5 and finally blow up rapidly to infinity. It seems that, no matter how small the time step h is, the norm of the eigenvalue λ_1 always becomes greater than 1 and then increases to infinity as time t increases. In fact, this assertion is strictly valid since

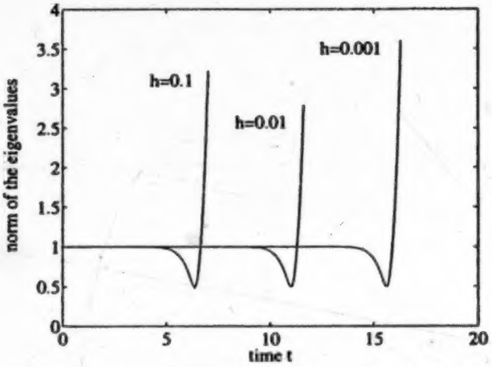

Figure 6.4: The norm of the eigenvalues of the transition matrix of the scheme

$$
\begin{aligned}
\|\lambda_1\| \geq & \frac{1}{2}(a+d) \\
\geq & 1 + \frac{1}{48}h^4 e^{2nh+\frac{1}{2}h} + \frac{1}{48}h^4 e^{2nh+\frac{3}{2}h} - \frac{1}{12}h^2 e^{nh+h} - \frac{1}{3}h^2 e^{nh+h} - \frac{1}{12}h^2 e^{nh+h} \\
\geq & 1 + \frac{1}{24}h^4 e^{2nh+\frac{1}{2}h} - \frac{1}{2}h^2 e^{nh+h} \\
\geq & 1 + \frac{1}{24}h^4 e^{2nh} - \frac{1}{2}h^2 e^{\frac{3}{2}nh} \\
\geq & \frac{1}{24}h^2 e^{\frac{3}{2}nh}(h^2 e^{\frac{1}{2}nh} - 12) \longrightarrow \infty \quad (n \to \infty)
\end{aligned}
$$

As $\|\lambda_1\| \geq \|\lambda_2\|$, the scheme (6.6) changes from being stable to being unstable as the computation time t increases, and therefore for large time t, the numerical results become meaningless.

In order to examine the significant differences between the exact and the numerical motions, we plot out the numerical solutions for the Eq.(6.6) with the initial condition $x_1^0 = 0$ and $x_2^0 = 0.1$ and with the time steps $h = 0.1, 0.01$, and 0.001 in Fig. 6.5. Taking Fig. 6.5(b) as an example, although the first several cycles of the graph agree well with the exact motion (Fig. 6.3), the graph decreases rapidly to zero (at $t = 10$) and becomes divergent finally (at $t = 12$).

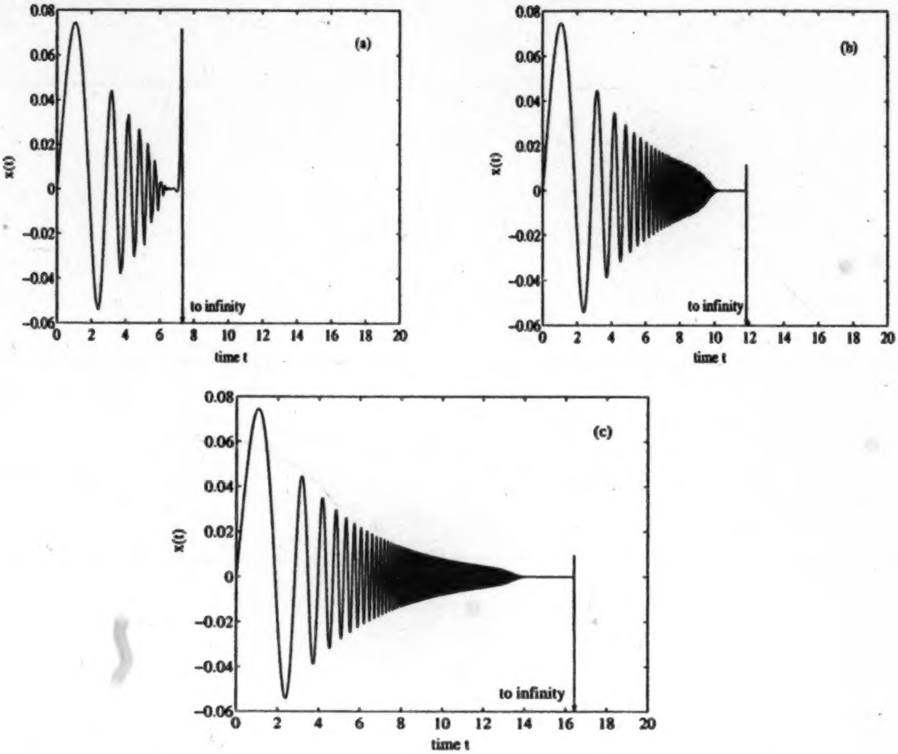

Figure 6.5: Numerical results for time steps (a) $h = 0.1$, (b) $h = 0.01$, and (c) $h = 0.001$.

This phenomenon can be explained by the behavior of the corresponding curve of $\|\lambda_1\|$ for $h = 0.01$ in Fig. 6.4, which shows that the scheme is stable for $t = 0$ to $t = 11.5$ and is unstable for $t \geq 11.5$. The other two graphs (Fig. 6.5(a) and (c)) behave similarly to that in Fig. 6.5(b). No matter how small the time step h is, the numerical result always becomes divergent, while the exact motion decreases and converges to zero gradually and smoothly as shown in Fig. 6.3. The error (difference between the numerical and exact solutions) of the scheme for $h = 0.01$ is displayed in Fig. 6.6, showing that the error grows rapidly to infinity as t increases. Hence, the numerical result is not acceptable no matter how small the chosen time step is. In fact, the Eq.(6.5) can not be solved correctly by Runge-Kutta method with an uniform time step.

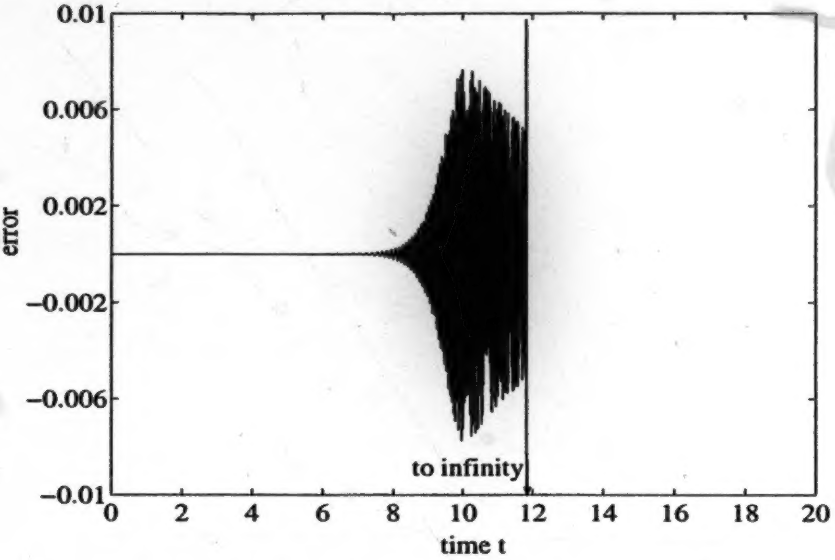

Figure 6.6: The numerical error of the scheme for $h = 0.01$.

6.4 An Aeroelastic System with A Piecewise Linear Model

In the previous sections, theoretical analyses have been carried out for the RK-schemes for several types of systems. We showed that stable schemes with small time steps usually provide sufficiently accurate numerical results for a finite time interval, unstable schemes, on the other hand, may result in numerical solutions qualitatively different from the exact motions. In this section, we focus on the error of the RK-scheme for an aeroelastic system with a freeplay model. This model, represented by a piecewise linear function, is not differentiable at the switching points. Although generally speaking the RK-method can always be applied and the numerical result may be accurate for some cases, the numerical scheme has not been proven stable and the numerical error cannot be estimated analytically. The stability cannot be analyzed easily since the eigenvalues of the system in the freeplay region may have positive real parts, which means that the RK-scheme could become unstable for the subsystem in that region. In the following discussion, the solutions resulting from the point transformation method are used as the exact solutions to compare with the numerical results. We will show that, based on several case studies, the fourth-order RK-scheme gives inconsistent numerical solutions when various time steps are used, confirming the problems of applying numerical schemes to piecewise continuous systems.

In order to concentrate on the numerical errors, without loss of generality, we consider a simplified version of the example in Chapter 4 by keeping only the first four variables, x_1, x_2, x_3 and x_4. More specifically, by leaving the ratio $r = (U_L^*/U^*)^2$ as a system parameter and evaluating all the others, this simplified system can be written as

$$X' = DX + F(X) \ , \tag{6.1}$$

with

$$D = \begin{pmatrix} 0 & 1 & 0 & 0 \\ 0.016 & -0.026 & 0.0029 + 0.0014r & 0.013 \\ 0 & 0 & 0 & 1 \\ -0.016 & -0.013 & -0.0029 - 0.0013r & -0.013 \end{pmatrix} ,$$

and

$$F(X) = \begin{cases} F_1(X) & \text{for} \quad x_1 < \alpha_f \\ F_2(X) & \text{for} \quad \alpha_f \le x_1 \le \alpha_f + \delta \\ F_3(X) & \text{for} \quad x_1 > \delta \ , \end{cases}$$

where

$$F_1(X) = \begin{pmatrix} 0 \\ -0.0334rx_1 + 0.00015r \\ 0 \\ 0.0084rx_1 - 0.000037r \end{pmatrix} , \quad F_2(X) = \begin{pmatrix} 0 \\ 0 \\ 0 \\ 0 \end{pmatrix} ,$$

and

$$F_3(X) = \begin{pmatrix} 0 \\ -0.0334rx_1 + 0.00044r \\ 0 \\ 0.0084rx_1 - 0.00011r \end{pmatrix} , \qquad \alpha_f = 0.0044 \ , \qquad \delta = 0.0087 \ .$$

Then, similar to the discussion in Chapter 4, the state space of the system Eq.(6.1) consists of three regions, each of which is governed by a strictly linear subsystem:

$$\begin{aligned}
R_1 &= \{X \in R^4 \mid x_1 < 0.0044\} : & X' &= DX + F_1(X)\,, \\
R_2 &= \{X \in R^4 \mid 0.0044 < x_1 < 0.0131\} : & X' &= DX + F_2(X)\,, \\
R_3 &= \{X \in R^4 \mid x_1 > 0.0131\} : & X' &= DX + F_3(X)\,.
\end{aligned}$$

Therefore the stability of the scheme can be analyzed by investigating the schemes for each subsystem. If there exists a time step h such that the schemes for all subsystems are stable, the scheme for the whole system may be stable. However, in the following we will show that for some cases such time step h cannot be found, and therefore the scheme may become unstable. Detailed discussions are given as follows.

The subsystem in R_1 can be written as

$$X' = AX + F1\,, \tag{6.2}$$

where

$$A = \begin{pmatrix} 0 & 1 & 0 & 0 \\ 0.016 - 0.0334r & -0.026 & 0.0029 + 0.0014r & 0.013 \\ 0 & 0 & 0 & 1 \\ -0.016 + 0.0084r & -0.013 & -0.0029 - 0.0013r & -0.013 \end{pmatrix},$$

and

$$F1 = \begin{pmatrix} 0 \\ 0.00015r \\ 0 \\ -0.000037r \end{pmatrix}.$$

The fourth-order RK-scheme for this subsystem written in a simplified form is

$$X_{n+1} = RX_n + Q(h, A, F1)\,, \tag{6.3}$$

where Q is a function of h, A and $F1$, and

$$R = I + hA + \frac{h^2}{2}A^2 + \frac{h^3}{6}A^3 + \frac{h^4}{24}A^4\,. \tag{6.4}$$

As the stability is determined by the eigenvalues of R, the scheme for this subsystem is stable for $0.01 < U^*/U_L^* < 1$ provided $h < 0.08$ since the norms of the eigenvalues of R are less than 1 when $h < 0.08$. Similar analysis can be carried out for the scheme for the subsystem in R_3, and the same conclusion is reached as well.

On the other hand, the scheme for the subsystem in R_2 can be written in the form similar to Eq.(6.4) with

$$R = I + hD + \frac{h^2}{2}D^2 + \frac{h^3}{6}D^3 + \frac{h^4}{24}D^4 \,. \tag{6.5}$$

The condition of h for the scheme to be stable in this region is complicated, depending on the value of the ratio U^*/U_L^*. The following discussion of the numerical error concentrates on three cases for $U^*/U_L^* = 0.02$, 0.12, and 0.4. Therefore, only the stability conditions for these three values of the ratio are reported. For $U^*/U_L^* = 0.02$, the scheme is stable when $0.31 \leq h \leq 1$; for $U^*/U_L^* = 0.12$, it is stable when $5 \leq h \leq 10$; for $U^*/U_L^* = 0.4$, the scheme is unconditionally unstable. For all three cases, the scheme for the subsystem in R_2 either is unconditionally unstable or requires $h > 0.08$ to be stable, which is contradict to the stability condition of the schemes for the subsystems in R_1 and R_3. Thus, for any given time step h, the stability condition of the scheme for the subsystems in R_1, R_2 and R_3 cannot be all satisfied.

The reason we choose these three cases lies in the fact that they are typical according to the bifurcation diagram as shown in Fig.6.7. Notice that r in Eq.(6.1) is the bifurcation parameter. This diagram, where the x-axis is the ratio of the velocities U^*/U_L^* and the y-axis is the maximum and minimum amplitudes for x_1, is computed for system Eq.(6.1) with the initial condition $x_1(0) = 0.01170190$, $x_2(0) = 0.00014569$, $x_3(0) = -0.00024094$ and $x_4(0) = 0.00001137$ by Formulation 1 of the point transformation method described in § 4.3.1. Notice that the unit for the amplitude has been transformed from radian to degree. From this diagram, when $U^*/U_L^* = 0.02$, 0.03, 0.07, 0.08, and 0.09, the motions may be classified as fixed points, while for the rest of $U^*/U_L^* \in (0, 0.2)$, the graph indicates that the motions are chaotic. When $U^*/U_L^* \in (0.2, 1)$, the motion is either period-one LCO or period-one with harmonics LCO. For all $U^*/U_L^* \geq 1$, the motions are divergent. Although this bifurcation diagram is very different from that of the original eight-dimensional system as shown in Fig.4.7, it still captures the essential features of the nonlinear dynamic responses, such as the fixed point, period-one LCO, period-one with harmonics LCO and chaotic motion.

Notice that there may be three fixed points for the whole system since each linear subsystem has one fixed point. However, through the following theoretical analysis, the fixed point of the whole piecewise linear system is unique.

The fixed point X_0^1 of the subsystem in R_1, obtained by solving $DX + F_1(X) = 0$, is

$$X_0^1 = \left(0.005\frac{3277+1432r}{3545+1583r}, 0, -0.01\frac{9040+121r}{3454+1583r}, 0\right)^T .$$

Similarly, the fixed points X_0^2 and X_0^3 of the subsystems in R_2 and R_3 are

$$X_0^2 = (0,0,0,0)^T \quad \text{and} \quad X_0^3 = \left(0.55\frac{87+38r}{3545+1583r}, 0, -1.1\frac{240+r}{3545+1583r}, 0\right)^T$$

respectively. As the first component of X_0^1 is greater than 0.0045 for $r > 0$, X_0^1 is in fact in R_2, which means that this fixed point can never be reached by any motion of the whole piecewise linear system. Similarly, X_0^2 cannot be a fixed point of the whole system since it is in R_1. With the first component greater than 0.0132 for $r > 0$, X_0^3 is the only possible fixed point of the whole system since it is within its own subsystem's domain, R_3.

Next, the numerical solutions using the fourth-order RK-scheme with different time steps for three selected cases $U^*/U_L^* = 0.02$, 0.12 and 0.4 are carefully examined. The results are reported in Table 6.1, where the initial conditions are $x_1(0) = 0.01170190$, $x_2(0) = 0.00014569$, $x_3(0) = -0.00024094$ and $x_4(0) = 0.00001137$ for Cases 1 and 2, and $x_1(0) = 0.01700663$ and $x_2(0) = x_3(0) = x_4(0) = 0$ for Case 3. The corresponding results obtained by using PT-method are reported in Table 6.2. In these two tables, "$t = 70$ →fixed" means that "when t exceeds 70, the motion stays at the unique fixed point of the system"; "p-1" means "period-one motion"; "p-1-h"

h	Case 1 $U^*/U_L^* = 0.02$	Case 2 $U^*/U_L^* = 0.12$	Case 3 $U^*/U_L^* = 0.4$
0.16	$t = 70$ →fixed	$t = 5710$ →fixed	p-1
0.08	chaotic	chaotic	p-1-h
0.04	$t = 75$ →fixed	$t = 5530$ →fixed	p-1
0.02	$t = 135$ →fixed	chaotic	p-1
0.01	$t = 200$ →fixed	chaotic	p-1
0.005	$t = 80$ →fixed	$t = 7620$ →fixed	p-1-h
0.0025	$t = 80$ →fixed	chaotic	p-1-h
0.00125	chaotic	chaotic	p-1-h
0.000625	$t = 80$ →fixed	$t = 1020$ →fixed	p-1-h
0.0003125	$t = 80$ →fixed	chaotic	
0.00015625	chaotic	chaotic	
0.000078125	$t = 550$ →fixed	chaotic	
0.00005	$t = 2625$ →fixed	chaotic	
0.000025	$t = 255$ →fixed	chaotic	
0.00001	$t = 170$ →fixed	chaotic	

Table 6.1: Case studies using RK-method for a freeplay model

	Case 1 $U^*/U_L^* = 0.02$	Case 2 $U^*/U_L^* = 0.12$	Case 3 $U^*/U_L^* = 0.4$
PT-method	$t = 284$ →fixed	chaotic	p-1-h

Table 6.2: Case studies using PT-method for a freeplay model

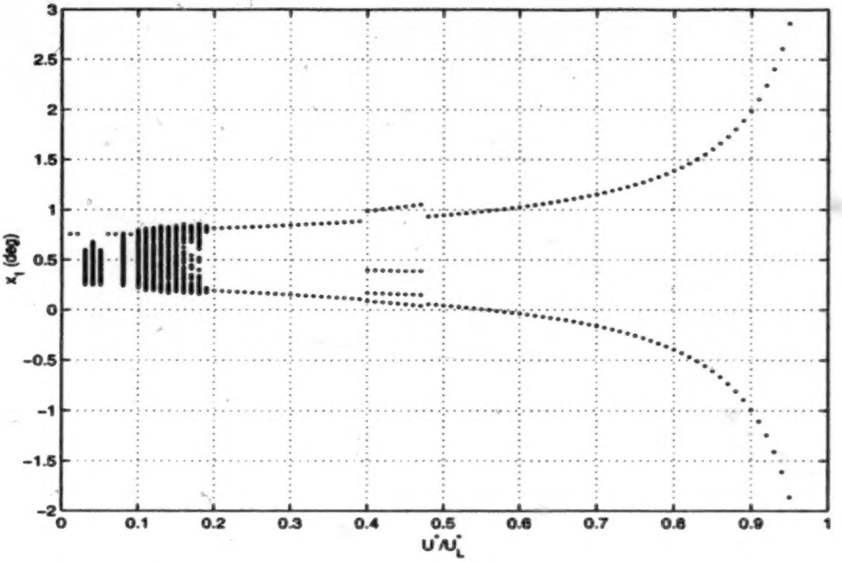

Figure 6.7: Bifurcation diagram for the simplified four dimensional freeplay model.

means "period-one with harmonics motion". The computing time for all the cases is $t = 9000$. This table shows that the numerical scheme with different time steps gives qualitatively different solutions. The details of the motion behavior of the numerical solutions and results obtained by using PT-method are shown in Figs. 6.8-6.20, in which the radians are transformed to degrees.

For Case 1, while most of the time steps result in fixed points, three of them ($h = 0.08$, 0.00125 and 0.00015625) lead to chaotic motions. Furthermore, even for the same asymptotic behavior, the fixed point, the transient states are different. For example, Fig. 6.8 gives different time histories for time steps $h = 0.02$ and $h = 0.005$, although both motions approach to the unique fixed point X_0^3. For the time steps which lead to chaotic motions, the trajectories are not all the same. For example, the time histories of x_1 for $h = 0.08$ and $h = 0.00125$ are displayed in Figs. 6.9(a) and (b) respectively; the corresponding phase pathes of x_2 versus x_1 are given in Figs. 6.10(a) and (b). It is obvious that both time histories and phase paths are quite different. Also, the time histories for x_3 and the phase paths of x_3–x_4 for these two time steps are

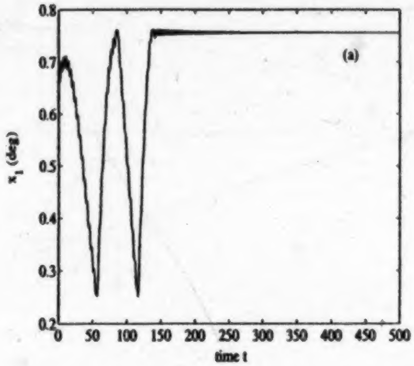

Figure 6.8: The time histories of x_1 for Case 1 with (a). $h = 0.02$ and (b). $h = 0.005$.

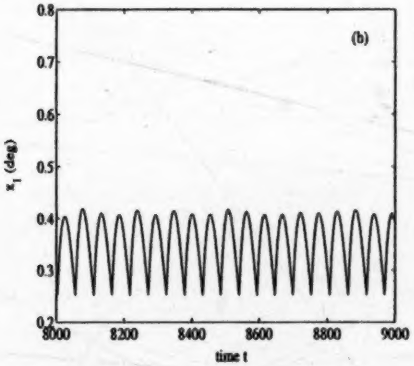

Figure 6.9: The time histories of x_1 for Case 1 with (a). $h = 0.08$ and (b). $h = 0.00125$.

different, as shown in Figs. 6.11 and 6.12. The chaotic motion resulting from the RK-method with $h = 0.00015625$ looks similar to that with $h = 0.00125$.

However, the PT-method gives only a fixed point with the transient time $t = 284$. The time history of x_1 resulting from the PT-method is shown in Fig. 6.18. It turns out that none of the RK results are the same as the PT result. For a case in which the numerical results are as sensitive as this one to time step h, certainly the RK-method is not recommended.

For Case 2, while most of the results are chaotic motions, some of them (h = 0.16, 0.04, 0.005, and 0.00625) are fixed points. The profiles for the

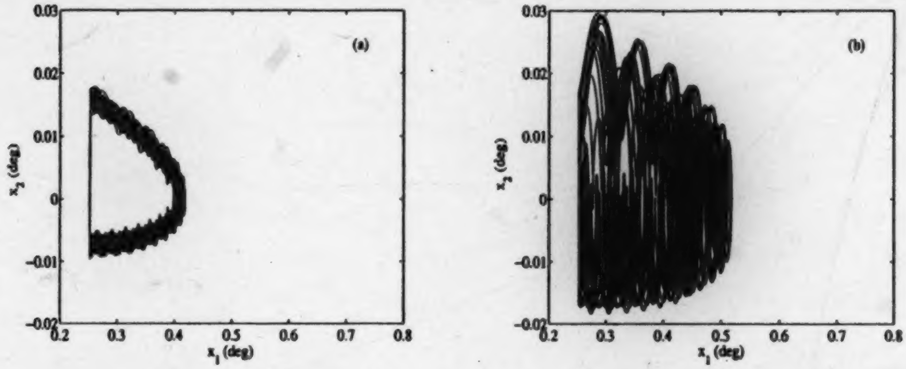

Figure 6.10: The phase paths of x_1–x_2 for Case 1 with (a). $h = 0.08$ and (b). $h = 0.00125$.

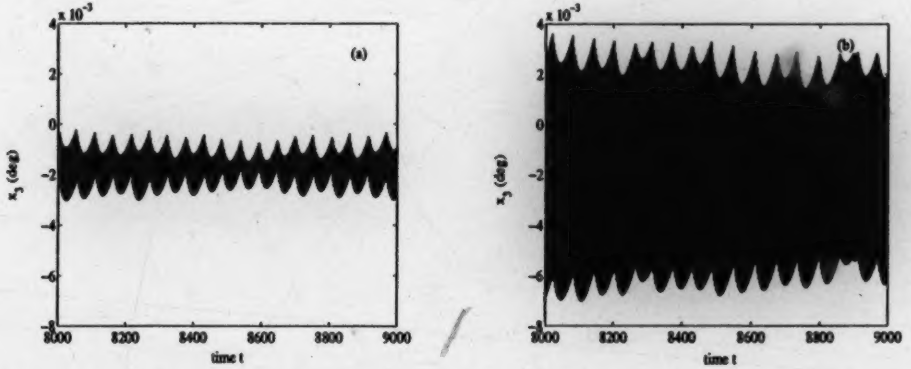

Figure 6.11: The time histories of x_3 for Case 1 with (a). $h = 0.08$ and (b). $h = 0.00125$.

chaotic motions are more or less the same, while the transient states for the fixed points are very different. The time histories and phase pathes for the motions with $h = 0.08$, 0.02 and 0.005 are displayed in Figs. 6.13–6.17. On the other hand, the PT-method gives a chaotic motion for this case. The time histories of x_1 and x_3 and the phase paths of x_1–x_2 and x_3–x_4 for Case 2 resulting from the PT-method are displayed in Figs. 6.19 and 6.20. Again, we reach the conclusion that the RK-scheme is not suitable here since with different time steps it gives inconsistent asymptotic results.

Even when the ratio is larger than 0.2, the RK-method with different time

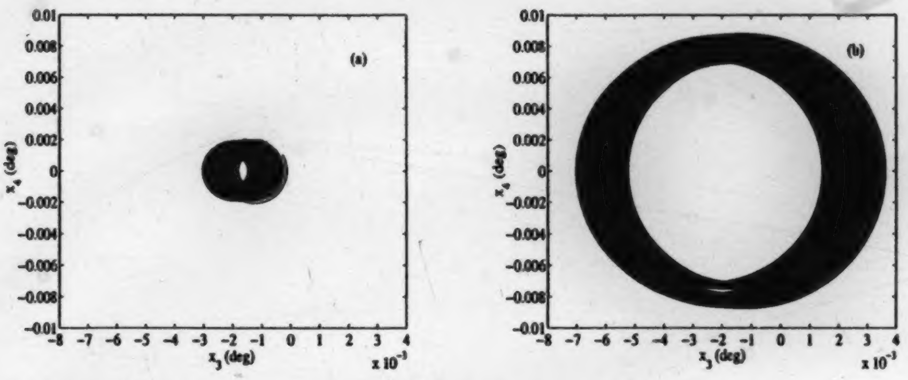

Figure 6.12: The phase paths of x_3–x_4 for Case 1 with (a). $h = 0.08$ and (b). $h = 0.00125$.

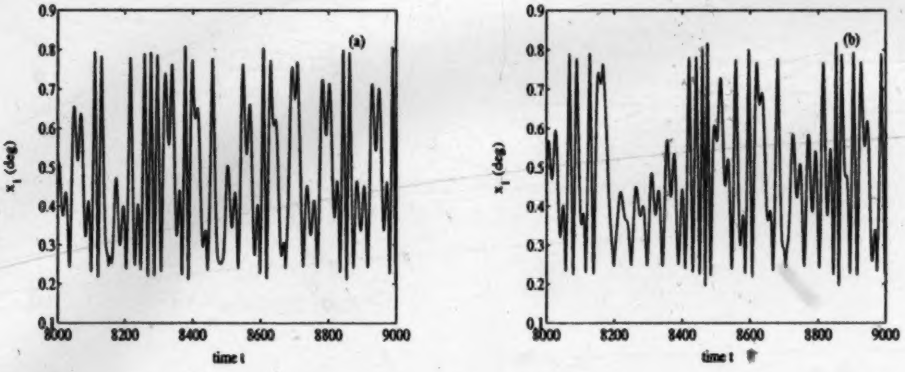

Figure 6.13: The time histories of x_1 for Case 2 with (a). $h = 0.08$ and (b). $h = 0.02$.

steps also gives different results. In Case 3, with $h = 0.16, 0.04, 0.02$, and 0.01, the motions resulting from the RK-method converge to period-one LCO; with $h = 0.08, 0.005, 0.0025, 0.00125, 0.000625...$, the motions converge to period-one with harmonics LCO. When using PT-method, we obtain only the period-one with harmonics LCO, which is similar to the result from the RK-method with small time steps (smaller than 0.005).

The errors of the RK-scheme for the piecewise linear system consist of accumulated error and the switching points location error. Since the system is piecewise linear, although the analytical error estimation method presented in

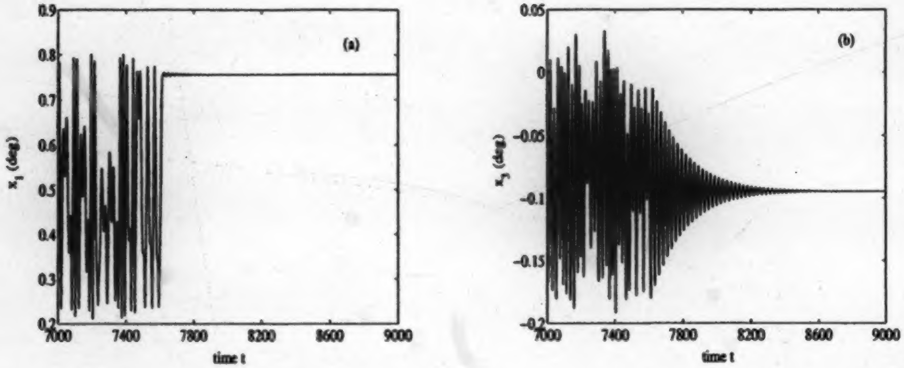

Figure 6.14: The time histories of (a). x_1 and (b). x_3 for Case 2 with $h = 0.005$.

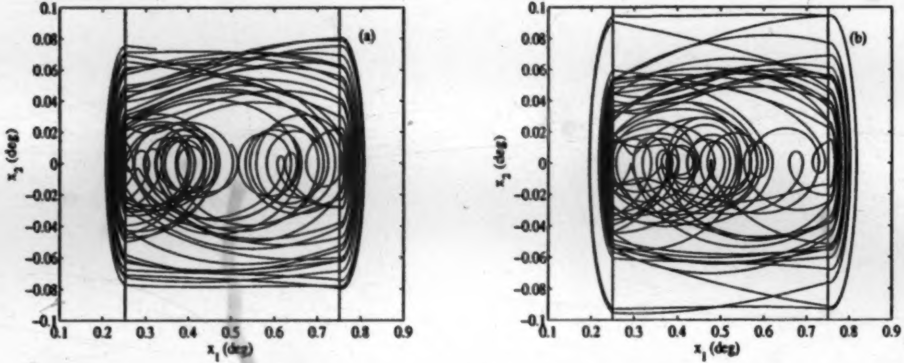

Figure 6.15: The phase paths of x_1–x_2 for Case 2 with (a). $h = 0.08$ and (b). $h = 0.02$.

the previous sections of this chapter can be applied to each subsystem in each region, the numerical error for the entire system cannot be achieved. However, these two types of errors will be illustrated through Case 1 in the following discussion and Figs. 6.21-6.22. Similar results can be obtained for the other cases.

Accumulated Error: In Case 1, the numerical results deviate from the exact motion at an early time. Fig. 6.21 displays the time histories resulting from the RK-method with different time steps compared to that from the PT-method. The smaller the time step h is, the longer time it takes for the deviation to become evident. For example, when $h = 0.08$, the discrepancy

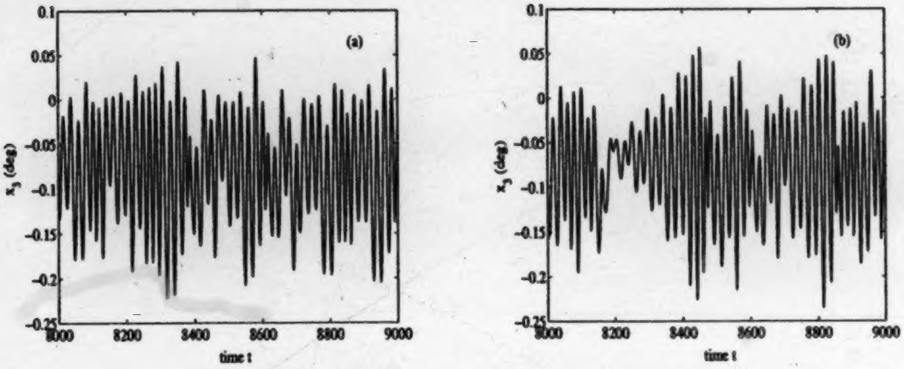

Figure 6.16: The time histories of x_3 for Case 2 with (a). $h = 0.08$ and (b). $h = 0.02$.

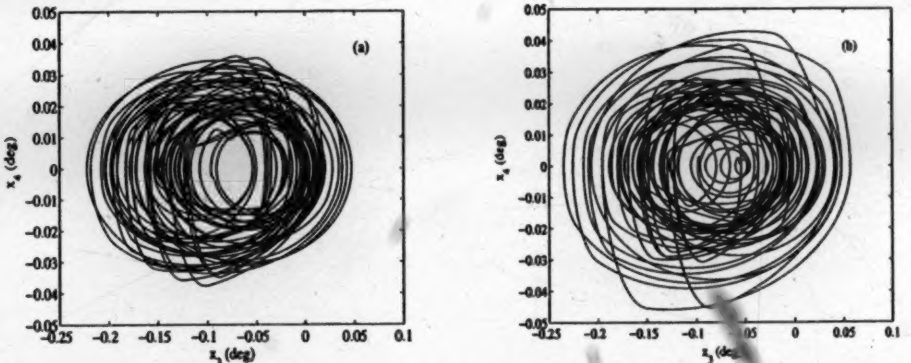

Figure 6.17: The phase paths of x_3–x_4 for Case 2 with (a). $h = 0.08$ and (b). $h = 0.02$.

between the numerical result and the exact motion can be seen as early as $t = 56$. Then, the error grows quickly, leading the motion from a fixed point to a qualitatively different solution: chaos. As h decreases to $h = 0.00125$, the discrepancy becomes evident only after $t = 85$.

Switching Point Location Error: The RK-method with an uniform time step cannot locate exactly the switching points, which is further confirmed in Fig. 6.22. This figure, with x_1 versus time t, shows location error of the switching points at $x_1 = 0.0044$ for Case 1. Here, the location error is defined as the difference between 0.0044 with the value of x_1 of the closer point to

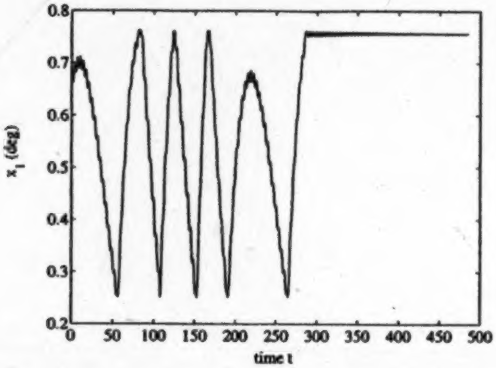

Figure 6.18: Time history of x_1 for Case 1 resulting from PT-method.

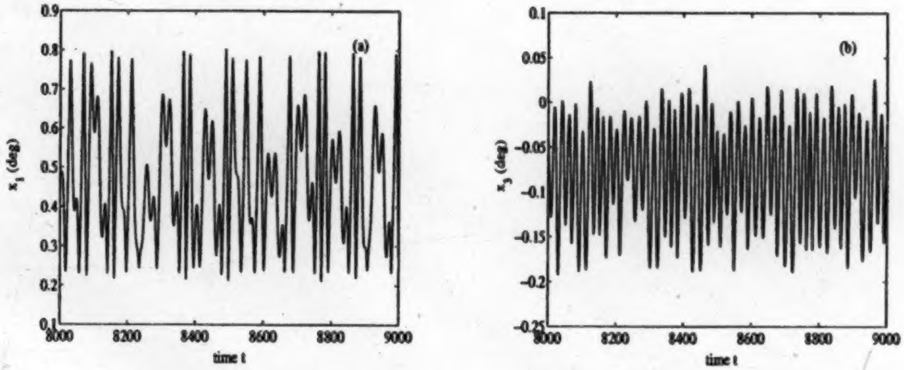

Figure 6.19: Time histories of x_1 and x_3 for Case 2, result from PT-method.

$\{X \in \mathbf{R} | x_1 = 0.0044\}$ when the trajectory passes through the subspace. It can be seen that larger time step results in larger location error. When the location error is small for small time steps (which can be seen in Fig. 6.22), from Tables 6.1 and 6.2, the numerical solutions become consistent and have similar asymptotic behavior as that of the solutions obtained by using PT-method. Hence, we reach the conclusion that the location of switching points is very important. The graph for the location error of the switching points at $x_1 = 0.0131$ for Case 1 is similar to Fig. 6.22.

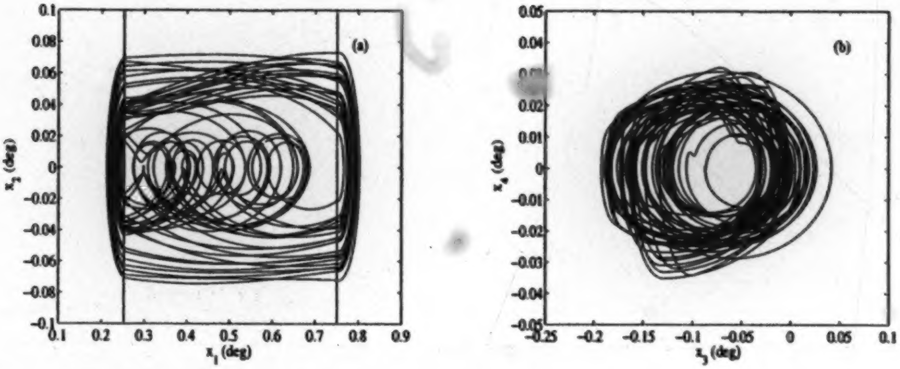

Figure 6.20: The phase paths of x_1–x_2 and of x_3–x_4 for Case 2, result from PT-method.

6.5 Concluding Remarks

In this chapter, we emphasize the importance and necessity of analytical techniques by investigating the errors of the fourth-order RK-schemes applied to a simple sinusoidal motion, aeroelastic systems with cubic springs, a rapidly time-variant system and an aeroelastic system with a freeplay model. First, for a simple sinusoidal motion, the numerical scheme is proven stable, and the analytical estimate (6.11) of the numerical error is obtained. For a finite time interval, we can always have sufficiently accurate numerical results by choosing small time steps such that the ratio h/T is sufficiently small. Since T is fixed for a motion and is known from the equation, it is easy to check the condition of h/T before the numerical computation. However, no matter how small the time step h is, the amplitude of the numerical solution always approaches zero as the computation time increases to infinity. Therefore, the scheme must be used with careful choice of h/T for long time computations. For a more complicated aeroelastic system with cubic springs, the stability and accuracy of the scheme rely heavily on the ratio h/T as well. However, the period T is unknown before the numerical computation, which makes it impossible to check the stability condition of the scheme in advance. Then, for a rapidly time-variant system, the scheme changes from being stable to being unstable. Even worse, since the period T decreases to zero, for any chosen

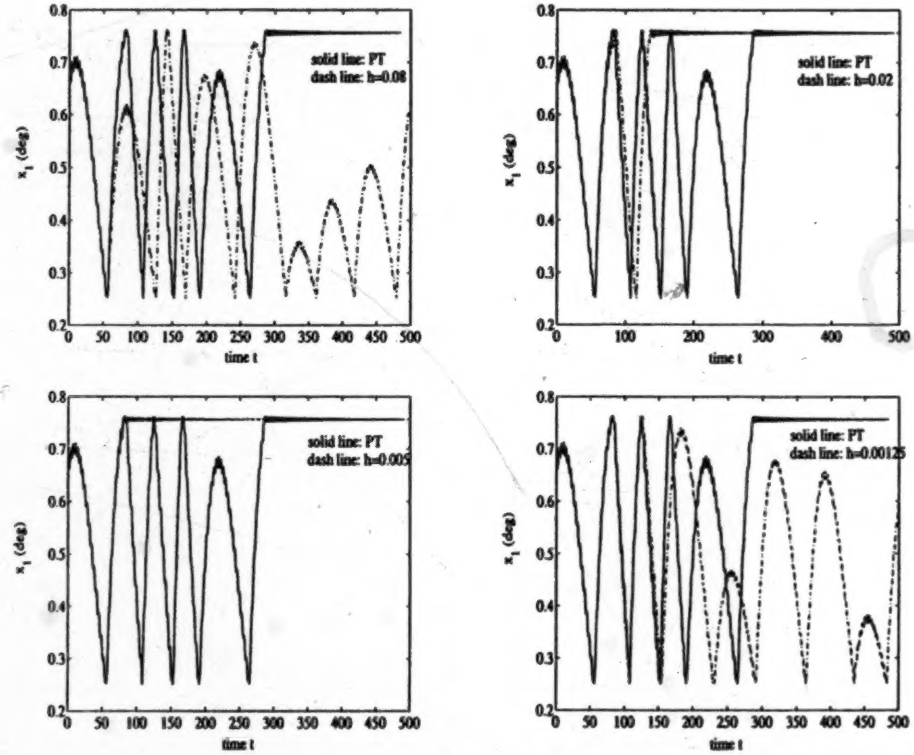

Figure 6.21: A comparison between the RK result and the PT result.

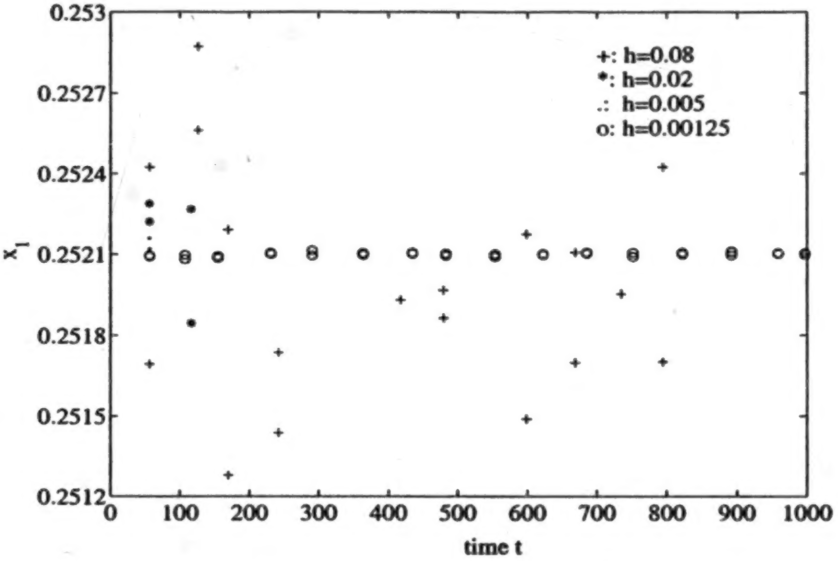

Figure 6.22: Switching point location errors in the RK-method for Case 1

time step h the ratio h/T always increases to infinity as the computation time t increases. As expected, the numerical simulations show the divergent solutions qualitatively different from the exact motion, which converges to zero. Finally, the scheme for the aeroelastic system with a freeplay model cannot be proven stable by using the standard analysis for the scheme. Particularly, for some cases, the schemes cannot be proven to be stable for all three regions with any chosen time step. Furthermore, from the error analysis of the scheme for the piecewise linear system, we conclude that the location error of switching points, as well as the normal accumulated error, plays an important role in the numerical results. By a careful examination of three cases, we observe that different time steps may result in inconsistent solutions and qualitatively different asymptotic behaviors such as the fixed point, the chaos, the period-one LCO and the period-one with harmonics LCO. Hence, analytical techniques proposed in this thesis not only provide predictions directly and fast but also for some cases are important and necessary, since numerical results may lead to inconsistent and wrong results especially when the scheme has not been proven stable.

Chapter 7

Conclusion

In this thesis, we consider a two-dimensional airfoil oscillating in pitch and plunge exposed to a subsonic flow with cubic, freeplay, and hysteresis structural nonlinearities. The mathematical model is a system of coupled integro-differential equations, which is reformulated to a set of eight first-order ordinary differential equations by the introducing of four new variables. Several analytical techniques, the center manifold theory, the principle of normal form, the perturbation method, and the point transformation method, have been applied to investigate the dynamic response of the 2-DOF aeroelastic system. Numerical results obtained by using the fourth-order Runge-Kutta method have been presented to compare with those obtained from analytical predictions.

For a self-excited aeroelastic system with cubic hard springs, the center manifold theory is used to reduce the 8-dimensional system to a 2-dimensional system, which is then simplified by the principle of normal form. From the simplified 2-dimensional system, the frequency prediction formula is first derived. The prediction of the amplitude is then obtained by using the perturbation method. Therefore, the amplitude and frequency of the LCO in the post-Hopf bifurcation are predicted analytically. Several test examples are given to show the excellent agreement between the numerical results and the analytical predictions. These examples include the aeroelastic system with weak/strong cubic nonlinearity in one/both DOF. Furthermore, in a straightforward manner, this center manifold technique can be extended to be suitable for general nonlinear system of ODEs with polynomial nonlinearities[88]. For the analytical predictions in the flutter response of cubic nonlinearity, several problems remain open and are listed below.

(a) The amplitudes and frequencies of period-two LCOs.

As mentioned at the end of Chapter 3, with some adjustment for the time dependent center manifold and time dependent normal form, the center manifold technique developed in Chapter 3 may be extended to predict the amplitudes and frequencies of period-two LCOs.

(b) The flutter response of a soft spring.

As this response depends on the initial conditions, the center manifold technique, which does not take into account any initial conditions, is not applicable for this case.

(c) The dynamic response of an aeroelastic system subject to two external forces with two different frequencies.

The dynamic response of an aeroelastic system subject to one external force or two external forces with the same frequencies was investigated in Lee et al.[49]. However, their technique cannot be extended for two different frequencies. If the time dependent center manifold and time dependent normal form can be derived for the aeroelastic system, this technique may be extended to predict the dynamic response of the aeroelastic system with two external forces where the reference frequencies are distinct.

Based on the point transformation method, two formulations are developed for the self-excited aeroelastic system with freeplay and hysteresis structural nonlinearities. The observed nonlinear phenomena are convergent, period-one, period-one with harmonics, period-two, period-two with harmonics, chaotic and divergent motions. Formulation 1 in § 4.3.1 and § 5.2.1 takes into account the initial conditions, which is particularly necessary for these two types of nonlinearities. It can be used to detect all the nonlinear behavior of the system. Formulation 2 in § 4.3.2 and § 5.2.2 can be used to predict the amplitude and frequency of period-one, period-one with harmonics, period-two, and period-two with harmonics LCOs. Formulation 2 is more efficient than Formulation 1 if only the LCO steady-state is of interest. Both formulations are capable of detecting the coexistence of stable LCOs. For the cases we considered, the numerical results obtained by using very small time-steps agree with those obtained by using the point transformation method. Furthermore, these two procedures can be generalized for the system subject to external forces and for the nonlinearities in both DOF. In fact, this techniques can be extended for general piecewise linear system. In this field, there are some related problems which need further investigation.

(d) The prediction of chaos.

As mentioned in Chapters 4 and 5, Formulation 2 in § 4.3.2 and § 5.2.2 cannot be used directly to predict any chaotic motion. However, it may be possible to extend the formulation to detect the chaos specifically for the freeplay and hysteresis models.

(e) The prediction of the frequency of harmonics component.

Although we detect the harmonics component in the nonlinear behavior by using both formulations, the frequency of the harmonics cannot be predicted from the formulations.

Finally, to emphasize the importance and necessity of analytical techniques, we carry out a detailed analysis of the errors resulting from the Runge-Kutta method for the aeroelastic system with cubic and freeplay nonlinearities. For the cubic model, the numerical scheme is stable for sufficiently small time steps, and the numerical error can be estimated analytically. For the freeplay model, on the other hand, the stability of the scheme cannot be theoretically analyzed in a straightforward manner and the numerical error cannot be estimated analytically. The error resulting from the fourth-order Runge-Kutta scheme for a simplified freeplay model is carefully studied, especially for the cases where the numerical results indicate qualitatively different system behavior. The result suggests that the analytical techniques such as those developed in Chapters 3, 4 and 5 are important and necessary since the numerical results are not always reliable, particularly for the aeroelastic system with freeplay and hysteresis models for which the numerical schemes have not been proven stable.

The present work assumes linear aerodynamics with nonlinear structures. As limit cycle behavior has been observed in the transonic regime, where strong aerodynamics nonlinearities are presented, our future work will take account the effect due to nonlinear aerodynamics as well as structural nonlinearities. Compared to the flutter analysis of nonlinear structures, nonlinear aerodynamic effects are more difficult to analyze since the fluid motion is governed by equations where analytical solutions cannot be found. However, if the unsteady aerodynamics model can be approximated by a curve function, the center manifold (time-dependent) technique and the point transformation method can be extended to study the dynamics response of the two- or three-degree-of-freedom aeroelastic system with cubic, freeplay and hysteresis nonlinear structures and with nonlinear aerodynamics.

Bibliography

[1] H. ALIGHANBARI AND S. J. PRICE, *The post-Hopf-bifurcation response of an airfoil in incompressible two-dimensional flow*, Nonlinear Dynamics, 10(1996), pp. 381-400.

[2] A. A. ANDRONOV, A. A. VITT, AND S. E. KHAIKIN, *Theory of Oscillators*, Addison-Wesley Publishing Company Inc., 1966.

[3] P. V. BAYLY AND L. N. VIRGIN, *Chaotic rattling of a piecewise nonlinear oscillator*, ASME-91-WA-DSC-17, 1991.

[4] K. J. BATHE AND E. L. WILSON, *Numerical Methods in Finite Element Analysis*, Prentice Hall, Inc. New Jersey, 1976. pp.345–362.

[5] P. BERGE, Y. POMEAU AND C. VIDAL, *Order Within Chaos*, Wiley, New York, 1986.

[6] W. J. BEYN, *Numerical Methods for Dynamical Systems*, Advances in Numerical Analysis (editor, W. Light), Oxford Science Publication, Oxford, 1991.

[7] R. L. BISPLINGHOFF AND H. ASHLEY, *Principles of Aeroelasticity*, John Wiley and Sons, Inc., New York, NY, 1962.

[8] R. L. BISPLINGHOFF, H. ASHLEY AND R. L. HALFMAN, *Aeroelasticity*, Addison-Wesley Publishing, Cambridge, Mass, 1955.

[9] E. J. BREITBACH, *Effect of structural nonlinearities on aircraft vibration and flutter*, Presented at the 45th Structures and Materials AGARD Panel Meeting, AGARD report 665. Voss, Norway, 1977.

[10] E. J. Breitbach, *Flutter analysis of an airplane with multiple structural nonlinearities in the control system*, NASA TP 1620, 1980.

[11] J. C. Butcher, *The Numerical Analysis of Ordinary Differential Equations: Runge-Kutta and General Linear Methods*, John Wiley & Sons, 1987.

[12] J. Carr, *Applications of Centre Manifold Theory*, Springer-Verlag, New York, 1981.

[13] A. R. Collar, *The expanding domain of aeroelasticity*, Journal of the Royal Aeronautical Society, L(1946), pp. 613-636.

[14] Y. Chan, *Numerical simulation of a two-dimensional airfoil with a hysteresis nonlinearity*, National Research Council Canada, NRC summer student project report IAR-97-1, Sept. 1997.

[15] M. D. Conner, P. Donescu and L. N. Virgin, *On the global convergence characteristics of numerically evaluated jacobian matrices*, Nonlinear Dynamics, 10(1996), pp. 165-174.

[16] M. D. Conner, D. M. Tang, E. H. Dowell and L. N. Virgin, *Nonlinear Behavior of a Typical Airfoil Section with Control Surface Freeplay: A Numerical and Experimental Study*, J. Fluids and Structures, (11)1997, pp. 89-109.

[17] E. J. Doedel and J. P. Kernevez, *AUTO: software for continuation and bifurcation problems in ordinary differential equations*, Applied Mathematics Report, California Institute of Technology, 1986.

[18] E. H. Dowell, *Aeroelasticity of Plates and Shells*, Noordhoff International Publishing, 1974.

[19] E. H. Dowell, H. C. Jr. Curtiss, R. H. Scanlan and F. Sisto, *A Modern Course in Aeroelasticity*, Sijthoff and Noordhoff, the Netherlands, 1978.

[20] E. H. DOWELL AND M. ILGAMOV, *Studies in Nonlinear Aeroelasticity*, Springer-Verlag New York Inc., 1988.

[21] J. H. FERZIGER, *Numerical Methods for Engineering Application*, John Wiley & Sons, 1998.

[22] H. W. FORSCHING, *Fundamentals of Aeroelasticity*, In German, Springer-Verlag, Berlin, 1974.

[23] Y. C. FUNG, *An Introduction to the Theory of Aeroelasticity*, Dover Publications Inc., New York, 1993.

[24] C. W. GEAR, *Numerical Initial Value Problems in Ordinary Differential Equations*, Prentice-Hall, Inc. 1971.

[25] L. GONG, Y. S. WONG AND B. H. K. LEE, *Dynamics of a Coupled System of Duffing's Equations*, Dynamics of Continuous, Discrete and Impulsive Systems, 4(1998), pp. 99-119.

[26] J. GUCKENHEIMER, AND P. HOLMES, *Nonlinear Oscillations, Dynamical Systems, and Bifurcation of Vector Fields*, Springer-Verlag, 1993.

[27] P. HARTMAN, *Ordinary Differential Equations*, 2nd ed. Birkauser, Boston, 1982.

[28] M. HATA, *Euler's finite difference scheme and chaos in* $\mathbf{R}^n$, Proc. Japan Acad. 58A(1982), pp. 178-181.

[29] A. J. HAUENSTEIN, R. M. LAURENSON, W. EVERSMAN, G. GALECKI, I. QUMEI AND A. K. AMOS,*Chaotic response of aerosurfaces with structural nonlinearities*, Proceedings of the AIAA/ASME/ASCE/AHS/ASC 31st Structures, Structural Dynamics, and Materials Conference (Long Beach, CA), AIAA, Washington, DC, 1990, pp. 1530-1539.

[30] A. J. HAUENSTEIN, J. A. ZARA, W. EVERSMAN AND I. QUMEI, *Chaotic and nonlinear dynamic response of aerosurfaces with structural nonlinearities*, Proceedings of the AIAA/ASME/ASCE/AHS/ASC 33rd

Structures, Structural Dynamics, and Materials Conference, Part 4 Structural Dynamics II (Dallas, TX), AIAA, Washington, DC, 1992, AIAA-92-2574-CP, pp. 2367-2375.

[31] C. HAYASHI, *Nonlinear Oscillations in Physical Systems*, McGraw Hill, New York, 1964.

[32] M. HENON, *On the numerical computation of Poincare maps*, Physica 5D, 1982, pp. 412-414.

[33] D. H. HODGES AND R. A. ORMISTON, *Stability of hingeless rotor blades in hover and pitch-link flexibility*, AIAA J., 15(1977), pp. 476-482.

[34] J. C. HOUBOLT, *A recurrence matrix solution for the dynamic response of elastic aircraft*, J. Aeronaut. Sci., 17(1950), pp. 540-550.

[35] A. HECK, *Introduction to Maple*, Springer-Verlag, New York, 1993.

[36] K. ISOGAI, *On the transonic-dip mechanism of flutter of a sweptback wing*, AIAA Journal, 17(7)(1979), pp. 793-795.

[37] E. C. JOHNSON, *Sinusoidal analysis of feedback-control systems containing nonlinear elements*, Trans. AIEE, 71(1952), pp. 169-181.

[38] D. J. JONES AND B. H. K. LEE, *Time marching numerical solution of the dynamic response of nonlinear systems*, Aeronautical Note NAE-AN-25, NRC No. 24131, National Research Council Canada, 1985.

[39] R. T. JONES, *The unsteady lift of a wing of finite aspect ratio*, NACA Rept. 681, 1940.

[40] K. A. KOUSEN AND O. O. BENDIKSEN, *Limit cycle phenomena in computational transonic aeroelasticity*, J. Aircraft, 31(1994), pp. 1257-1263.

[41] N. KRYLOV AND N. BOGOLIUBOV, *Introduction to Nonlinear Mechanics*, translation by Solomon Lifschitz, Princeton University Press, Princeton, 1947.

[42] Y. A Kuznetsov, *Elements of Applied Bifurcation Theory*, Springer, Berlin, 1995.

[43] R. M. Laurenson and R. M. Trn, *Flutter analysis of missile control surfaces containing structural nonlinearities*, AIAA J. 18(1980), pp. 1245-1251.

[44] B. H. K. Lee and J. Desrochers, *Flutter analysis of a two-dimensional airfoil containing structural nonlinearities*, National Research Council of Canada, Aeronautical Report, LR-618, NRC No. 27833, 1987.

[45] B. H. K. Lee and A. Tron, *Effects of structural nonlinearities on flutter characteristics of the CF-18 aircraft*, J. Aircraft, 26(1989), pp. 781-786.

[46] B. H. K. Lee, L. Gong and Y. S. Wong, *Analysis and computation of nonlinear dynamic response of a two-degree-of-freedom system and its application in aeroelasticity*, AIAA-96-1248, AIAA Dynamics Specialists Conference, April 18-19, 1996, Salt Lake City, UT.

[47] B. H. K. Lee, L. Gong and Y. S. Wong, *Effects of structural nonlinearities in aeroelasticity*, Nonlinear Analysis, Theory, Methods and Applications, Proceedings of the Second World Congress of Nonlinear Analysts, 30(1997), pp. 2699-2709.

[48] B. H. K. Lee, L. Gong and Y. S. Wong, *Analysis and computation of nonlinear dynamic response of a two-degree-of-freedom system and its application in aeroelasticity*, J. Fluids Structures, 11(1997), pp. 225-246.

[49] B. H. K. Lee, L. Y. Jiang and Y. S. Wong, 1999 *Flutter of an airfoil with a cubic nonlinear restoring force*, AIAA Paper 98-1725, 39th AIAA/ASME/ASCE/AHS/ASC Structures, Structural Dynamics, and Materials Conf. 20-23 April, Long Beach, CA, 1998.

[50] B. H. K. Lee, L. Y. Jiang and Y. S. Wong, 1999 *Flutter of an airfoil with a cubic nonlinear restoring force*, J. Fluids Structures, 13(1999), pp. 75-101.

[51] B. H. K. Lee and P. LeBlanc, 1986 *Flutter analysis of a two-dimensional airfoil with cubic nonlinear restoring force*, National Research Council of Canada, Aeronautical Note, NAE-AN-36, NRC No. 25438, 1986.

[52] B. H. K. Lee, S. J. Price, and Y. S. Wong, *Nonlinear Aeroelastic Analysis of Airfoils: Bifurcation and Chaos*, Progress in Aerospace Sciences, 35(1999), pp. 205-334.

[53] Q. S. Li, *A new exact approach for analyzing free vibration of SDOF systems with nonperiodically time varying parameters*, J. Vibration and Acoustics, 122(2)(2000), pp. 175-179.

[54] T. Y. Li and J. A. Yorke, *Period three implies chaos*, Amer. Math., Monthly, 82(1975), pp. 985-992.

[55] W. B. Lin and W. H. Cheng, *Nonlinear flutter of loaded lifting surfaces (I) and (II)*, Journal of the Chinese Society of Mechanical Engineers, 14(1993), pp. 446-466.

[56] L. Liu, Y. S. Wong, and B. H. K. Lee, *Application of the centre manifold theory in nonlinear aeroelasticity*, CEAS/AIAA/ICASE/NASA Langley International Forum on Aeroelasticity and Structural Dynamics 1999, NASA/CP- 1999-209136/PT2, pp. 533-542.

[57] L. Liu, Y. S. Wong, and B. H. K. Lee, *Application of the centre manifold theory in nonlinear aeroelasticity*, J. Sound and Vibration, 234-4(2000), pp. 641-659.

[58] L. Liu, Y. S. Wong, and B. H. K. Lee, *The point transformation method in nonlinear aeroelasticity*, Proceedings of the Second Interna-

tional Workshop on Scientific Computing and Applications, Kananaskis, Alberta, CA, May 28-June 1st, 2000.

[59] L. LIU, Y. S. WONG, AND B. H. K. LEE, *Nonlinear aeroelastic analysis using the point transformation method, Part I and II*, J. Sound and Vibration, submitted.

[60] L. LIU, B. H. K. LEE, AND Y. S. WONG, *Dynamical Analysis of Nonlinear Aeroelastic System with Hysteresis*, Proceedings of International Forum on Aerodynamics and Structural Dynamics 2001, June 5-7, Madrid, Spain.

[61] L. LIU, Y. S. WONG AND B.H.K. LEE, *Error analysis of Runge-Kutta's discretizations of aeroelastic systems*, Applied Mathematics and Computations, submitted.

[62] JR. S. C. MCINTOSH, JR. R. E REED AND W. P. RODDEN, *Experimental and theoretical study of nonlinear flutter*, J. Aircraft, 18(1981), pp. 1057-1063.

[63] Y. MAEDA, *Euler's discretization revisited*, Proc. Japan Acad., 71A(1995), pp. 58-61.

[64] MANY AUTHORS, *Aeroelastic effects from a flight mechanics standpoint*, North Atlantic Treaty Organization, Advisory Group for Aerospace Research and Development, Flight Mechanics Panel, 1970.

[65] C. MOLER AND C. VAN LOAN, *Nineteen dubious ways to compute the exponential of a matrix*, SIAM Review 20(1978), pp. 801-836.

[66] F. C. MOON, *Chaotic Vibrations: An Introduction for Applied Scientists and Engineers*, John Wiley & Sons, Inc. 1987.

[67] A. H. NAYFEH AND D. T. MOOK, *Nonlinear Oscillations*, John Wiley & Sons, New York, 1995.

[68] A. H. NAYFEH AND B. BALACHANDRAN, *Applied Nonlinear Dynamics: Analytical, Computational and Experimental Methods*, John Wiley & Sons, Inc. 1995.

[69] A. NATARAJAN, R. K. KAPANIA AND D. J. INMAN, *Near-exact analytical solutions to linear time-variant systems*, Proceedings of the 42nd AIAA/ASME/ASCE/AHS/ASC Structures, Structural Dynamics, and Materials Conference and Exhibit, Seattle, WA, USA, 16-19 April, 2001.

[70] T. O'NEIL, H. GILLIAT AND T. STRGANAC, *Investigation of Aeroelastic Response for a System with Continuous Structural Nonlinearities*, AIAA Paper, 96-1390, 1996.

[71] S. J. PRICE, H. ALIGHANBARI AND B. H. K. LEE, *The Aeroelastic Response of a Two-Dimensional Airfoil with Bilinear and Cubic Structural Nonlinearities*, Journal of Fluids and Structures, 9(1995), pp. 175-193.

[72] S. J. PRICE, B. H. K. LEE, AND H. ALIGHANBARI, *Post instability behavior of a two-dimensional airfoil with a structural nonlinearity*, J. Aircraft, 31(1994), pp. 1395-1401.

[73] R. H. SCANLAN AND R. ROSENBAUM, *Introduction to the Study of Aircraft Vibration and Flutter*, The Macmillan Company, New York, NY, 1951.

[74] R. SEYDEL, *From Equilibrium to Chaos*, Elsevier, New York, 1988.

[75] S. F. SHEN, *An approximate analysis of nonlinear flutter problems*, J. Aerosp. Sci., 26(1959), pp. 25-32.

[76] S. F. SHEN, *Author's reply to: Remarks on analytical results of certain nonlinear flutter problems*, J. Aerosp. Sci., 26(1952), pp. 52-53.

[77] S. F. SHEN AND C. C. HSU, *Analytical results of certain nonlinear flutter problems*, J. Aeronaut. Sci., 25(1958), pp. 136-137.

[78] J. J. STOKER, *Nonlinear vibrations in mechanical and electrical systems*, Interscience Publishers, New York, 1950.

[79] D. M. TANG AND E. H. DOWELL, *Flutter and stall response of a helicopter blade with structural nonlinearity*, J. Aircraft, 29(1992), pp. 953-960.

[80] D. M. TANG AND E. H. DOWELL, *Comparison of theory and experiment for nonlinear flutter and stall response of a helicopter blade*, J. Sound Vib., 165(1993), pp. 251-276.

[81] J. M. T. THOMPSON AND H. B. STEWART, *Nonlinear Dynamics and Chaos*, John Wiley & Sons Ltd. 1986.

[82] C. T. TRAN AND D. PETOT, *Semi-empirical model for the dynamic stall of airfoils in view of the application to the calculation of responses of a helicopter blade in forward flight*, Vertica, 5(1)1981, pp. 35-53.

[83] Y. UEDA, *Steady motions exhibited by Duffing's equation: a picture cook of regular and chaotic motions*, New Approaches to Nonlinear Problems in Dynamics (editor, P. J. Holmes), SIAM, Philadelphia, 1980, pp. 311-322.

[84] F. VERHULST, *Nonlinear Differential Equations and Dynamical Systems*, Springer, Berlin, 1990.

[85] S. WIGGINS, *Introduction to Applied Nonlinear Dynamical Systems and Chaos*, Springer-Verlag, New York, 1996.

[86] S. WOLFRAM, *The Mathematica Book*, Wolfram Media, Inc., 1996.

[87] Y. S. WONG, B. H. K. LEE AND L. GONG, *Dynamic response of a two-degree-of-freedom system with a cubic nonlinearity*, 3rd Int. Conf. on Computational Physics, Chung Li, Taiwan, 1995.

[88] Y. S. WONG, L. LIU AND B. H. K. LEE, *Frequency and amplitude prediction of limit cycle oscillations of an airfoil containing concentrated structural nonlinearities*, 42nd AIAA/ASME/ASCE/AHS/ASC

Structures, Structural Dynamics, and Materials Conference and Exhibit, Seattle, WA, USA, April 16-19, 2001, AIAA 2001-1293.

[89] D. S. WOOLSTON, H. L. RUNYAN AND R. E. ANDREWS, *An investigation of effects of certain types of structural nonlinearities on wing and control surface flutter*, J. Aeronaut. Sci., 24(1957), pp. 57-63.

[90] D. S. WOOLSTON, H. L. RUNYAN AND T. A. BYRDSONG, *Some effects of system nonlinearities in the problem of aircraft flutter*, NACA TN 3539, 1955.

[91] M. YAMAGUTI AND Y. MAEDA, *On the discretization of O.D.E.*, ZAMM. Z. angew. Math. Mech., 76(1996)S4, pp. 217-219.

[92] M. YAMAGUTI AND H. MATANO, *Euler's finite difference scheme and chaos*, Proc. Japan Acad., 55A(1979), pp. 78-80.

[93] Z. C. YANG AND L. C. ZHAO, *Analysis of limit cycle flutter of an airfoil in incompressible flow*, J. Sound Vib. 123(1988), pp. 1-13.

[94] L. C. ZHAO AND Z. C. YANG, *Chaotic motions of an airfoil with nonlinear stiffness in incompressible flow*, J. Sound Vib., 138(1990), pp. 245-254.

Appendix A

Nomenclature

a_h	non-dimensional distance from airfoil mid-chord to elastic axis
b	airfoil semi-chord
c	chord
h	plunge displacement
m	airfoil mass
r	response amplitude of plunge motion
r_α	radius of gyration about elastic axis
t	time
x_α	non-dimensional distance from elastic axis to centre of mass
$C_L(\tau)$	aerodynamic lift coefficients
$C_M(\tau)$	pitching moment coefficients
DOF	degree of freedom

$G(\xi)$	nonlinear plunge stiffness term
J	Jacobian matrix
LCO	limit cycle oscillation
$M(\alpha)$	nonlinear pitch stiffness term
$P(\tau)$	externally applied force
PSD	power spectral density
$Q(\tau)$	externally applied moment
R	response amplitude of pitch motion
U	free stream velocity
U^*	non-dimensional velocity, $U^* = \dfrac{U}{b\omega_\alpha}$
U_L^*	non-dimensional linear flutter speed
X, Y	system variable vectors
V, Z	complex variables
ξ	nondimensional plunge displacement, $\xi = \dfrac{h}{b}$
α	pitch angle of airfoil
ω	frequency of the motion.
μ	airfoil/air mass ratio, $\mu = \dfrac{m}{\pi\rho b^2}$
τ	non-dimensional time, $\tau = \dfrac{Ut}{b}$
δ	perturbation parameter,
	pitch angle for the central region of the freeplay stiffness
ψ_1, ψ_2	constants in Wagner's function
ϵ_1, ϵ_2	constants in Wagner's function

β_α, β_{α^3}	constants in nonlinear pitch stiffness term $M(\alpha)$
β_ξ, β_{ξ^3}	constants in nonlinear plunge stiffness term $G(\xi)$
ζ_ξ, ζ_α	viscous damping ratios in plunge and pitch
$\bar{\omega}$	frequency ratio, $\bar{\omega} = \dfrac{\omega_\xi}{\omega_\alpha}$
ω_ξ, ω_α	natural frequencies in plunge and pitch
$\phi(\tau)$	Wagner's function

Appendix B

Center Manifold Theory

This appendix includes only the result that is related to Chapter 3. More details and results can be found in the books[12, 85].

B.1 Definitions and Theorems

We first define an invariant manifold for the equation:

$$\dot{\mathbf{x}} = N(\mathbf{x}) \tag{B.1}$$

where $\mathbf{x} \in \mathbf{R}^n$.

Definition 1. (invariant manifold) A set $S \subset \mathbf{R}^n$ is said to be local invariant manifold for Eq.(B.1) if for $\mathbf{x}_0 \in S$, the solution $\mathbf{x}(t)$ of Eq.(B.1) with $\mathbf{x}(0) = \mathbf{x}_0$ is in S for $|t| < T$ where $T > 0$. If we can always choose $T = \infty$, then we say that S is an invariant manifold.

We then consider the system:

$$\begin{cases} \dot{\mathbf{x}} = A\mathbf{x} + f(\mathbf{x}, \mathbf{y}) \\ \dot{\mathbf{y}} = B\mathbf{y} + g(\mathbf{x}, \mathbf{y}) \end{cases} \tag{B.2}$$

where $\mathbf{x} \in \mathbf{R}^n$, $\mathbf{y} \in \mathbf{R}^m$ and A and B are constant matrices such that all the eigenvalues of A have zero real parts while all the eigenvalues of B have negative real parts. The functions f and g are C^2 (the second derivatives exist and are continuous) with $f(0,0) = 0$, $f'(0,0) = 0$, $g(0,0) = 0$, and $g'(0,0) = 0$. (Here, f' is the Jacobian matrix of f.)

Definition 2. (center manifold) If $\mathbf{y} = h(\mathbf{x})$ is an invariant manifold for Eq.(B.2) and h is smooth, it is called a center manifold if $h(0) = 0$ and $h'(0) = 0$.

We use the term center manifold in place of local center manifold if the meaning is clear.

Theorem 3. (existence of center manifolds) There exists a center manifold for Eq.(B.2), $\mathbf{y} = h(\mathbf{x})$, $|\mathbf{x}| < \delta$, where h is C^2. The flow on the center manifold is governed by the n-dimensional system

$$\dot{u} = Au + f(u, h(u)) \ . \tag{B.3}$$

The next theorem tells us that Eq.(B.3) contains all the necessary information needed to determine the asymptotic behavior of small solutions of Eq.(B.2).

Theorem 4. (reduction principle)

(a) If the zero solution of Eq.(B.3) is stable (asymptotically stable) (unstable), the zero solution of Eq.(B.2) is stable (asymptotically stable) (unstable).

(b) Suppose that the zero solution of Eq.(B.3) is stable. Let $(\mathbf{x}(t), \mathbf{y}(t))$ be a solution of Eq.(B.2) with $(\mathbf{x}(0), \mathbf{y}(0))$ sufficiently small. Then there exists a solution $u(t)$ of Eq.(B.3) such that as $t \to \infty$,

$$\begin{cases} \mathbf{x}(t) = u(t) + O(e^{-\gamma t}) \\ \mathbf{y}(t) = h(u(t)) + O(e^{-\gamma t}) \end{cases} \tag{B.4}$$

where $\gamma > 0$ is a constant.

The next result shows that in principle the center manifold can be approximated to any degree of accuracy. For functions $\phi : \mathbf{R}^n \to \mathbf{R}^m$ which are C^1 in a neighborhood of the origin define

$$(M\phi)(\mathbf{x}) = \phi'(\mathbf{x})[A\mathbf{x} + f(\mathbf{x}, \phi(\mathbf{x}))] - B\phi(\mathbf{x}) - g(\mathbf{x}, \phi(\mathbf{x})). \tag{B.5}$$

Theorem 5. (approximation of the center manifold) Let ϕ be a C^1 mapping of a neighborhood of the origin in $\mathbf{R}^n$ into $\mathbf{R}^m$ with $\phi(0) = 0$ and

$\phi'(0) = 0$. If as $\mathbf{x} \to 0$, $(M\phi)(\mathbf{x}) = O(|\mathbf{x}|^q)$ where $q > 1$, $|h(\mathbf{x}) - \phi(\mathbf{x})| = O(|\mathbf{x}|^q)$ [illegible] $\to 0$.

B.2 Properties of Center Manifolds

Several interesting and important properties of center manifolds are presented as follows. For the details and proofs, consult the books[12, 85].

(1) In general Eq.(B.2) does not have a unique center manifold. However, if h and h_1 are two center manifolds for Eq.(B.2), by Theorem 5, $h(\mathbf{x}) - h_1(\mathbf{x}) = O(|\mathbf{x}|^q)$ as $\mathbf{x} \to 0$ for all $q > 1$.

(2) If f and g are C^k $(k \geq 2)$, h is C^k. If f and g are analytic, in general Eq.(B.2) does not have an analytic center manifold.

(3) Center manifold need not be unique, but there are some points which must always be on any center manifold. For example, suppose that $(\mathbf{x}_0, \mathbf{y}_0)$ is a small equilibrium point of Eq.(B.2) and let $\mathbf{y} = h(\mathbf{x})$ be any center manifold for Eq.(B.2). Then we must have $\mathbf{y}_0 = h(\mathbf{x}_0)$. Similarly, if Γ is a small periodic orbit of Eq.(B.2), Γ must lie on all center manifolds.

(4) If $(\mathbf{x}(t), \mathbf{y}(t))$ is a solution of Eq.(B.2) which remains in a neighborhood of the origin for all $t \geq 0$, there is a solution $u(t)$ of Eq.(B.3) such that the representation Eq.(B.4) holds.

(5) In many problems the initial data is not arbitrary, for example, some of the components might always be nonnegative. If $S \subset \mathbf{R}^{n+m}$ with $0 \in S$ and if Eq.(B.2) defines a local dynamical system on S, Theorem 4 is valid when Eq.(B.2) is studied on S.